STRUCTURAL AND BIOCHEMICAL ANALYSIS OF DYNEIN LIGHT CHAIN-MEDIATED HOMODIMERIZATION OF CYTOSKELETAL AND NUCLEAR PORE PROTEINS

Erin MacKenzie Romes

A dissertation submitted to the faculty of the University of North Carolina at Chapel Hill in partial fulfillment of the requirements for the degree of Doctor of Philosophy in the Department of Biochemistry and Biophysics.

Chapel Hill

2012

Approved by:

Kevin Slep, PhD

Richard Cheney, PhD

Nikolay Dokholyan, PhD

Hengming Ke, PhD

Matthew Redinbo, PhD

Stephen Rogers, PhD

ABSTRACT

ERIN M. ROMES: Structural and biochemical analysis of dynein light chain-mediated homodimerization of cytoskeletal and nuclear pore proteins
(Under the direction of Dr. Kevin C. Slep)

The dynein light chain, Lc8/Dyn2, is a ubiquitous protein that acts as a scaffold, binding to many different target proteins in various cellular contexts. Here we describe *S. cerevi*siae Dyn2's biophysical and structural interaction with the dynein intermediate chain, Pac11 at the dynein complex, and also Dyn2's interaction with a nuclear pore protein, Nup159 in the cytoplasmic fibrils. We also demonstrate the structural and binding similarities between the *Drosophila* homolog, Lc8 binding to a centriole duplication protein, Ana2 and Dyn2's interaction with Pac11 or Nup159. We obtained the first high-resolution crystal structure of Dyn2 bound to Nup159 peptides and subsequent structures of a homodimer of Dyn2 bound to two identical peptides of Pac11, and a homodimer of Lc8 bound to two identical Ana2 peptides. We also characterized the thermodynamic binding profiles of Dyn2/Lc8 interacting with Pac11, Ana2, or Nup159 peptide binding sites and discovered that both Dyn2 and Lc8 are capable of two modes of binding peptides, endothermically or exothermically with K_Ds in the range of 0.5 to 20 μM.

Results from these experiments highlight Dyn2/Lc8's ability to act as a "dimerization machine" to possibly optimize Pac11, Ana2 and Nup159's respective functions in the cell. Each of the Dyn2/Lc8 target proteins we have described here represents an essential component in their respective contexts. Pac11 is an essential scaffold that binds directly to

the dynein motor chain to modulate dynein velocity and processivity through various binding interactions, Ana2 is an essential centriole duplication protein that is responsible for nucleating a single procentriole so that a cell does not experience genomic instability as a result of improper chromosome distribution, and Nup159 is an essential protein in regulating mRNA export out of the nucleus through the nuclear pore. We provide evidence that Dyn2/Lc8 interacting in each of these processes affords the target protein the ability to optimize through dimerization.

ACKNOWLEDGEMENTS

First of all, I would like to thank my advisor, Dr. Kevin Slep for mentoring me through this huge stage of growth in my career. He helped me learn to find vision in a project and not to get too discouraged when that project was not proceeding according to that vision. I would also like to thank my committee members: Dr. Richard Cheney, Dr. Nikolay Dokholyan, Dr. Hengming Ke, Dr. Matt Redinbo, and Dr. Steve Rogers for guiding me through the essential experiments that resulted in published manuscripts. Finally, thank you to Michael Miley in the Crystallography Core at UNC for the technical assistance and advice.

I would like to thank the Slep lab members for technical assistance and well-mannered frivolity. I would like to thank Lauren Slevin for mentoring me through the new field of centrioles, technical support, and for her assistance with editing this dissertation. I would especially like to thank Jaime Campbell for helping me establish the Slep lab and for hours of moral support over the years.

Lastly, I would like to thank my family; none of this would be possible without them. I would like to apologize for hours of lost conversation and quality time due to other lab priorities. I am so fortunate to have Dennis, Linda, and Jonathan Toth to cheer me on from Michigan. The person who deserves most of the credit is my husband, Drew. My life would not be the same without his shoulder to cry on, a dinner to celebrate the small victories, and his unconditional support throughout all of it.

So thank you to all of you!

TABLE OF CONTENTS

CHAPTER 1 : INTRODUCTION 1

The benefit of a ubiquitous scaffolding protein 1

Lc8/Dyn2 is ubiquitously expressed, and a promiscuous protein 3

Lc8/DYNLL/Dyn2 interactions that are independent of the dynein complex illuminate a role as a dimerization machine 7

Motors of the cytoskeleton 9

The structure of processive kinesin 12

Cytoplasmic dynein structure 13

Function and regulation of the dynein holoenzyme 18

Lc8/Ctp interacts with Ana2 on centrioles 20

Dyn2 interacts with Nup159 on the cytoplasmic side of the nuclear pore 27

Research Objectives 29

References 32

CHAPTER 2 : THE STRUCTURE OF A YEAST DYNEIN DYN2-PAC11 COMPLEX AND EFFECT ON SINGLE MOLECULE DYNEIN MOTOR ACTIVITY 40

Preface 40

Summary 40

Experimental Procedures 41

Results 45

Discussion 57

References 60

CHAPTER 3 : THE STRUCTURE AND BINDING MODE OF THE DYNEIN LIGHT CHAIN, LC8, WITH AN ESSENTIAL CENTRIOLE DUPLICATION FACTOR, ANA2 62

Preface 62

Summary 62

Experimental Procedures 63

Results 66

Discussion 71

References 73

CHAPTER 4 : THE STRUCTURE OF A YEAST DYN2-NUP159 COMPLEX AND THE MOLECULAR BASIS FOR THE DYNEIN LIGHT CHAIN – NUCLEAR PORE INTERACTION 75

Preface 75

Summary 75

Experimental Procedures 76

Results 80

Discussion 94

References 97

CHAPTER 5 : DISCUSSION AND FUTURE WORK 100

Discussion 100

Future Work 108

References 110

LIST OF TABLES

Table 2-1 Data Collection and Refinement Statistics of Dyn2 and Pac11 pep2

Table 3-1 Data Collection and Refinement Statistics of Lc8 and Ana2 pep1

Table 4-1 Data Collection and Refinement Statistics of Dyn2 and Nup159 pep2

LIST OF FIGURES

Figure 1-1. Dyn2/Lc8 binds to proteins with coiled-coil domains and a QT motif. 4

Figure 1-2. Structure of the *Drosophila* Lc8 in complex with the rat dynein IC shows an Lc8 dimer bound to two IC β-strands by two parallel β-sheets..... 6

Figure 1-3. Cartoon of the dynein holoenzyme shows how all of the canonical dynein associating factors interact at the N-terminus of the DHC. 15

Figure 1-4. Centriole duplication involves seven essential proteins in higher eukaryotes. 22

Figure 1-5. A cartoon diagram of the Nuclear Pore Complex illustrates how exported mRNA interacts with the cytoplasmic fibrils. 27

Figure 2-1. Dynein intermediate chains contain conserved dynein light chain binding motifs near the amino terminal coiled-coil domain. 46

Figure 2-2. The structure of Dyn2 in complex with Pac11 pep2 shows a Dyn2 dimer bound to two Pac11 pep2s that form the end β-strands on two antiparallel β-sheets formed within the core of the Dyn2 dimer. 48

Figure 2-3. The crystal structure of Dyn2 in complex with Pac11 pep2 shows an extensive hydrogen bonding network that involves backbone/backbone β-strand interactions as well as involvement by the residue side chains..... 51

Figure 2-4. Dyn2's ability to dimerize and bind Pac11 pep2 is abrogated through key mutations..... 53

Figure 3-1. Lc8 interacts with two Ana2 peptides with an exothermic binding mode but exhibits different affinities..... 67

Figure 3-2. The crystal structure of the Lc8-Ana2 pep1 is a 2:2 complex formed by an Lc8 homodimer binding two Ana2 pep1. 70

Figure 4-1. *S. cerevisiae* Dyn2 is a conserved dynein light chain involved in diverse macromolecular complexes including the nuclear pore complex and the cytoplasmic dynein motor complex..... 81

Figure 4-2. Structure of the Dyn2-Nup159 pep2 complex shows a quaternary complex composed of a Dyn2 dimer, bound to two Nup159 pep2 peptides through parallel, composite □-sheets..... 84

Figure 4-3. Dyn2 homodimerizes via an extensive network of van der Waals contacts and hydrogen bonds..... 86

Figure 4-4. Dyn2 binds substrates through a highly conserved, positively charged composite groove formed by Dyn2 dimerization. 88

Figure 4-5. The Dyn2:Nup159 pep2 interaction is mediated by an extensive interaction network that recognizes ten contiguous Nup159 residues, dually conferring specificity and substrate plasticity. 90

Figure 4-6. The Dyn2 interaction with Nup159 pep2 and pep4 occur in a 1:1 stoichiometry, and exhibit similar affinities but differ in their thermal binding modes..... 91

Figure 4-7. Crystallographic contacts array Dyn2 dimers linearly in an arrangement that affords polarized binding to arrayed Dyn2 binding motifs. 93

LIST OF SUPPLEMENTAL FIGURES

Supplemental Figure 2-1. Pac11 pep2 does not bind to Dyn2 H58K or Dyn2 F76K/Y78E as measured by ITC..... 61

Supplemental Figure 3-1. Ana2 peptide ITC controls were necessary to determine the peptide contribution to the overall heat of dilution in each injection. 74

Supplemental Figure 4-1. The dynein light chain is highly plastic with regard to target peptide binding. 99

LIST OF ABBREVIATIONS

AAA+ Family= ATPases Associated with various cellular Activities Family

ATP = Adenosine Triphosphate

DID = Dynein light chain Interacting Domain

FG = Phenylalanine-Glycine

GST = Glutathione S-Transferase

HC = dynein heavy chain

IC = dynein intermediate chain

ITC = Isothermal Titration Calorimetry

KD = knock down

LB = Luria Broth

LC = dynein light chain

LIC = dynein light intermediate chain

LIS1 = lissencephaly 1

MTBD = microtubule binding domain

NPC = nuclear pore complex

PDB = protein data bank

RMSD = Root Mean Square Deviation

SEC-MALS = Size Exclusion Chromatography and Multi-Angle Light Scattering

WT = wild type

CHAPTER 1

INTRODUCTION

The benefit of a ubiquitous scaffolding protein

In many cases separate proteins with the same or similar function evolved to act in specialized, and often highly regulated functions, such as separate kinases evolving to differentially distinguish protein targets for phosphorylation (Manning, 2002). There is a benefit to having one ubiquitous protein that can accomplish the same function in multiple cellular locations. Ubiquitous proteins do not use as much genetic space as having two separate proteins with the same function, and do not require as much regulatory support for proteins that are not subject to rigorous regulation scrutiny. All of these assumptions are contingent on the ubiquitous protein binding with the same mode in different cellular contexts or having some flexibility in binding.

In the case of scaffolding proteins, their function is to optimize the effectiveness of another protein by providing the opportunity to form a stable complex of two or more proteins so that binding avidity is increased. Additionally, scaffolding proteins often do not have a significant catalytic or biochemical function, but are often the subject of regulation due to their allosteric control of a functional complex (Good, 2011).

The ability for a protein to interact with another copy of itself, or homodimerize, is necessary for proper function in many cases, and there are a few mechanisms for how the process of dimerization can occur. Dimerization often occurs through two specially formatted

α-helical domains that come together to form a coiled-coil. Coiled-coils require a specific heptad pattern in the amino acid sequence to stabilize the intra-, and inter-helix interactions (Zhou, 1992; Marsden, 2010). Some proteins contain the amino acid sequence pattern for a coiled-coil, but the coils are not long enough for specificity in an exclusive dimerization partner (Marsden, 2010). In cases such as this a scaffolding protein may provide enough specificity or stability for the coiled-coil to satisfactorily dimerize into a fully functional complex. Short coils have also been shown to convert from an α-helical to a β-strand form; a transition that is dependent on certain sequence cues, temperature, and peptide concentration (Aposolovic, 2010; Kammerer, 2006). This transition to β-strands may not be intentional (as in the case of amyloid formation in neurodegenerative diseases), but may provide flexibility as a gain-of-function interaction site for protein-mediated dimerization.

Coiled-coil domains are sufficient for dimerization in some cases but specific patterns and longer amino acid chains are required to accomplish a dimer than a β-strand-β-strand interaction between a β-sheet and target protein β-strand (Su, 1994; Khakshoor, 2010). Su et al. determined that at least three heptad repeats (21 residues) are necessary for forming a stable two-stranded α-helical coiled-coil, and five heptad repeats (35 residues) are optimal for stabilizing length (Su, 1994). Some coiled-coils successfully form obligate dimers that only function properly when they are homodimerized as is the case for cytoskeleton motor proteins like cytoplasmic dynein and kinesins that are not processive as monomers (Peckham, 2011).

We propose that the dynein light chain, Lc8/Dyn2, acts as a protein mediator to assist in dimerization, which in turn strengthens a weakly interacting dimer. We hypothesize protein dimerization through scaffolding mediators such as Lc8/Dyn2 may provide a

platform for recruitment that might also allow for a point of regulation. Lc8/Dyn2's mediation may afford less dedicated peptide sequence for a target binding protein that would otherwise rely on a coiled-coil for dimerization, and it may provide greater specificity for forming a homodimer than a coiled-coil of the same length.

The objective of this thesis is to investigate structural and biochemical properties of Dyn2/Lc8 across diverse systems: the dynein motor, centrioles, and at the nuclear pore. These assays will be used to distill the common function of dimerization, as well as to highlight differences between Dyn2/Lc8's interactions in these systems. The remainder of the introduction will present the three systems: 1) the microtubule cytoskeleton and its motor proteins, specifically dynein, 2) centriole structure and duplication, and 3) the structure and functional regulation of the nuclear pore complex.

Lc8/Dyn2 is ubiquitously expressed, and a promiscuous protein

Lc8/DYNLL/Dyn2 was originally characterized as a dynein light chain by King et al. due to its ability to co-purify and immunoprecipitate with cytoplasmic dynein (King, 1996). In fact, only about 30% of Lc8 in rat brain tissue is tightly associated with cytoplasmic dynein (King, 1996), so the other 70% is presumed to interact transiently with cytoplasmic dynein or in the cytosol. As with Dyn2, the higher dynein light chain orthologs, LC8 and DYNLL, bind partners outside of binding to the dynein intermediate chain and a dynein light intermediate chain, including the signaling molecules nNOS and Pak1, the apoptosis regulator Bim/Bmf, the myosin Va motor, and the mRNA localization protein Swallow (McCauley, 2007; Lightcap, 2008; Espindola, 2000; Benison, 2007).

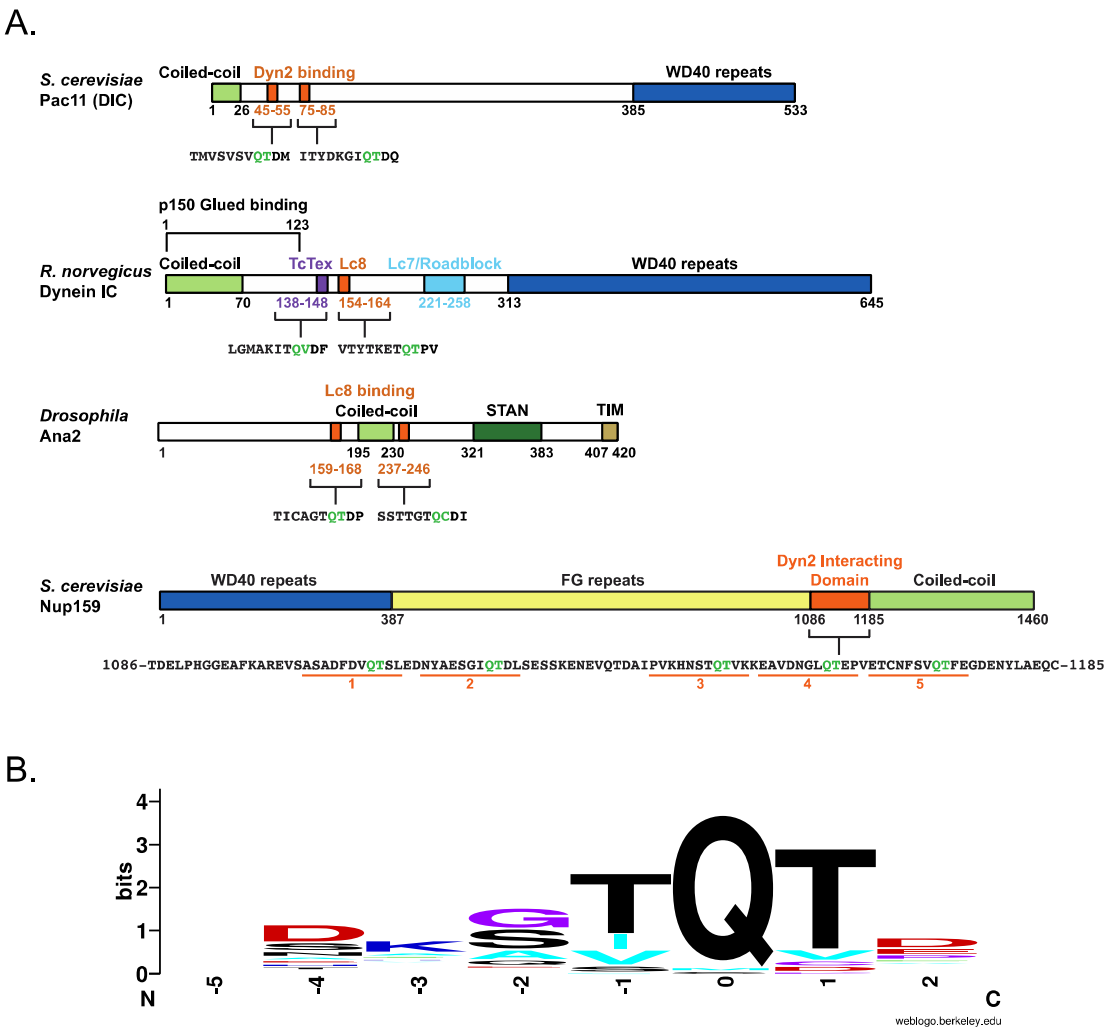

Figure 1-1. Dyn2/Lc8 binds to proteins with coiled-coil domains and a QT motif.

A. Dyn2 binds to the *S. cerevisiae* dynein IC, Pac11, in two locations in the central portion of the protein. There is an N-terminal coiled-coil (all light green) and a C-terminal WD40 motif (all dark blue) with much of the remaining central structure predicted to be unstructured. The IC from rat also contains an N-terminal coiled-coil (resi. 1-70), and C-terminal WD repeat domain that is responsible for interaction with the heavy chain (McKenney, 2011; Ma, 1999). The N-terminal coiled-coil also corresponds to the dynactin, p150 binding site (resi. 1-123) (Vaughan, 1995). Mammalian IC also contain binding sites for the three types of dynein light chains: TcTex (resi. 138-148; purple), Lc8 (resi. 154-164; all orange), and Lc7/Roadblock (resi. 221-258; cyan) (Williams, 2007; Hall, 2010). There are two Lc8 binding sites within Ana2 that bookend the predicted coiled-coil region (resi. 195-230). Ana2 also contains two motifs that show unique sequence conservation among the STIL/Ana2/Sas-5 family called STAN (for STil/ANa2; dark green) and TIM (for truncated in microcephaly; tan). The final Dyn2 binding protein is Nup159, which shows an N-terminal WD40 motif, a central domain composed of FG repeats (typical of nuclear pore proteins; yellow), the Dynein light chain interacting domain (DID) contains five Dyn2 binding sites, and a C-terminal coiled-coil. **B.**

Sequence conservation of 45 Dyn2/Lc8 natural binding sites includes 41 from Rapali, 2011 and the Pac11 and Ana2 binding sites. Sequence homology is colored according to the following amino acid code; RHK (blue), DE (red), FYW (green), AVILM (cyan), STNQ (black), and CGP (purple).

Lc8/DYNLL/Dyn2 is also a promiscuous protein, involved in a diversity of protein interactions, in a number of different cellular contexts. The binding motifs for the light chain orthologs have been widely debated due to a number of sequence and binding mode exceptions (Rapali, 2011; Benison, 2007; Radnai, 2010). In *S. cerevisiae*, Dyn2 interacts with the dynein intermediate chain, Pac11, through tandem canonical 10-12 residue stretches, each containing a conserved QT motif (Fig. 1-1A) (Stuchell-Brereton, 2011). Many authors recognize the Lc8 binding motif has a high probability of a glutamine followed by a threonine/valine (Fig. 1-1B). There are, however a number of binding interactions where Lc8 does not utilize this motif, such as p21 activated kinase 1 (Pak1) that contains a divergent serine then proline at the QT positions in the binding cleft (Lightcap, 2008). As of 2011, Rapali et al. reported 41 naturally occurring Lc8 binding motifs and most of the candidates also contained a separate dimerization domain, such as a coiled-coil (Rapali, 2011).

Lc8 is capable of not only binding very diverse sequences, but it is also promiscuous in its binding mode, being able to utilize an exothermic or endothermic interaction in some cases. An exothermic binding mode is more commonplace for Lc8 and many other proteins because it indicates the formation of an extensive hydrogen-bonding network to overcome the entropic penalties. Lc8 is capable of binding endothermically, as in the case of nNOS (Nyarko, 2011), which likely indicates an entropic consolidation of hydrophobic surfaces and rearrangement of structural waters (Lumry, 1970; Eftink, 1983). A protein that is capable of binding a target motif through an exothermic motif, or an endothermic motif if necessary

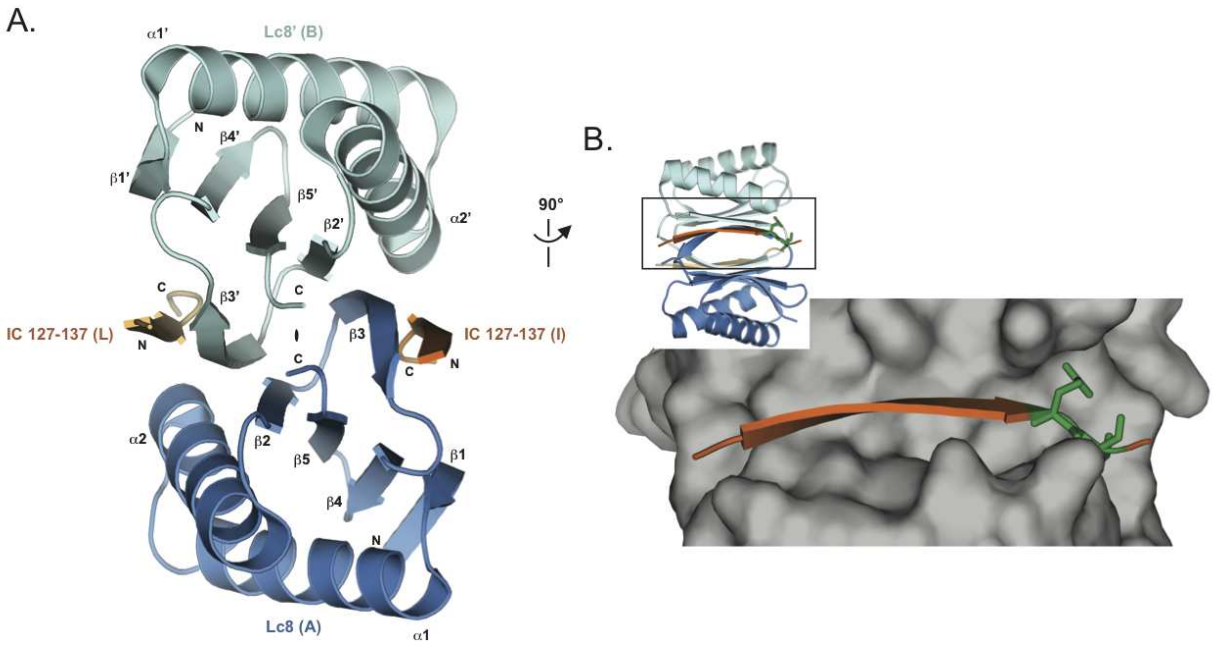

Figure 1-2. Structure of the *Drosophila* Lc8 in complex with the rat dynein IC shows an Lc8 dimer bound to two IC β-strands by two parallel β-sheets.

A. A cartoon diagram of the Lc8-IC crystal structure shows a quaternary structure of Lc8 dimerized in blue (chain A) and cyan (chain B) with two IC β-strands (residues 127-137) in dark (chain I) or light orange (chain L). There is a two-fold non-crystallographic rotational symmetry operator indicated in the z-axis between the two parallel β-sheets composed of five anti-parallel β-strands arranged β1-β4-β5-β2-β3'. Two α-helices from each monomer are arranged on top and bottom of the β-sheet sandwich that is peripherally bound to the IC through β-strand-β-strand interactions. **B.** The Lc8 dimer is turned 90° from A. and displayed in surface (gray) to show the zoomed in Lc8 binding pocket. IC (dark orange) binding residues show the wide binding pocket with few steric restrictions. The conserved Q135 and T136 are shown in green sticks to highlight their location near the end of the binding pocket. Figure made with pdb 2PG1 (Williams, 2007).

allows a protein to be more flexible in the selected binding partners, and therefore more promiscuous.

The regulation of Lc8 binding to a number of different partners occurs through a common mechanism of phosphorylation. Although this phosphorylation event has only been characterized as affecting Bim in the apoptosis pathway (Benison, 2009; Song, 2008), it is believed that phosphorylation is used to control Lc8's ability to homodimerize, and therefore

mediate dimerization of target proteins. Previous work has shown that Lc8 is phosphorylated on Ser88 by p21-activated kinase (Pak1), although the specific kinase utilized is hotly debated (Song, 2008; Benison, 2009). Song et al. used an S88E phosphomimetic mutation to show that phosphorylation at this specific Ser88 dissociates the Lc8 dimer and abolishes Lc8's ability to bind Bim (Song, 2008).

Lc8 is composed of five β-strands that form an anti-parallel β-sheet with two α-helices on one face (Fig. 1-2A). Lc8 homodimerizes and forms two parallel β-sheets that are sandwiched by the outer α-helices. One β-strand from each monomer completes the other monomer's sheet and forms an anti-parallel β-strand interaction with the peptide that binds each monomer of Lc8 (Williams, 2007; Benison, 2007; Fan, 2001; Lightcap, 2008). It is therefore remarkable that Lc8 binds many different targets with different thermodynamic binding modes through the same binding cleft (Fig. 1-2B).

While studies to date have biophysically characterized the Lc8/DYNLL, dynein light chains from *Drosophila*, rat, and human, molecular and biophysical details of the *S. cerevisiae* Dyn2 have remained outstanding. *S. cerevisiae* is a leading model system for biophysical, biochemical and genetic investigations of the nuclear pore complex and the cytoplasmic dynein motor complex.

Lc8/DYNLL/Dyn2 interactions that are independent of the dynein complex illuminate a role as a dimerization machine

Ubiquitous Lc8/DYNLL/Dyn2 has been structurally characterized as binding to a variety of targets independent of the dynein complex, such as neuronal Nitric Oxide Synthase (nNOS) (Chaudhury, 2008), Anastral spindle 2 (Ana2) (Wang, 2011), and a nuclear pore

protein (Nup159) (Stelter, 2007). There are even a few species of algae and flowering plants, such as *Arabidopsis*, that do not contain the dynein motor, but maintain the Lc8 homolog of the dynein light chain (Wickstead, 2007). Since only about 30% of Lc8 is tightly associated with cytoplasmic dynein (King, 1996) and some species do not contain other dynein complex proteins (Wickstead, 2007) it is probable Lc8 acts in a greater capacity than just as a scaffolding protein for the dynein motor complex.

Evidence suggests that although other dynein associating factors can act independent of the dynein motor, such as another dynein light chain, TcTex, which remodels actin in neurite outgrowth (Chuang, 2005), many of their characterized functions indirectly affect the dynein motor. A number of proteins that have been shown to interact with Lc8/DYNLL are assumed to also interact with the dynein complex such as Bim (Puthalakath, 1999), Bmf (Day, 2004), and Gephyrin (Fuhrmann, 2002). We challenge these presumed interactions due to the lack of experiments exclusively showing the importance of the dynein motor in these interactions, and a few experiments showing the converse; that the dynein motor domain is not always included in associating factor functions.

Although *lc8Δ*/*dyn2*Δ does not have a strong phenotype, the deletion phenotypes of the proteins with which Lc8/Dyn2 interacts at the dynein motor complex have more severe deletion phenotypes (*Pac11*/*DIC*, *STIL*/*Ana2*, *Nup159*) (Stuchell-Brereton, 2011; Arquint, 2012; Gorsch, 1995). *pac11Δ* in *S. cerevisiae* shows an inability to move the nucleus into the budding cell for proper cell division (Stuchell-Brereton, 2011). In 60% of *STIL*-depleted U2OS cells there were fewer than two centrioles, which supports that STIL/Ana2 is necessary for centriole duplication (Arquint, 2012). In the final example, Nup159 is an essential nuclear pore protein that when deleted or mutated in *S. cerevisiae* causes an

accumulation of poly(A)+ RNA in the nucleus (Gorsch, 1995). These strong phenotypes in a variety of cellular processes draw attention to the importance of having functional binding interactions with Dyn2/Lc8 to ensure optimal processing in the aforementioned contexts.

Given the diverse set of dynein light chain binding partners, both at the dynein complex and independent of the complex, it has been postulated that the dynein light chain functionally serves as a dimerization machine. This role correlates with the structures of higher Dyn2 orthologs that show dynein light chains complexed 2:2 with a variety of target peptides (Lightcap, 2008; Fan, 2001; Williams, 2007; Benison, 2008; Wang, 2003). In this study we aim to further our structural and biophysical understanding of Dyn2/Lc8 to derive a model for Dyn2's role as a dimerization machine.

Motors of the cytoskeleton

The cytoskeleton is a network of proteins involved in cell organization, cell motility, internal cellular restructuring, and division. In eukaryotes there are two protein polymers that form polar cellular tracks for the various cellular functions; actin and tubulin. Like tubulin, actin is important in forming networks across the cytoplasm for signal transduction, cellular movement, and the movement of cargos intracellularly. Actin forms a single filament composed of two strands unlike tubulin's unique, hollow tubes of typically 13 protofilaments, called microtubules, which can then interact with a host of proteins for force generation and cargo transport. Actin contains a single class of motor proteins, called non-muscle myosins that are able to move long distances along a single actin filament (Mehta, 2001). There are two microtubule families of motor proteins that facilitate aspects of force generation and cargo transport. The kinesin family of proteins moves toward the plus end

direction of microtubules (with the exception of kinesin 14 family members) with many different types of kinesins thus delineated because they perform different tasks. The cytoplasmic dynein complex is a 1.2 MDa multifunctional motor protein that processes toward the minus end of microtubules with great importance in cell division, intracellular organelle transport and organization, and delivery of cargos across great distances within a cell (Nyarko, 2004). It is believed that dynein can accomplish such a great variety of tasks through the presentation of different scaffolding and regulatory proteins, called associating factors. Kinesin, however, has several different proteins to accomplish the various plus end directed functions that a single cytoplasmic dynein can accomplish with its associating factors. All three families of cytoskeletal motor proteins utilize ATP hydrolysis to generate force for their various functions, but myosin (such as the 119 kDa *Dictyostelium* Myosin-1B) and kinesin (such as the approximately 400 kDa Kinesin-1 complex) are much smaller and simpler than the comparative behemoth, dynein (1.2 MDa cytoplasmic complex) (Mooseker, 1995; Kull, 2000; Nyarko, 2004). While much is known about kinesin and myosin family members, far less is known about structure and regulation of the dynein motor and dynein regulators.

In vitro experiments of cytoplasmic dynein and kinesin have aided in our understanding of force generation and how these motors might work together to deliver cargos *in vivo*. Unlike kinesin's regular 8 nm steps along a single microtubule protofilament, dynein primarily takes 8 nm steps, but it has the ability to take 4 to 24 nm steps and can switch protofilaments (Gennerich, 2007; Reck-Peterson, 2006). This flexibility in dynein's step size is likely afforded by the inherent flexibility in dynein's dimerization domain that acts like a lever arm, whereas kinesin's linker domain is much shorter and not as flexible as a

lever arm (Vale, 2003). Under the load of a cargo, cytoplasmic dynein was additionally shown to have the ability to take steps backward (toward the plus end) in the presence of ATP, and even to take forward and backward steps in the absence of ATP hydrolysis (Gennerich, 2007). A WT stall force of 4.5 pN was measured for a single yeast motor (Gennerich, 2007), although yeast dynein has a slower measured velocity and lower dissociation rates as compared to other species of dynein (Cho, 2008). A number of studies aim to measure the cumulative possible velocity and capable force of multiple motors on a load (Gross, 2002; Hendricks, 2010; Leidel, 2012) to better understand how cargos might transport *in vivo*. There are two possible models for how dynein and kinesin might work tethered to the same cargo. Dynein and kinesin can either coordinate their movement, which would imply that one set of motors does not function during a given translation, or dynein and kinesin ensembles can have a tug-of-war, where the winner dictates the direction of movement (Bryantseva, 2012). Although *in vivo* evidence for either model is slim, it appears as though the two models work in concert, with some cargo-bound motors being more weakly bound to the microtubule than others (Bryantseva, 2012). Some of the dynein associating factors are also capable of binding kinesins, such as the p150 subunit of dynactin, so it is possible that the associating factors could provide mediation to coordinate dominance of motors. Many *in vitro* studies of dynein are done in the absence of regulatory associating factors that are also predicted to have a great impact on velocity, processivity, and possibly even force generation.

The structure of processive kinesin

The kinesin motor is comprised of a heavy chain that homodimerizes to form a functional motor, which can process toward the plus end of microtubules with invariant 8 nm steps. The heavy chain contains an approximately 30 kDa globular motor domain that contains the highly conserved microtubule-binding site and catalytic site. Kinesins contain a coiled-coil, or stalk, for dimerization, and a tail that binds to the light chain scaffolding protein (Sack, 1999). The kinesin family can be divided into groups based on the organization of these three domains within the peptide, although the structural folds within the catalytic head domains are invariant (Endow, 2010). The tail has been less well characterized in kinesin, however, the kinesin light chain bound to the tail mediate binding to vesicles and organelles.

In classic kinesin, three distinct light chains (KLC) have been reported, and are the result of alternative gene splicing. It is hypothesized that the three light chain isoforms provide functional differences for the specialized roles necessary for kinesin (Cyr, 1991). Recently, the crystal structures and specific binding interactions were solved to elucidate the differential binding properties of cargo selectivity for the KLC1 and KLC2 tetratricopeptide repeats binding a kinesin cargo, JIP, (Zhu, 2012). Although kinesin light chain's mechanism for binding cargos has not been fully worked out, it is clear that the three isoforms utilize their tetratricopeptides to connect to cargo, unlike dynein's many different scaffolding proteins binding with different modes.

Cytoplasmic dynein structure

Cytoplasmic dynein in metazoans is composed of a catalytic homodimer of heavy chains (HC), and a number of non-catalytic subunits; two dynein intermediate chains (IC), three light intermediate chains (LIC), and three light chains (LC) (Fig. 1-3B). In fungi, such as *S. cerevisiae*, there are only three reported non-catalytic subunits that are canonical dynein components: the intermediate chain, Pac11, a light intermediate chain, Dyn3, and a light chain, Dyn2. Dynein also binds to other non-canonical associating factors such as the dynactin complex, lissencephaly 1 (LIS1)/Pac1, and the RZZ complex (Rod, Zwilch, Zw10) to regulate processivity and contribute to function. The absence of the dynactin or LIS1 components by depletion phenotypically copies the loss of dynein function (Kardon, 2009), therefore these associating factors provide an essential component to dynein *in vivo*.

Structure of the dynein heavy chain

The heavy chain of cytoplasmic dynein is composed of an amino terminal (N-terminal) dimerization domain that is a predicted coiled-coil, and a carboxy terminal (C-terminal) motor domain (Fig. 1-3A). The N-terminal domain of dynein is predicted to contain the binding sites for the canonical associating proteins. In rat, cytoplasmic dynein binding sites for IC, LIC 1 and 2 binding to the HC were identified to have partial overlap but distinct binding regions using a series of co-immunoprecipitation experiments (Tynan, 2000). These experiments were found to corroborate mapping of the HC binding sites on *Dictyostelium* with a 72% homologous region between *Dictyostelium* and rat (Habura, 1999). It has also been shown through alignments that even some of the most divergent fungal species show high conservation in this particular region of the dynein HC, but the sequence by itself is not sufficient for HC dimerization (Habura, 1999). Although a great deal has recently been

discovered about the dynein motor structure and possible mechanism, there have not been significant studies on the role that the dimerization domain of the HC plays in coordinating dynein associating factors.

The motor domain of dynein is composed of six ATP binding domains (although only four of six are actually capable of binding ATP) that are concatenated in a single polypeptide, thus making dynein a unique member of the ATPases Associated with various cellular Activities (AAA+) family. Recently, the crystallographic structure of the motor domain of the cytoplasmic dynein heavy chain in *Dictyostelium* was solved to 2.8 Å (Kon, 2012) and in *S. cerevisiae* to 3.3 Å resolution (Schmidt, 2012). Both of these structures are high enough resolution that peptide backbone and side chains can be more accurately determined than previous structures. These two structures allow for a better understanding of the organization of the dynein motor ring, as well as a more complete prediction of the motor mechanism. As previously mentioned, the first four AAA domains of the dynein motor contain sequence motifs necessary to bind and hydrolyze ATP, while the final two AAA domains are highly divergent and believed to provide more of a structural role (Cho, 2008). AAA1 is shown to be the main hydrolysis site because mutations at this site in the Walker A or Walker B motif abolish motility and decrease overall ATP turnover (Kon, 2004; Cho, 2008). The microtubule binding domain (MTBD) is an extension of AAA4 and contains the globular head that makes contact with the microtubule, as well as a coiled-coil stalk which shifts the registry in order to complete the ATP hydrolysis communication from the ring into the MTBD (Carter, 2010; Kon, 2011). Recent publications show the importance of the stalk of the MTBD, the AAA5 strut contacting the stalk, and the linker domain that folds over the ring to communicate the

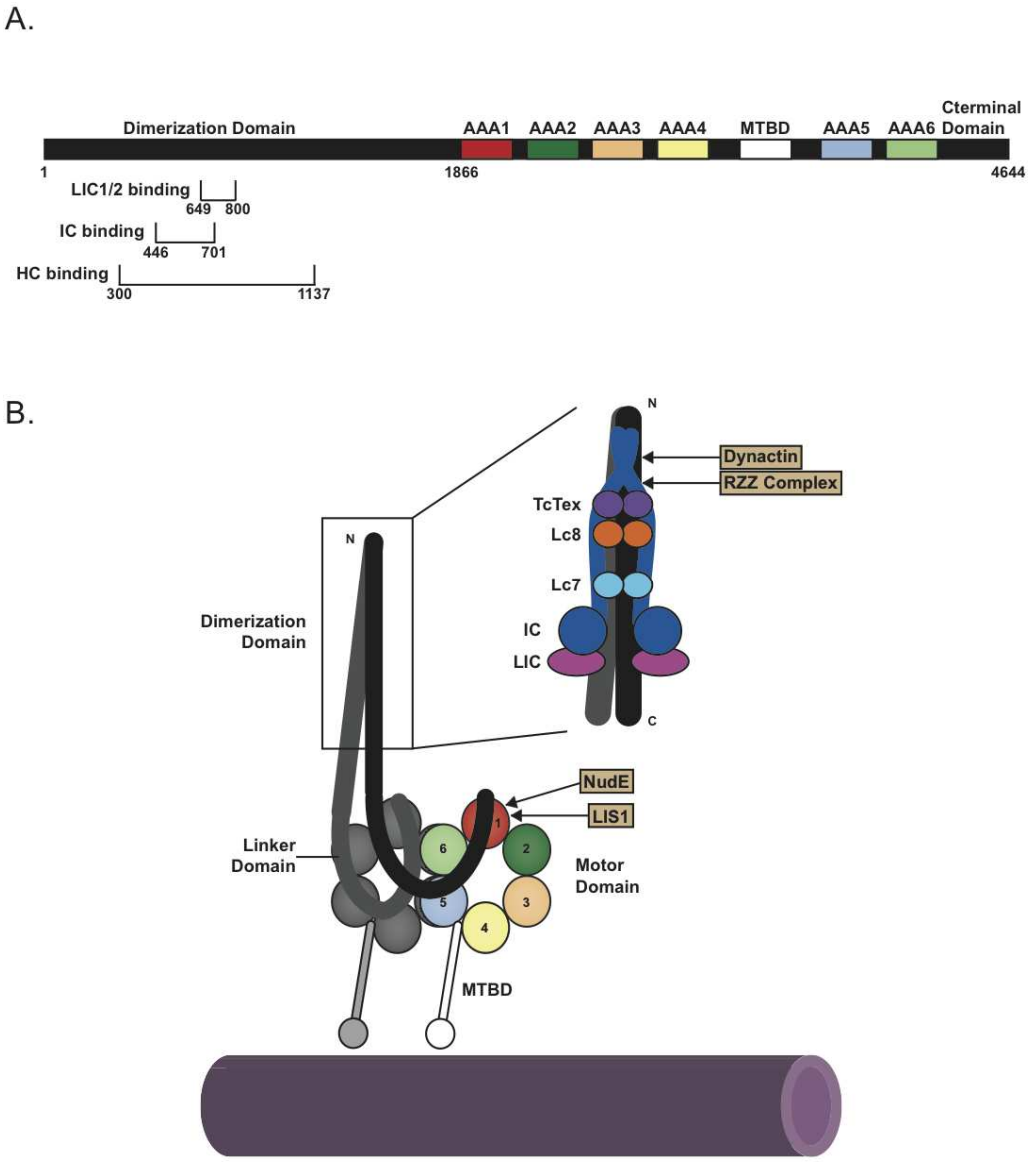

Figure 1-3. Cartoon of the dynein holoenzyme shows how all of the canonical dynein associating factors interact at the N-terminus of the DHC.

A. The domain arrangement of the dynein heavy chain contains an N-terminal dimerization domain with binding sites for LIC1 and LIC2, IC, and the HC (residue numbers for rat; Tynan, 2000). The motor domain contains six concatenated AAA domains with a microtubule binding domain (MTBD) between AAA4 and AAA5. **B.** A cartoon of the canonical dynein complex shows a ring of AAA domains with the MTBD protruding between AAA4 and AAA5 to bind the microtubule. The N-terminal linker folds over the ring in different conformations depending on the ATP hydrolysis state of the motor. The dimerization domain zoom shows a cartoon of how the dynein LCs (purple, orange, light blue), LIC (pink), and IC (dark blue) might bind along the shaft of the dimerization domain. Tan boxes point to locations where other dynein associating factors interact with the dynein holoenzyme to regulate dynein. This figure is based on Kardon, 2009.

ATP hydrolysis through the ring and into the MTBD (Carter, 2008; Carter, 2011; Kon, 2011; Kon, 2012; Schmidt, 2012).

Structure of the canonical cytoplasmic dynein associating factors

Although a full length structure of a dynein intermediate chain has not been published, the domain structure and binding sites for other dynein associating factors have been determined using sequence analysis and biochemical assays (Stuchell-Brereton, 2011; Benison, 2007; Makokha, 2002; Williams, 2007; Hall, 2009). The very N-terminal portion of the IC contains a short, predicted coiled-coil (Makokha, 2002) and also contains the p150, dynactin subunit, binding site (Vaughan, 1995). The IC N-terminal domain follows an inherently disordered domain that gains structure upon binding to Lc8 (Nyarko, 2004), and contains binding sites for the other two LCs. The two light chain-binding sites for human TcTex and Lc8 were determined by x-ray crystallography to form a β-strand-β-strand interaction with the backbone of IC (Williams, 2007; Benison, 2007). The third LC that binds to the central domain of the IC, Lc7/Roadblock, interacts with two α-helices from the IC to form the binding site (Susalka, 2002; Hall, 2010). The final C-terminal domain of the IC contains seven WD-repeat motifs (Susalka, 2002;) predicted to form a β-propeller (Garcia-Higuera, 1996), which then binds to the dynein heavy chain (Ma, 1999).

The LICs of dynein are isoforms of a single gene that undergoes differential phosphorylation and alternative splicing to form two cytoplasmic proteins (Hughes, 1995). Sequence analysis has shown that there appears to be no significant relationship between the LICs and the LCs, nor are there regions of predicted α-helical, or β-sheet secondary structure in the LICs (Hughes, 1995). The N-terminal domain of LIC contains a P-loop consensus sequence, which is used for binding nucleotides, and this putative ATP hydrolysis domain

also shares some homology with the ABC transporter family (Hughes, 1995). Although there is not very much known about the LIC's function, its sequence homology with the ABC transporter family indicates LIC may bind and hydrolyze ATP (Mische, 2008). Mutations in the putative ATP-binding residues of *C. elegans* LIC (*dli-1*) have shown complete rescue of function, indicating that ATP hydrolysis is not necessary for LIC's function (Yoder, 2001).

In addition to Lc8/Dyn2 there are two more dynein light chains, Lc7/Roadblock and TcTex have similar secondary structural elements to Dyn2/Lc8, but Lc7's secondary structure is a different fold, and they all have little sequence homology with each other. The light chains are thus named because they are less than 10 kDa on average, and are all non-catalytic subunits. The Lc7/Roadblock structure in humans (Ilangovan, 2005), mouse (Song, 2005), and *Drosophila* (Hall, 2010) were all shown to contain five β-strands that homodimerize to form one contiguous β-sheet with each monomer contributing two peripheral α-helices on either side of the β-sheet. The IC binds Lc7 with two amphipathic helices laid across the β-sheet and forms interactions throughout the molecule (Hall, 2010). The final category of dynein LC, TcTex, shares 1.6 Å RMSD strucutural homology with LC8, but is very divergent in sequence with almost no homology (Williams, 2005). TcTex binds non-overlapping sequences on target proteins in the same β-strand-β-strand interaction mode as Lc8 where each monomer binds a peptide along the midline β-sheet. TcTex, like Lc8, contains five β-strands and two α-helices that are arranged in the same fashion as Lc8 except that the central β-strands and α-helices are much longer (Williams, 2005; Williams, 2007). Although the three categories of dynein LC are structurally different and bind targets differently, they all share similar folds that incorporate a β-sheet with peripheral α-helices.

Function and regulation of the dynein holoenzyme

Dynein's role in vivo

Cytoplasmic dynein has a variety of roles that are instrumental in cell movement, division, and intracellular transport of cargos. One of dynein's primary roles in metazoans is in organelle transport such as movement of the Golgi apparatus (Corthesy-Theulaz, 1992; Holzbaur, 1994), lysosomes, and endosomes (Lin, 1992). For many of the larger organelles there are several dynein motors attached at any one time, which serves the role of overcoming the stall force for a single dynein motor, and to keep the organelle processively moving along the microtubule track (Bryantseva, 2012). The dynein complex has also been implicated in transport of vesicles, viruses, and packaged mRNA through LC mediation (Holzbaur, 1994; Vallee, 2004). It is not yet clear how dynein is specifically targeted to transport these particular cargos.

Dynein is also responsible for positioning the chromatin in metaphase and plays a role in inactivating the spindle assembly checkpoint, which allows a cell to progress into anaphase (Bader, 2010). This role at kinetochores involves a number of associating proteins to sense and attach dynein to ingressing microtubules. Pools of dynein are also concentrated at the spindle poles and cell cortex during mitosis to assist in positioning the astral microtubules of the spindle (Busson, 1998). In *S. cerevisiae*, dynein's sole responsibility is to position the mitotic spindle in the budding yeast so that the mother and daughter cells have proper DNA segregation (Eschel, 1993; Kahana, 1998; Moore, 2008). It is for this reason that many *in vivo* studies of cytoplasmic dynein utilize *S. cerevisiae* because dynein deletion cells are still viable (Geiser, 1997). The Cin8 pathway is synthetic with the PAC genes (perish in

the absence of Cin8) so the Kar9 and Cin8 pathways have some overlap with dynein and complete other functions typically associated with dynein in metazoans (Geiser, 1997).

Intermolecular regulation of the dynein motor domain

The dynein motor domain is internally regulated by AAA2-4 as well as by external adaptors that are crucial in adjusting the motor to its cellular function (Kardon, 2009). LIS1 is the only known associating protein to bind directly to the dynein motor domain. LIS1 binds directly between AAA3 and AAA4 to regulate communication between the catalytic motor and the microtubule-binding stalk, which prolongs dynein's interaction with the MT and thereby increases processivity (Huang, 2012; McKenney, 2010). It appears as though this LIS1 binding interaction is most important during high bearing loads like transport of nuclei, movement of kinetochores, and during high tension in the cytoskeleton (McKenney, 2010). NudE is also important in the high load interactions and to recruit LIS1 and dynein to kinetochores (Stehman, 2007). NudE, however, interacts directly with the IC and LIC to abrogate dynein force production (McKenney, 2010).

Dynactin is a 1 MDa complex that has a role in modulating nearly every function of dynein's behavior. In vitro experiments have shown that dynactin acts as a clutch for increasing dynein processivity (Kardon, 2009 PNAS). There are two microtubule-binding domains in the p150 subunits of dynactin that were thought to tether dynein to the microtubule to enhance processivity (Waterman-Storer, 1995). Mutant and deletion constructs of dynactin show that these microtubule-binding domains are dispensable and therefore not sufficient for increasing processivity (Kim, 2007).

Besides dynactin's function in increasing dynein's processivity, dynactin has also been reported to play a role in linking dynein to cargo (Holleran, 2001; Watson, 2005).

Interactions through the p150 subunit as well as the ARP1 scaffolding subunit both mediate interactions between dynein and cargo (Kardon, 2009). The ARP1 subunit directly interacts with a protein on the cytosolic surface of the Golgi, βIII spectrin, in the process of dynein-dynactin mediated vesicle trafficking from the endoplasmic reticulum (Holleran, 2001). The p150 subunit not only binds to ARP1 and the dynein IC, but also to a number of microtubule plus end binding proteins such as EB1 and CLIP170 to target dynein to stably congress at microtubule plus ends (Hayashi, 2005; Hayashi, 2007). Dynein's binding interactions with non-canonical proteins not only have the ability to modulate dynein's behavior, but more importantly they alter dynein's functionality in attachment and delivery of specific cargos during certain times.

Through biochemical and structural studies we are gaining more insight as to how the dynein motor domain is organized and functions to promote motility *in vitro*, but there is still a great deal to learn about how this molecular machine selects and attaches to cargos for its *in vivo* functions. One hypothesis for dynein targeting cargos in fungi is that dynein is targeted to the plus ends of microtubules through the LIS1/NudE interaction or through the dynactin interaction to probe the cytoplasm for cargos as microtubules cycle through dynamic instability (Kardon, 2009). The mechanism for dynein targeting cargos in metazoans is less clear.

Lc8/Ctp interacts with Ana2 on centrioles

Centriole duplication is a cell cycle-regulated process that plays a vital role in ensuring a cell is able to properly segregate its genetic material during mitosis (Fig. 1-4). Improperly formed or over-duplicated centrioles can result in a number of cellular

aberrations that amount to disease states such as primary microcephaly, male sterility, and cancer (Kitagawa, 2011; Nigg, 2009). The process and regulation of centriole duplication has recently become a popular topic because it is poorly understood and has possible clinical implications in drug therapies.

Centriole structure

The structure of a centriole consists of a cylinder decorated by microtubule triplets with nine-fold radial symmetry; mature centrioles contain distal appendages that help assemble components to build the centrosome, the structure responsible for nucleating the bipolar mitotic spindle. The centrosome consists of a pair of centrioles: a mature ("mother" centriole), and a procentriole tethered by interconnecting fibers. A cloud of protein matrix, called pericentriolar material surrounds the centriole pair (Azimzadeh, 2011; Bornens, 2012).

During centriole duplication, the nucleating procentriole forms perpendicular to the original centriole at the proximal end. The first structure for nucleating a daughter centriole is a central hub that forms like a wheel spoke with nine-fold symmetry accompanied by microtubule triplets around the periphery (Azimzadeh, 2012; Brito, 2012; Nigg, 2011). The central cartwheel, at the proximal end of a procentriole, remains within the daughter to form the scaffold for the remainder of the barrel structure (Brito, 2012; Kitagawa, 2011). The microtubule triplets on the daughter centriole are then elongated around a central lumen to a specified length that is dependent on cell type and species (Schmidt, 2009; Tang, 2009).

Centriole biogenesis

Centriole biogenesis can occur by either nucleating a procentriole (daughter) off of an existing centriole (mother) during duplication, or centrioles can form *de novo* (Brito, 2012; Rodrigues-Martins, 2007). Although these two processes are distinct, they utilize a conserved

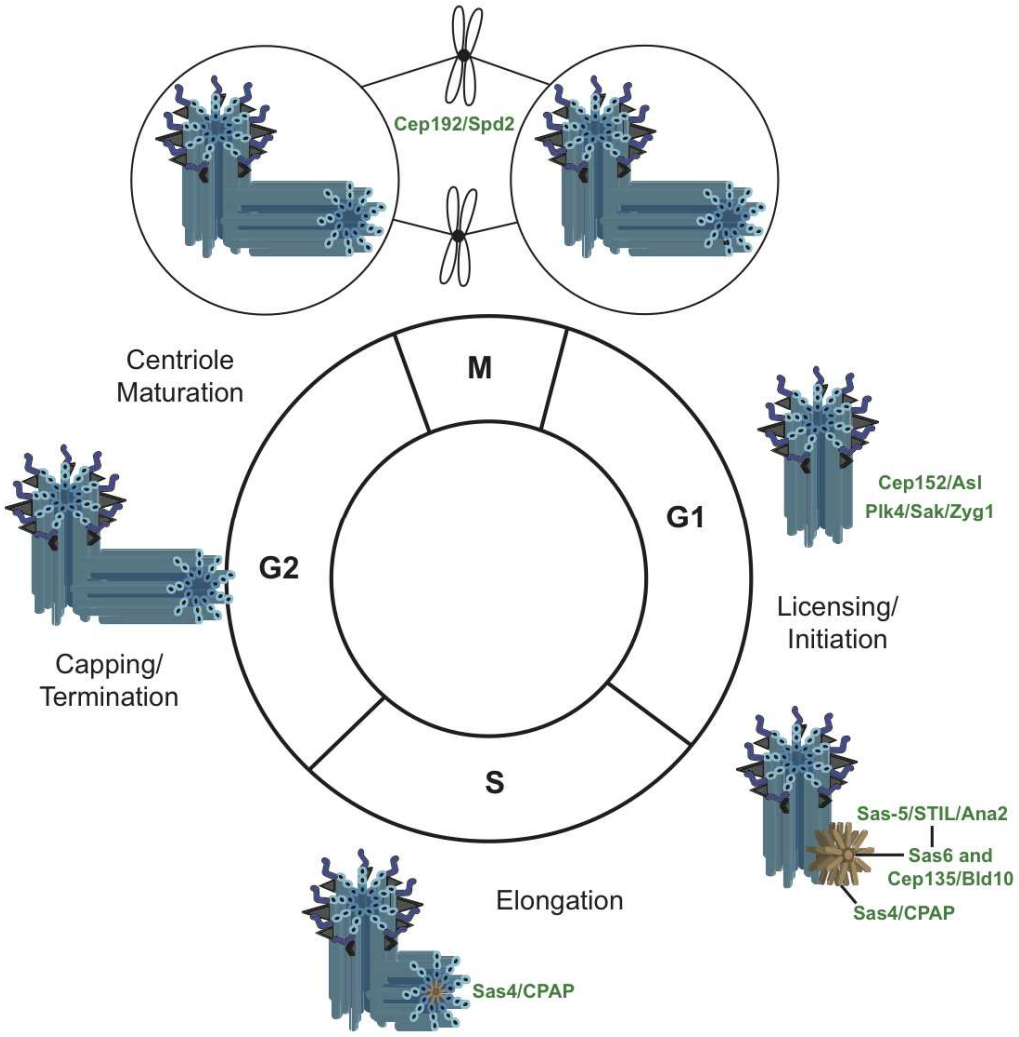

Figure 1-4. Centriole duplication involves seven essential proteins in higher eukaryotes.

In the end of G1/early S phase of the cell cycle the duplication licensing protein, Plk4/Sak/Zyg1 is recruited by Cep152/Asl to begin formation of the cartwheel with Sas4/CPAP (brown). Sas6 and Cep135/Bld10 accumulate at formation of the cartwheel, and Sas-5/STIL/Ana2 interacts with Sas6 to initiate a single daughter centriole. Sas4/CPAP also acts to stabilize newly formed centriole microtubules in the elongation phase of duplication. In the final phase of centriole duplication Cep192/Spd2 stabilizes mitotic microtubules to nucleate the spindle.

set of proteins to coordinate with the DNA replication cycle (Brito, 2012). The onset of centriole biogenesis coincides with late G1-phase when DNA is unwound to prime the replication machinery (Brito, 2012). There are three main phases of centriole duplication,

each of which contains opportunities for regulation: initiation/licensing, elongation, and capping/termination. The initial step of priming the centriole replication machinery is the onset of the licensing phase, which will commence assembling the daughter centriole cartwheel during the following S-phase of the cell. There are only a few proteins that are essential for centriole duplication including Cep152/Asl, Plk4/Sak/Zyg1, STIL/Sas-5/Ana2, Sas6, Cep135/Bld10, CPAP/Sas4, and Cep192/Spd2 (Vulprecht, 2012; Kitagawa, 2009). When any one of these seven proteins is deficient then centrioles duplicate irregularly or not at all. Although the cascade of proteins involved in the first steps appears to be hierarchical, the specific order of events and players is still poorly understood. The first known protein involved in the initial cascade is Cep152/Asl to recruit Plk4/SAK to centrioles and to act as a scaffold for CPAP/Sas4 to assemble or stabilize centriolar microtubules during the elongation phase (Carvalho, 2010; Stevens, 2010). Sas6 forms the initial cartwheel during initiation, and Sas-5/STIL1/Ana2 is a required Sas6 binding partner that is also required for controlling the number of procentrioles. The coiled-coil and C-terminal half of Ana2 is sufficient for binding to the N-terminal portion of Sas6 (Stevens, 2010).

When centrosome duplication is disturbed there is an increased incidence of genomic instability due to compromised segregation of chromosomes. Therefore, the number of procentrioles generated on a mother centriole and the number of rounds of centriole duplication are crucial to fidelity of balanced centrosome number (Nigg, 2011).

The second phase of assembly is the elongation of the daughter centriole from the cartwheel assembly, which occurs during S to G2 phase of the cell cycle. During this phase, initial microtubules are elongated using the γ-TuRC complex, and the other two microtubules within each triplet set utilize the stably nucleating microtubule as a template. There is an

unknown intrinsic property of the elongation machinery to make the daughter centriole a homogeneous length for the designated cell type and species, although post-translational modifications are suspected (Brito, 2012). The elongation machinery is also capable of distinguishing between daughter and mother centrioles with proteins like centrobin, so that only daughter centrioles elongate (Marthiens, 2012). Centrobin's recruitment to α-tubulin core components is dependent on Sas6, so centrobin is capable of distinguishing between centriole types due to the formation of the inner cartwheel (Gudi, 2011). In the absence of centrobin, 58% of cells show daughter centrioles with stunted growth (Gudi, 2011). Therefore, centrobin acts in the elongation/stabilization phase that is directly dependent on the proper assembly of Sas6 during initiation.

The final phase of centriole duplication is capping and disengagement of the newly matured centriole. A daughter centriole acquires distal and subdistal appendages that designate it as a fully matured centriole that is capable of replicating in future rounds of mitosis. During this final phase Cep192 targets AurA to mitotic centrosomes to assist in AurA oligomerization so that it can drive spindle microtubule assembly (Joukov, 2010).

The role STIL/Sas-5/Ana2 plays in centriole licensing and elongation

STIL is a large, cytosolic protein in human cells that shares significant homology with Ana2 (from *Drosophila*) and Sas-5 (in *C. elegans*) and is also thought to be their functional ortholog (Arquint, 2012; Stevens, 2010). There is a coiled-coil domain in the central region of each of the STIL/Ana2 family members that was shown to be essential for Ana2 interacting with Sas6 (Stevens, 2010; Wang, 2011), but not Sas-5 interacting with Sas6 (Stevens, 2010). Although STIL/Ana2/Sas-5 proteins show great variety in length, there are two areas of high sequence conservation between the 1300 amino acids in chordates and the

400 amino acid length arthropods (Arquint, 2012). Near the C-terminus there is an area of approximately 90 amino acids called the STAN motif (for STil/Ana2) that shows 31% identity between *Drosophila* Ana2 and zebrafish STIL (Stevens, 2010). The most divergent member of the STAN motif is in the *C. elegans* Sas-5 sharing only 12% identity with the zebrafish STIL. At the very C-terminus there is a second motif that shows high sequence similarity, called TIM (Truncated In Microcephaly) (Arquint, 2012). This area of sequence was named because truncation of the very C-terminus of human STIL results in fewer asymmetrically divided progenitor neurons due to abnormal centriole function, thus resulting in microcephaly (Kumar, 2009).

STIL, Ana2, and Sas-5 were shown to be functional orthologs because they all function in licensing only one daughter centriole to nucleate from a mother and share sequence motifs (Arquint, 2012), as a result they are one of the seven essential proteins in centriole duplication (Delattre, 2004). This mechanism for licensing a single daughter centriole is still unclear, but depletion of endogenous STIL causes 60% of U2OS cells to contain fewer than two centrioles (Arquint, 2012). STIL and Ana2 studies also showed that overexpression of STIL/Ana2 results in multiple daughter centrioles nucleating off a single mother centriole that results in genomic instability (Arquint, 2012; Stevens, 2010). These experiments demonstrate the importance for regulating STIL/Ana2/Sas-5 for gaining a single daughter centriole on all duplicating mother centrioles. The protein responsible for this regulation is a serine/threonine phosphatase called PP2A (Kitagawa, 2011). The majority of Sas-5 is in the phosphorylated form during steady state in *C. elegans*. Upon dephosphorylation by PP2A, Sas-5 is targeted to centrioles for a duplication event (Kitagawa, 2011).

Dynein Lc8 from Drosophila interacts with Ana2 to assist in mitotic spindle orientation

In addition to centriole duplication, Ana2 forms a complex with a number of astral microtubule binding proteins to orient the mitotic spindle for asymmetric division of *Drosophila* neuroblasts (Wang, 2011). Ana2 mutant neuroblast spindle poles were disengaged from centrosomes, which resulted in disorganized spindles and misoriented assemblies (Wang, 2011). Severe spindle misorientation in asymmetrically dividing cells like neuroblast progenitors can result in hyperproliferation and tumorigenesis (Caussinus, 2005).

The dynein light chain from *Drosophila*, Lc8 was shown to interact with the central domain of Ana2 which contains a coiled-coil; co-localizing to the distal ends of centrioles (Wang, 2011). Lc8 mutants on their own were also shown to have a similar, although less severe, misoriented spindle phenotype as the Ana2 mutants (Wang, 2011).

We hypothesize that the domain containing the coiled-coil within Ana2 has demonstrated importance for binding interactions with Lc8 and Sas6, and this validates Ana2's need to dimerize. Although Lc8 mutants were only shown to produce a moderate number of cells with a severe phenotype, we hypothesize this phenotype may be more severe when Ana2 is incapable of dimerizing through its coiled-coil domain. We plan to test the importance of Lc8's role in mediating Ana2 dimerization through Ana2 mutational studies in our future work.

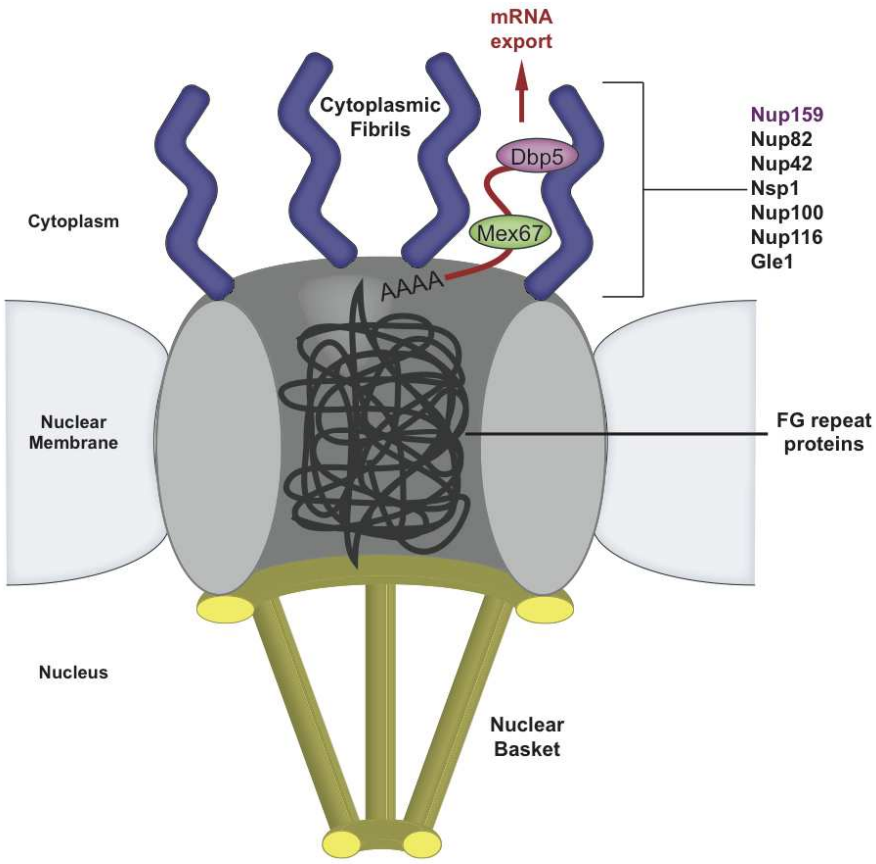

Figure 1-5. A cartoon diagram of the Nuclear Pore Complex illustrates how exported mRNA interacts with the cytoplasmic fibrils.

The nuclear pore is composed of a ring of transmembrane proteins with a nuclear basket structure and cytoplasmic fibrils that have both been identified as structurally and functionally important in nuclear pore transport. The central core of the pore contains a web of proteins with FG repeats, which can move aside to permit translocation. Dbp5 interacts with the mRNA export machinery and the cytoplasmic fibril as the final step in nuclear pore exit.

Dyn2 interacts with Nup159 on the cytoplasmic side of the nuclear pore

The *S. cerevisiae* Nuclear Pore Complex (NPC) is a 66 MDa structure composed of approximately 30 different proteins that embed in the nuclear envelope and facilitate transport across this barrier (Fig. 1-5) (Rout, 2000). NPC proteins are highly conserved in function and sequence across eukaryotes and carry out biologically conserved functions:

mRNA export into the cytoplasm and gated transport of specific proteins into and out of the nucleus.

The proteins that make up this highly coordinated and complex structure form an eight-fold symmetrical pore from a limited number of structural folds (Maul, 1971). The types of domains in the nuclear pore proteins, or nucleoporins (Nups), are primarily α-solenoids, β-propellers, Phe-Gly (FG) rich repeats, coiled-coil domains, and transmembrane domains (Schwartz, 2005; Alber, 2007). Transmembrane domains traverse the double nuclear envelope membrane and underlie the NPC core topology and biogenesis (Gerace, 1988; Tcheperegine, 1999). FG repeats are primarily concentrated in the core interior where they function as a physical or entropic barrier to entering proteins while reversibly binding nuclear transport receptors and selectively allowing their passage (Rout, 2000; Ribbeck, 2001). On either side of the core, asymmetrically distributed elements are positioned to facilitate asymmetric, unidirectional transport. The nucleoplasmic side of the NPC contains proteins tethered into a basket-like structure that protrudes 95 nm into the nucleus, potentially serving as a molecular checkpoint for pre-mRNA before it exits the nucleus (Fahrenkrog, 1998; Galy, 2004). On the cytoplasmic surface, NPC fibrils stretch 50 nm into the cytoplasm (Fahrenkrog, 1998). Cytoplasmic fibrils are primarily composed of nucleoporins from the Nup82 complex that bind translation initiation factors and mRNA export machinery (Allen, 2002). The Nup82 complex consists of Nup82, Nup159 and Nsp1 that work with Nup116, Nup42, Gle1, and Nup100, to mediate mRNA export in concert with the mRNA nuclear export receptor Mex67 and the DEAD box RNA helicase Dbp5 (Alber, 2007; Stelter, 2007; Bailer, 2000; Hodge, 2011).

Nup159 is a prime component of the Nup82 complex and plays a directed role in coordinating nucleoporins involved in mRNA export rather than protein trafficking between the cytoplasm and nucleus (Del Priore, 1997). Nup159 has an extended multi-component architecture that facilitates its roles in mRNA export, as well as filament localization in the NPC structure (Del Priore, 1997; Weirich, 2004; Gorsch, 1995; Schmitt, 1999). Nup159's N-terminal domain constitutes a seven-bladed β-propeller that extends into the cytoplasm and mediates Dbp5 binding (Miller, 2004). Deletion of Nup159's N-terminal domain results in a temperature-sensitive phenotype, lethal at 37°C and hallmarked by Dbp5 mislocalization and constitutive mRNA export defects at 23°C (Del Priore, 1997; Gorsch, 1995). Nup159's central 700 amino acids form an FG-rich repeat domain. C-terminal to the FG-rich repeats is a 100 amino acid region termed the dynein light chain interacting domain (DID) that uses a pentameric array of dynein light chain binding motifs to bind the yeast dynein light chain Dyn2 (Stelter, 2007). C-terminal to the DID, Nup159 contains a predicted helical region (Kraemer, 1995) that is essential for Nup159's stability and localization on the NPC, and has recently been shown to form a heterotrimeric structure with Nup82 and Nup116 (Del Priore, 1997; Gorsch, 1995; Yoshida, 2011). Higher-order oligomerization of the Nup82 complex requires both the Nup159 DID region as well as Dyn2 (Stelter, 2007). The functional role of a dynein light chain at the nuclear pore is independent of its role in the cytoplasmic dynein microtubule motor complex (Stelter, 2007).

Research Objectives

This dissertation describes work done to further our understanding of how Lc8/Dyn2 interacts both with the canonical dynein proteins as well as in other cellular functions.

We set out to characterize the *S. cerevisiae* dynein light chain, Dyn2 interacting in the protein complex for which it was named, the dynein complex. It was previously established that Dyn2 interacts directly with the intermediate chain, Pac11 (also *S. cerevisiae*) but the Dyn2 binding sites on Pac11 were not structurally or biophysically characterized. We solved the co-complex of Dyn2 binding to a peptide of one of the two reputed Pac11 binding sites as well as biophysically characterized the binding affinity of Dyn2 for Pac11 at this site. We hypothesize that Dyn2-mediated dimerization of Pac11 modulates Pac11's function in attaching to the dynein heavy chain or directly modulating the processivity of the dynein complex. We designed two mutations in Dyn2 to determine whether Dyn2-mediated dimerization of Pac11 is necessary for affecting Pac11's ability to bind the dynein heavy chain. One double point mutant knocks out Dyn2's ability to bind Pac11 but maintains a Dyn2 homodimer, and a single point mutation that ablates Dyn2's ability to homodimerize and also the ability to bind Pac11. Our collaborators will assess the processivity of the dynein complex with *in vitro* tracking assays utilizing these Dyn2 mutants in future work.

In our initial investigations of Lc8 interacting with the centriole duplication protein, Ana2 we plan to focus on establishing the structural and biochemical binding parameters for this Lc8 interaction. We determined two potential Lc8 binding sites on Ana2 through sequence analysis and found that both Ana2 peptides bind Lc8 with measureable affinity. Although one of the Ana2 peptide binding sites does not follow the canonical Lc8/Dyn2 recognition sequence, it was still able to have affinity consistent with previously measured Lc8 affinities, but weaker than the canonical motif. We hypothesize that this non-canonical binding motif utilizes a different set of hydrogen bonds for binding, but we will test this hypothesis in our future work. To date we have been unable to obtain a crystal structure of

Lc8 in complex with the non-canonical Ana2 peptide-binding site, and we will continue to improve the refinement of the crystals for solving this structure. Lastly, we aim to determine whether Ana2's interaction with Lc8 is necessary for dimerization, and whether dimerization of Ana2 is required for Ana2 to function properly in centriole duplication and in orienting the mitotic spindle. These *in vivo* experiments will be part of our future experimentation to determine the importance of the Lc8-Ana2 complex.

For studying how the dynein light chain interacts at the nuclear pore I chose to focus on the *S. cerevisiae* LC homolog, Dyn2. The budding yeast is a highly utilized model organism for studying dynein, and Dyn2 had not been structurally characterized. This body of work describes the first structure of the *S. cerevisiae* Dyn2, bound to a Nup159 peptide where only biochemical interactions have been shown with Dyn2. We show that Nup159 is the first known example of a single macromolecule that is capable of binding to Lc8/Dyn2 with one endothermic profile and another site with exothermic favorability. We hypothesized that even though there was only 50% sequence identity between *S. cerevisiae* Dyn2 and *Drosophila* Lc8 there would be a similar structural organization and mechanism for binding peptides.

We set out to establish the binding parameters for strength of interaction between Dyn2/Lc8 and target peptides and determined Dyn2/Lc8's relative affinity for Pac11, Ana2 at two binding sites, and Nup159 at two binding sites. Importantly, we provide evidence here that Dyn2 acts in more capacities than just as a scaffolding protein for Pac11, Ana2 and Nup159. Here we find that Dyn2/Lc8 acts to mediate/stabilize dimerization as a possible point of regulation for three particular targets at the dynein complex, via its centriole interaction, and at the nuclear pore.

References

1. Alber, F., Dokudovskaya, S., Veenhoff, L. M., Zhang, W., Kipper, J., Devos, D., Suprapto, A., Karni-Schmidt, O., Williams, R., Chait, B. T., Sali A., and Rout, M. P. (2007) *Nature* **450,** 695-701

2. Allen, N. P. C., Patel, S. S., Huang, L., Chalkley, R. J., Burlingame, A., Lutzmann, M., Hurt, E. C., and Rexach, M. (2002) Mol. Cell. Proteomics 1, 930-946

3. Aposolovic, B., Danial, M., Klok, H. A. (2010) Chem. Soc. Rev. 39, 3541-3575

4. Arquint, C., Sonnen, K. F., Steirhof, Y.-D., and Nigg, E. A. (2011) J. Cell Sci. 125, 1342-1352

5. Arquint, C., Sonnen, K. F., Stierhof, Y.-D., and Nigg, E. A. (2012) J. Cell Sci. 125, 1342-1352

6. Azimzadeh, J., and Marshall, W. F. (2011) Curr. Biol. 20, R816-R825

7. Azimzadeh, J., and Bornens, M. (2012) J. Cell Sci. 120, 2139-2142

8. Bader, J. R., and Vaughan, K. T. (2010) Semin. Cell Dev. Biol. 21, 269-275

9. Bailer, S. M., Balduf, C., Katahira, J., Podtelejnikov, A., Rollenhagen, C., Mann, M., Pante, N., and Hurt, E. C. (2000) J. Biol. Chem. 275, 23540-23548

10. Benison, G., Karplus, P. A., and Barbar, E. (2007) J. Mol. Biol. 371, 457-468

11. Benison, G., Chiodo, M., Karplus, P. A., and Barbar, E. (2009) Biochemistry 48, 11381-11389

12. Bornens, M. (2012) Science 335, 422-426

13. Brito, D. A., Gouveia, S. M., and Bettencourt-Dias, M. (2012) Curr. Opin. Cell Biol. 24, 4-13

14. Bryantseva, S. A. and Zhapparova, O. N. (2012) Cell Biol. Int. 36, 1-6

15. Busson, S., Dujardin, D., Moreau, A., Dompierre, J., and De Mey, J. R. (1998) Curr. Biol. 8, 541-544

16. Carter, A. P., Garbarino, J. E., Wilson-Kubalek, E. M., Shipley, W. E., Cho, C., Milligan, R. A., Vale, R. D., and Gibbons, I. R. (2008) Science 322, 1691-1695

17. Carter, A. P. and Vale, R. D. (2010) Biochem. Cell Biol. 88, 15-21

18. Carter, A. P., Cho, C., Jin, L., and Vale, R. D. (2011) Science 331, 1159-1165

19. Carvalho-Santos, Z., Machado, P., Branco, P., Tavares-Cadete, F., Rodrigues-Martins, A., Pereira-Leal, J. B., and Bettencourt-Dias, M. (2010) J. Cell Sci. 123, 1414-1426

20. Caussinus, E., and Gonzalez, C. (2005) Nat. Genet. 37, 1125-1129

21. Chaudhury, A., Rao, Y. M., and Goyal, R. K. (2008) Am. J. Physiol. Gastrointest. Liver Physiol. 295, G442-G451

22. Cho, C., Reck-Peterson, S. L., and Vale, R. D. (2008) J. Biol. Chem. 283, 25839-25845

23. Chuang, J. Z., Yeh, T. Y., Bollati, F., Conde, C., Canavosio, F., Caceres, A., and Sung, C. H. (2005) Dev. Cell 9, 75-86

24. Corthesy-Theulaz, I., Pauloin, A., and Pfeffer, S. R. (1992) J. Cell Biol. 118, 1333-1345

25. Cyr, J. L., Pfister, K. K., Bloom, G. S., Slaughter, C. A., and Brady, S. T. (1991) PNAS 88, 10144-10148

26. Day, C. L., Puthalakath, H., Skea, G., Strasser, A., Barsukov, I., Lian, L.Y., Huang, D. C. S., Hinds, M. G. (2004) Biochem. J. 377, 597-605

27. Del Priore, V., Heath, C. V., Snay, C. A., MacMillan, A., Gorsch, L. C., Dagher, S., and Cole, C. N. (1997) J. Cell Sci. 110, 2987-2999

28. Delattre, M. Leidel, S., Wani, K., Baumer, K., Bamat, J., Schnabel, H., Feichtinger, R., Schnabel, R., and Gonczy, P. (2004) Nat. Cell Biol. 6, 656-664

29. Eftink, M. R., Anusiem, A. C., and Biltonen, R. L. (1983) Biochemistry 22, 3884-3896

30. Endow, S. A., Kull, F. J., and Liu, H. (2010) J. Cell Sci. 123, 3420-3424

31. Eshel, D., Urrestarazu, L. A., Vissers, S., Jauniaux, J. C., van Vliet-Reedijk, J. C., Planta, R. J., and Gibbons, I. R. (1993) PNAS 90, 11172-11176

32. Espindola, F.S., Suter, D. M., Partata, L. B. E., Cao, T., Wolenski, J. S., Cheney, R. E., King, S. M., and Mooseker, M. S. (2000) Cell Motil. Cytoskeleton 47, 269-281

33. Fahrenkrog, B., Hurt, E. C., Aebi, U., and Pante, N. (1998) J. Cell Biol. 143, 577-588

34. Fan, J., Zhang, Q., Tochio, H., Li, M., and Zhang, M. (2001) J. Mol. Biol. 306, 97-108

35. Fuhrmann, J. C., Kins, S., Rostaing, P., El Far, O., Kirsch, J., Sheng, M., Triller, A., Betz, H., and Kneussel, M. (2002) J. Neurosci. 22, 5393-5402

36. Galy, V., Gadal, O., Fromont-Racine, M., Romano, A., Jacquir, A., and Nehrbass, U. (2004) Cell 116, 63-73

37. Garcia-Higuera, I., Fenoglio, J., Li, Y., Lewis, C., Panchenko, M. P., Reiner, O., Smith, T. F., and Neer, E. J. (1996) Biochemistry 35, 13985-13994

38. Geiser, J. R., Schott, E. J., Kingsbury, T. J., Cole, N. B., Totis, L. J., Bhattacharyya, G., He, L., and Hoyt, M. A. (1997) Mol. Biol. Cell 8, 1035-1050

39. Gennerich, A., Carter, A. P., Reck-Peterson, S. L., and Vale, R. D. (2007) Cell 131, 952-965

40. Gerace, L. (1988) Ann. Rev. Cell Biol. 4, 335-374

41. Good, M. C., Zalatan, J. G., and Lim, W. A. (2011) Science 332, 680-686

42. Gorsch, L. C., Dockendorff, T. C., Cole, C. N. (1995) J. Cell Biol. 129, 939-955

43. Gross, S. P., Welte, M. A., Block, S. M., and Wieschaus, E. F. (2002) J. Cell Biol. 156, 715-724

44. Gudi, R., Zou, C., Li, J., and Gao, Q. (2011) J. Cell Biol. 193, 711-725

45. Habura, A., Tikhonenko, I., Chisholm, R. L., and Koonce, M. P. (1999) J. Biol. Chem. 274, 15447-15453

46. Hall, J., Karplus, P. A., and Barbar, E. (2009) J. Biol. Chem. 284, 33115-33121

47. Hall, J. Son, Y., Karplus, P. A., and Barbar, E. (2010) J. Biol. Chem. 285, 22566-22575

48. Hayashi, I., Wilde, A., Mal, T. K., and Ikura, M. (2005) Mol. Cell 19, 449-460

49. Hayashi, I., Plevin, M. J., and Ikura, M. (2007) Nat. Struct. Mol. Biol. 14, 980-981

50. Hendricks, A. G., Perison, E., Ross, J. L., Schroeder III, H. W., Tokito, M., and Holzbaur, E. L. F. (2010) Curr. Biol. 20, 697-702

51. Hodge, C. A., Tran, E. J., Noble, K. N., Alcazar-Roman, A. R., Ben-Yishay, R., Scarcelli, J. J., Folkmann, A. W., Shav-Tal, Y., Wente, S. R., Cole, C. N. (2011) Genes Dev. 25, 1052-1064

52. Holleran, E. A., Ligon, L. A., Tokito, M., Stankewich, M. C., Morrow, J. C., and Holzbaur, E. L. F. (2001) J. Biol. Chem. 276, 36598-36605

53. Holzbaur, E. L. F., and Vallee, R. B. (1994) Annu. Rev. Cell Biol. 10, 339-372

54. Huang, J., Roberts, A. J., Leschziner, A. E., and Reck-Peterson, S. L. (2012) Cell 150, 975-986

55. Hughes, S. M., Vaughan, K. T., Herskovits, J. S., and Vallee, R. B. (1995) J. Cell Sci. 108, 17-24

56. Ilangovan, U., Ding, W., Zhong, Y., Wilson, C. L., Groppe, J. C., Trbovich, J. T., Zuniga, J., Demeler, B., Tang, Q., Gao, G., Mulder, K. M., and Hinck, A. P. (2005) J. Mol. Biol. 352, 338-354

57. Joukov, V., De Nicolo, A., Rodriguez, A., Walter, J. C., and Livingston, D. M. (2010) PNAS 107, 21022-21027

58. Kahana, J. A., Schlenstedt, G., Evanchuk, D. M., Geiser, J. R., Hoyt, M. A., and Silver, P. A. (1998) Mol. Biol. Cell 9, 1741-1756

59. Kammerer, R. A. and Steinmetz, M. O. (2006) J. Struct. Biol. 155, 146-153

60. Kardon, J. R., and Vale, R. D. (2009) Nat. Rev. Mol. Cell Biol. 10, 854-865

61. Kardon, J. R., Reck-Peterson, S. L., and Vale, R. D. (2009) PNAS 106, 5669-5674

62. Khakshoor, O., Lin, A. J., Korman, T. P., Sawaya, M. R., Tsai, S. C., Eisenberg, D., and Nowick, J. S. (2010) J. Am. Chem. Soc. 132, 11622-11628

63. Kim, H., Ling, S. C., Rogers, G. C., Kural, C., Selvin, P. R., Rogers, S. L., and Gelfand, V. I. (2007) J. Cell Biol. 176, 641-651

64. King, S. M., Barbarese, E., Dillman III, J. F., Patel-King, R. S., Carson, J. H., and Pfister, K. K. (1996) J. Biol. Chem. 271, 19358-19366

65. Kitagawa, D., Busso, C., Fluckiger, I., and Gonczy, P. (2009) Dev. Cell 17, 900-907

66. Kitagawa, D., Vakonakis, I., Olieric, N., Hillbert, M., Keller, D., Olieric, V., Bortfeld, M., Erat, M. C., Fluckiger, I., Gonczy, P., and Steinmetz, M. O. (2011) Cell 144, 364-375

67. Kon, T., Nishiura, M., Ohkura, R., Toyoshima, Y. Y., and Sutoh, K. (2004) Biochemistry 43, 11266-11274

68. Kon, T., Sutoh, K. and Kurisu, G. (2011) Nat. Struct. Mol. Biol. 18, 638-642

69. Kon, T., Oyama, T., Shimo-Kon, R., Imamula, K., Shima, T., Sutoh, K., and Kurisu, G. (2012) Nature 484, 345-350

70. Kraemer, D. M., Strambio-de-Castillia, C., Blobel, G., and Rout, M. P. (1995) J. Biol. Chem. 270, 19017-19020

71. Kull, F. J. (2000) Essays Biochem. 35, 61-73

72. Kumar, A., Girimaji, S. C., Duvvari, M. R., and Blanton, S. H. (2009) Am. J. Hum. Gen. 84, 286-290

73. Leidel, C., Longoria, R. A., Gutierrez, F. M., and Shubeita, G. T. (2012) Biophys. J. 103, 492-500

74. Lightcap, C. M., Sun, S., Lear, J. D., Rodeck, U., Polenova, T., and Williams, J. C. (2008) J. Biol. Chem. 283, 27314-27324

75. Lin, S. X., and Collins, C. A. (1992) J. Cell Sci. 101, 125-137

76. Lumry, R. and Rajender, S. (1970) Biopolymers 9, 1125-1227

77. Ma, S., Trivinos-Lagos, L., Graf, R., and Chisholm, R. L. (1999) J. Cell Biol. 147, 1261-1274

78. Makokha, M., Hare, M., Li, M., Hays, T., and Barbar, E. (2002) Biochemistry 41, 4302-4311

79. Manning, G., Plowman, G. D., Hunter, T., and Sudarsanam, S. (2002) Trends Biochem. Sci. 27, 514-520

80. Marsden, H. R. and Kros, A. (2010) Angew. Chem. Int. Ed. 49, 2988-3005

81. Marthiens, V., Piel, M., and Basto, R. (2012) J. Cell Sci. 125, 3281-3292

82. Maul, G. G. (1971) J. Cell Biol. 51, 558-563

83. McCauley, S. D., Gilchrist, M., and Befus, A. D. (2007) Life Sci. 80, 959-964

84. McKenney, R. J., Vershinin, M., Kunwar, A., Vallee, R. B., and Gross, S. P. (2010) Cell 141, 304-314

85. Mehta, A. (2001) J. Cell Sci. 114, 1981-1998

86. Miller, A. L., Suntharalingam, M., Johnson, S. L., Audhya, A., Emr, S. D., and Wente, S. R. (2004) J. Biol. Chem. 279, 51022-51032

87. Mische, S., He, Y., Ma, L., Li, M., Serr, M., and Hays, T. S. (2008) Mol. Biol. Cell 19, 4918-4929

88. Moore, J. K., Li, J., and Cooper, J. A. (2008) Traffic 9, 510-527

89. Mooseker, M. S., and Cheney, R. E. (1995) Annu. Rev. Cell Dev. Biol. 11, 633-675

90. Nigg, E. A., and Raff, J. W. (2009) Cell 139, 663-678

91. Nigg, E. A., and Stearns, T. (2011) Nat. Cell Biol. 13, 1154-1160

92. Nyarko, A., Hare, M., Hays, T. S., and Barbar, E. (2004) Biochem. 43, 15595-15603

93. Nyarko, A., Hall, J., Hall, A., Hare, M., Kremerskothen, J., and Barbar, E. (2011) Biophys. Chem. 159, 41-47

94. Peckham, M. (2011) Biochem. Soc. Trans. 39, 1142-1148

95. Puthalakath, H., Huang, D. C., O'Reilly, L. A., King, S. M., and Strasser, A. (1999) Mol. Cell 3, 287-296

96. Radnai, L., Rapali, P., Hodi, Z., Suveges, D., Monar, T., Kiss, B., Becsi, B., Erdodi, F., Buday, L., Kardos, J., Kovacs, M., and Nyitray, L. (2010) J. Biol. Chem. 285, 38649-38657

97. Rapali, P., Radnai, L., Suveges, D., Harmat, V., Tolgyesi, F., Walgren, W. Y., Katona, G., Nyitray, L., and Pal, G. (2011) PLoS One 6, e18818

98. Ribbeck, K., and Gorlich, D. (2001) EMBO J. 20, 1320-1330

99. Rodrigues-Martins, A., Riparbelli, M., Callaini, G., Glover, D. M., and Bettencourt-Dias, M. (2007) Science 316, 1046-1050

100. Rout, M. P., Aitchison, J. D., Suprapto, A., Hjertaas, K., Zhao, Y., and Chait, B. T. (2000) J. Cell Biol. 148, 635-651

101. Sack, S., Kull, F. J., and Mandelkow, E. (1999) Eur. J. Biochem. 262, 1-11

102. Schmidt, H., Gleave, E. S., and Carter, A. P. (2012) Nat. Struct. Mol. Biol. 19, 492-497

103. Schmidt, T. I., Kleylein-Sohn, J., Westendorf, J., Le Clech, M., Lavoie, S. B., Stierhof, Y. D., and Nigg, E. A. (2009) Curr. Biol. 19, 1005-1011

104. Schmitt, C., von Kobbe, C., Bachi, A., Pante, N., Rodrigues, J. P., Boscheron, C., Rigaut, G., Wilm, M., Seraphin, B., Carmo-Fonseca, M., and Izaurralde, E. (1999) EMBO J. 18, 4332-4347

105. Schwartz, T. U. (2005) Curr. Opin. Struct. Biol. 15, 221-226

106. Song, C., Wen, W., Rayala, S. K., Chen, M., Ma, J., Zhang, M., and Kumar, R. (2008) J. Biol. Chem. 283, 4004-4013

107. Song, J., Tyler, R. C., Lee, M. S., Tyler, E. M., and Markley, J. L. (2005) J. Mol. Biol. 354, 1043-1051

108. Stehman, S. A., Chen, Y., McKenney, R. J., and Vallee, R. B. (2007) J. Cell Biol. 178, 583-594

109. Stelter, P., Kunze, R., Flemming, D., Hoepfner, D., Diepholz, M., Philippsen, P., Boettcher, B., and Hurt, E. C. (2007) Nat. Cell Biol. 9, 788-796

110. Stevens, N. R., Dobbelaere, J., Brunk, K., Franz, A., and Raff, J. W. (2010) J. Cell Biol. 188, 313-323

111. Stuchell-Brereton, M. D., Siglin, A., Li, J., Moore, J. K., Ahmed, S., Williams, J. C., and Cooper, J. A. (2011) Mol. Biol. Cell 15, 2690-2701

112. Su, J. Y., Hodges, R. S., and Kay, C. M. (1994) Biochemistry 33, 15501-15510

113. Susalka, S. J., Nikulina, K., Salata, M. W., Vaughan, P. S., King, S. M., Vaughan, K. T., and Pfister, K. K. (2002) J. Biol. Chem. 277, 32939-32946

114. Tang, C. J., Fu, R. H., Wu, K. S., Hsu, W. B., and Tang, T. K. (2009) Nat. Cell Biol. 11, 825-831

115. Tcheperegine, S. E., Marelli, M., and Wozniak, R. W. (1999) J. Biol. Chem. 274, 5252-5258

116. Tynan, S. H., Gee, M. A., and Vallee, R. B. (2000) J. Biol. Chem. 275, 32769-32774

117. Vale, R. D. (2003) J. Cell Biol. 163, 445-450

118. Vallee, R. B., Williams, J. C., Varma, D., and Barnhart, L. E. (2004) J. Neurobiol. 58, 189-200

119. Vaughan, K. T., and Vallee, R. B. (1995) J. Cell Biol. 131, 1507-1516

120. Vulprecht, J., David, A., Tibelius, A., Castiel, A., Konotop, G., Liu, F., Bestvater, F., Raab, M. S., Zentgraf, H., Izraeli, S., and Kramer, A. (2012) J. Cell Sci. 125, 1353-1362

121. Wang, C., Li, S., Januschke, J., Rossi, F., Izumi, Y., Garcia-Alvarez, G., Gwee, S. S. L., Soon, S. B., Sidhu, H. K., Yu, F., Matsuzaki, F., Gonzalez, C., and Wang, H. (2011) Dev. Cell 21, 520-533

122. Wang, W., Lo, K. W., Kan, H., Fan, J., and Zhang, M. (2003) J. Biol. Chem. 278, 41491-41499

123. Waterman-Storer, C. M., Karki, S., and Holzbaur, E. L. (1995) PNAS 92, 1634-1638

124. Watson, P., Forster, R., Palmer, K. J., Pepperkok, R., and Stephens, D. J. (2005) Nat. Cell Biol. 7, 48-55

125. Weirich, C. S., Erzberger, J. P., Berger, J. M., and Weis, K. (2004) Mol. Cell 16, 749-760

126. Wickstead, B., and Gull, K. (2007) Traffic 8, 1708-1721

127. Williams, J. C., Xie, H., and Hendrickson, W. A. (2005) J. Biol. Chem. 280, 21981-21986

128. Williams, J. C., Roulhac, P. L., Roy, A. G., Vallee, R. B., Fitzgerald, M. C., and Hendrickson, W. A. (2007) Proc. Natl. Acad. Sci. 104, 10028-10033

129. Yoder, J. H., and Han, M. (2001) Mol. Biol. Cell 12, 2921-2933

130. Yoshida, K., Seo, H., Debler, E. W., Blobel, G., and Hoelz, A. (2011) PNAS 108, 16571-16576

131. Zhou, N. E., Zhu, B.-Y., Kay, C. M., and Hodges, R. S. (1992) Biopolymers 32, 419-426

132. Zhu, H., Lee, H. Y., Tong, Y., Hong, B.-S., Kim, K.-P., Shen, Y., Lim, K. J., Mackenzie, F., Tempel, W., and Park, H.-W. (2012) PLoS One 7, e33943

CHAPTER 2

THE STRUCTURE OF A YEAST DYNEIN DYN2-PAC11 COMPLEX AND EFFECT ON SINGLE MOLECULE DYNEIN MOTOR ACTIVITY

Preface

This work is a manuscript in preparation. Lu Rao (Laboratory of Arne Gennerich at Albert Einstein College of Medicine) performed the expression and preparation of rhodamine labeled Dyn2 and Pac11 as well as the single molecule motility assays, which are not presented here but will be part of the final manuscript. Ashutosh Tripathy assisted me with the size exclusion chromatography-multi-angle light scattering experiments as well as the isothermal microtitration calorimetry. I performed the remaining experiments and protein preparation. My advisor, Kevin Slep, and I designed the project and experiments I performed. Kevin Slep, Arne Gennerich, Lu Rao, and I wrote and edited the final manuscript.

Romes, EM, Rao, L, Tripathy, A, Slep, K, and Gennerich, A. (manuscript in progress).

Summary

The dynein complex is a 1.2 MDa complex that consists of a motor on the heavy chain and a dimerization domain that binds to dynein associating proteins (Nyarko, 2004). The dynein associating proteins modulate dynein's functional efficiency on the microtubule tracks as well as function as scaffolds with which to attach dynein cargos (Kardon, 2009; Rapali, 2011; Williams, 2007). The dynein intermediate chain, Pac11 is believed to function

in both of these capacities and binds directly to a dynein light chain, Dyn2 to assist and/or stabilize dimerization of Pac11 at two binding sites (Stuchell-Brereton, 2011). We determined the binding affinity of Dyn2 for the Pac11 second binding site (pep2) to have a K_D of 620 nM, which is the tightest Dyn2 binding interaction characterized to date. We also present the 1.90 Å resolution crystal structure of full length Dyn2 in complex with a peptide from the second of two Pac11 binding sites (pep2). Based on this crystal structure we designed a double point mutant (F76K/Y78E) that ablates Dyn2's ability to bind to the Pac11 pep2, but maintains Dyn2's ability to dimerize. We additionally confirmed that a single point mutant discussed in previous work on the *Drosophila* homolog, Lc8 (H55K), ablates Dyn2 dimerization and consequently also the ability of Dyn2 to bind to the Pac11 pep2. These point mutation tools will likely prove useful in dissecting whether Dyn2's role in dimerization is necessary for the function of Pac11 interacting with the dynein heavy chain or with cargo. Future experiments will aim to determine the role that Dyn2 plays in modifying dynein processivity and localization, as well as whether Dyn2's function as a dimerization machine affects Pac11's ability to modulate dynein processivity.

Experimental Procedures

Cloning, Expression, and Purification of Full Length Dyn2 from S. cerevisiae - Full length Dyn2 was cloned from *S. cerevisiae* S288c as described (Romes, 2012). Briefly, Dyn2 was cloned into pGEX-6P-2, (GE Healthcare) yielding an N-terminal, cleavable GST tag. GST-Dyn2 was expressed in BL21 DE3 (pLysS) and induced using 0.1 mM isopropyl-1-thio-β-D-galactopyranoside at 18° C for 16 hours. Cells were harvested, resuspended in lysis buffer and lysed by sonication. Dyn2 was purified using a Glutathione-S-sepharose column,

eluted and incubated with PreScission protease (GE Healthcare) to cleave the GST tag. A final purification step was performed using an ion exchange SP Sepharose Fast Flow column (GE Healthcare). The Dyn2 peak was collected and exchanged into 50 mM NaCl, 25 mM Hepes, pH 6.8, and 0.1% β-mercaptoethanol. The final, purified Dyn2 protein was concentrated to 5 mg/mL, snap frozen in liquid nitrogen and stored at -80°C. The final Dyn2 protein contained an N-terminal GPLGS cloning artifact.

Cloning, Expression and Purification of Dyn2 mutants - Dyn2 H58K and F76K/Y78E mutagenesis was done with the Quikchange method (Strategene) with the following complimentary oligonucleotides for the H58K mutant: 5'-GGATGTCAAATACGGCAATACCTGGAAAGTGATTGTCGGAAAGAACTTTGGG-3' (where the underlined portion codes for the mutated codon) and 5'-CCCAAAGTTCTTTCCGACAATCACTTTCCAGGTATTGCCGTATTTGACATCC-3', and the complimentary oligonucleotides for F76K/Y78E: 5'-GTGACACACGAAAAGGGCCATAAAGTTGAATTCTATATCGGTCCACTGGCG-3' and 5'-CGCCAGTGGACCGATATAGAATTCAACTTTATGGCCCTTTTCGTGTGTCAC-3'. Both the single and double mutants were confirmed by sequencing. The expression and purification of Dyn2 H58K and Dyn2 F76K/Y78E follow the same protocols and buffers as for WT Dyn2.

Synthesis of Pac11 Peptides – Pac11 peptides one (pep1) (YMVSVSVQTDM, residues 45-55) and two (pep2) (ITYDKGIQTDQ, residues 75-85), were synthesized at the UNC Microprotein Sequencing and Peptide Synthesis Facility. Pep1 was designed with an amino terminal tyrosine in order to quantify the peptide concentration once solubilized. Lyophilized peptides were solubilized in 50 mM NaCl, 25 mM Hepes, pH 6.8 and 0.1% β-mercaptoethanol.

Crystallization – Final concentrations of 0.5 mM Dyn2 and 0.6 mM Pac11 pep2 were incubated together to form a complex in 50 mM NaCl, 25 mM Hepes, pH 6.8, and 0.1% β-mercaptoethanol for 30 minutes at ambient temperature. Crystals were obtained by the hanging drop protocol using 2 μL of the Dyn2-Pac11 pep2 mixture and 1 μL of the 1 mL well solution: 0.4 M sodium phosphate monobasic, 0.1 M 1,6-hexanediol, and 25% polyethylene glycol 3350. Crystals grew at 20°C into full-sized thin, individual plates in two weeks. Crystals were transferred to cryoprotection of well solution supplemented with 20% ethylene glycol and flash frozen in liquid nitrogen.

Data Collection, Structure Determination, and Refinement – Diffraction data were collected on Dyn2-Pac11 pep2 crystals at the Advanced Photon Source SER-CAT beamline 22-ID with 1° oscillations over 180° from a single crystal. Data were indexed, integrated and scaled using HKL2000 (Otwinowski, 1997). The structure was determined using the AutoMR molecular replacement program (PHENIX crystallographic suite (Adams, 2010)) and a modified 4DS1 (Romes, 2012) coordinate file in which a monomeric, apo Dyn2 search model was used. The model was built using AutoBuild (PHENIX) (Adams, 2010) and refined iteratively through manual builds in Coot (Emsley, 2010) followed by refinement runs using phenix.refine (PHENIX) (Adams, 2010). Refinement statistics were monitored using a Free R, calculated using 7.8% of the data, randomly excluded from refinement (Brunger, 1992).

Isothermal Microtitration Calorimetry – Pac11 pep2 was exchanged into buffer B using G-25 Sephadex Quick Spin Columns (Roche) to remove additional salts. WT Dyn2, Dyn2 H58K, and Dyn2 F76K/Y78E were individually exchanged into buffer B as before: 50 mM NaCl, 25 mM Hepes, pH 6.8, and 0.1% β-mercaptoethanol. Binding was measured by

ITC at 26°C on a Microcal AutoITC200 (GE Healthcare). 19 x 2 μL injections of 1.0 mM Pac11 pep2 were automatically injected into 200 μL of 50 μM WT Dyn2. The data were analyzed with the Origin 7.0 software package (OriginLab) and the resulting isotherm was fit to a one-site binding model. The experiment was performed in triplicate and the mean K_D value with standard deviation is shown in Fig. 2-4A.

Dyn2 H58K and Dyn2 F76K/Y78E experiments were performed with Pac11 pep2 solubilized in buffer B (but not desalted) and the same concentrations as for WT Dyn2 and did not show binding (Fig. 2-4 F,G). 19 x 2 μL injections of 3.0 mM Pac11 pep2 were automatically injected into 200 μL of 300 μM Dyn2 H58K (not desalted) or 300 μM Dyn2 F76K/Y78E (not desalted). There was significant heat contributed by the Pac11 pep2 in the control experiment of 19 x 2 μL injections of 3.0 mM Pac11 pep2 that were automatically injected into 200 μL of buffer B. Because each injection produced a significant heat of dilution, the control experiment was subtracted from the raw 3.0 mM Pac11 pep2 into 300 μM Dyn2 H58K or 300 μM F76K/Y78E, and no binding was observed for either experiment (Fig. S2-1 C-E).

Pac11 pep2 was exchanged into buffer B using G-25 Sephadex Quick Spin Columns (Roche) to remove additional salts and the resulting concentration was used for further Dyn2 mutant experiments. 19 x 2 μL injections of 0.5 mM Pac11 pep2 were automatically injected into 200 μL of 50 μM Dyn2 H58K or 50 μM Dyn2 F76K/Y78E and no binding was observed (Fig. S2-1 A,B).

Size Exclusion Chromatography and Multi-Angle Light Scattering – Dyn2 H58K and Dyn2 F76K/Y78E were exchanged into buffer B: 50 mM NaCl, 25 mM Hepes, pH 6.8, and 0.1% β-mercaptoethanol using 3000 Da Amicon Ultra Spin Concentrators. Dyn2 WT was

concentrated to 6.0 mg/mL, Dyn2 H58K was concentrated to 10.0 mg/mL, and Dyn2 F76K/Y78E was concentrated to 6.0 mg/mL and all three proteins were monitored for precipitation during concentration. 50 μL injections of Dyn2 WT, H58K or F76K/Y78E were individually injected onto a Superdex 200 10/300 GL size exclusion column in buffer B with 0.2 g/L sodium azide and then passed consecutively through a Wyatt DAWN HELEOS II light scattering instrument and a Wyatt Optilab rEX refractometer. The light scattering and refractive index data were used to calculate the weight-averaged molar mass (M_W) and the mass fraction in each peak using the Wyatt Astra V software program (Wyatt Technology Corp.) (Wyatt, 1993).

Protein Data Bank Accession Number – Coordinates for the Dyn2-Pac11 pep2 complex have been deposited in the Research Collaboratory for Structural Bioinformatics PDB under accession code 4HT6.

Results

The dynein intermediate chain contains two conserved binding motifs for two Dyn2 homodimers in lower eukaryotes, or for one Dyn2/Lc8 homodimer and one TcTex homodimer in higher eukaryotes. In a sequence alignment of ICs from 12 species of eukaryotes ranging from fungi to higher order humans (Fig. 2-1A) the putative LC binding domains contain regions of sequence identity. There is one invariant QT motif that is preserved among all 12 species and one, more N-terminal QT motif that is conserved among fungi but not as highly conserved among higher eukaryotes. The more N-terminally conserved Q is a putative light chain binding site for Lc8/Dyn2 in fungi where the QT motif

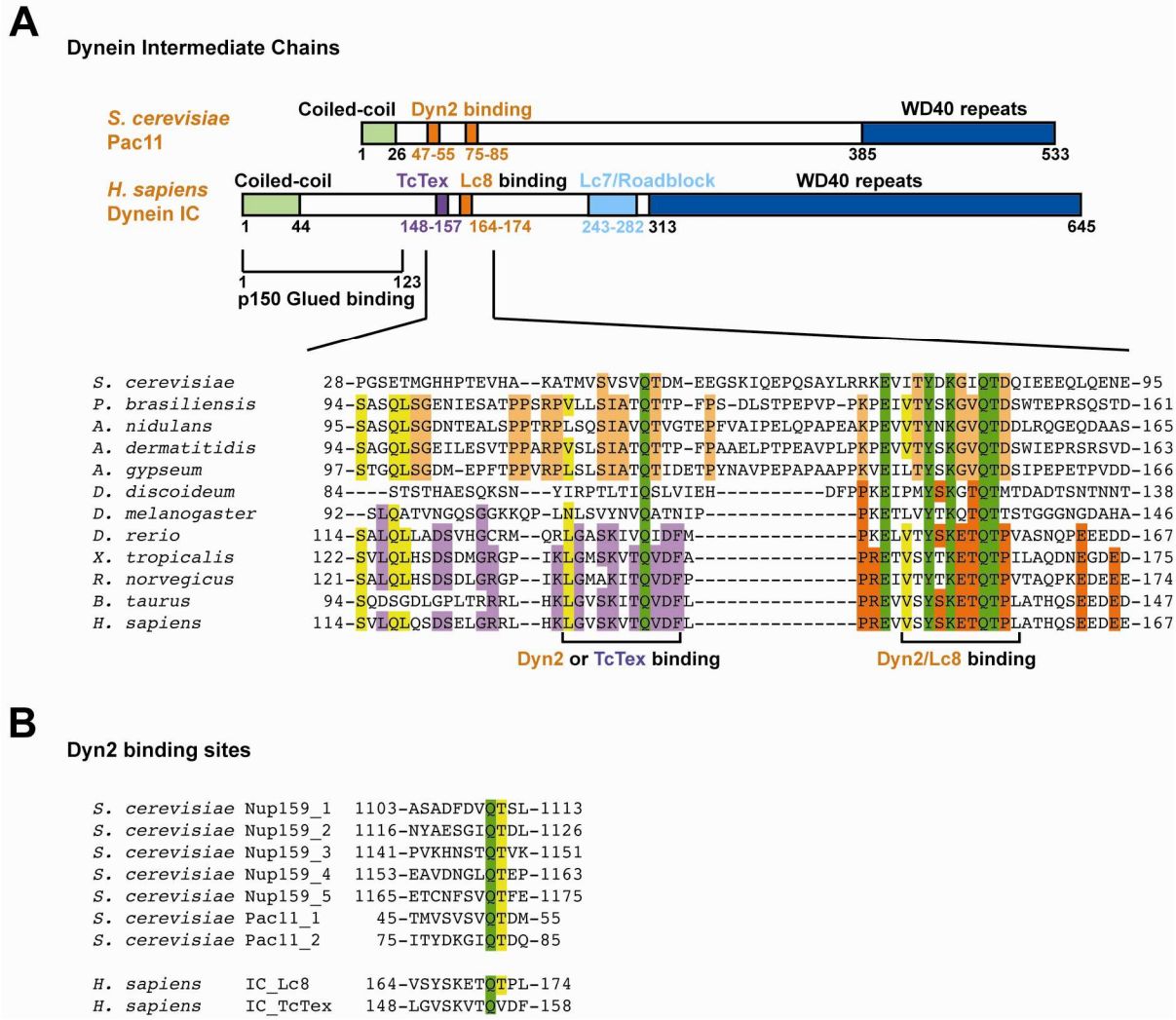

Figure 2-1. Dynein intermediate chains contain conserved dynein light chain binding motifs near the amino terminal coiled-coil domain.

A. Domain diagrams of dynein intermediate chains from *S. cerevisiae* and *H. sapiens* demonstrate a conserved amino terminal coiled-coil, a conserved binding site for Dyn2/Lc8 in *S. cerevisiae* or TcTex in *H. spaiens*, a highly conserved binding site for Dyn2/Lc8 homologs which contains the invariant QT motif, and a carboxy terminus WD repeat domain. The *H. sapiens* intermediate chain also contains a p150Glued-binding site between residues 1-123. A 12 species sequence alignment demonstrates residues 100% identical (green) and greater than 65% identical among all species (yellow). There is also conservation indicated among the five yeast species (orange is greater than 80% identical) and among the seven higher eukaryotes (purple is greater than 57% identical near the TcTex binding site, dark orange is greater than 57% identical near the Lc8 binding site). The reported and predicted dynein light chains bind to the intermediate chain with eleven residue motifs as indicated at the bottom. Residue numbers are indicated for each species. **B.** Reported Dyn2/Lc8/TcTex binding motifs display a highly conserved QT binding motif except for QV for *H. sapiens* TcTex.

is invariant, and a TcTex binding site in higher eukaryotes where QV is prevalent but not invariant.

Lower order eukaryotes, such as fungi only contain one type of dynein LC so both of the invariant QT motifs and surrounding conserved sequence are potentially used by Lc8/Dyn2 for recognition and binding. The higher order eukaryotes maintain a high level of conservation surrounding the QT and QV motif (with the exception of *D. melanogaster* and *D. discoideum*) with residues that are not homologous between the fungi and higher eukaryotes' putative binding sites. Previously reported Lc8/Dyn2 binding sites are represented in Fig. 2-1B and demonstrate the prevalence of the QT motif for recognition. Although binding motifs other than QT have been shown for Lc8/Dyn2, the five Dyn2 binding sites from the nuclear pore protein, Nup159, the two yeast IC (Pac11) sites, and the two LC binding sites on the human IC demonstrate that the QT motif is most utilized. The sequence surrounding the QT motif is highly variable, which illuminates Lc8/Dyn2's promiscuity in protein binding targets. Even though the putative binding sites for TcTex share some conservation with the Dyn2 binding site, TcTex and Lc8/Dyn2 do not share any sequence homology (Williams, 2005). These two dynein LCs share similar structure (RMSD 1.6 Å between Lc8 and TcTex in *Drosophila*), but they are otherwise divergent proteins.

The Dyn2 and Pac11 pep2 complex forms as the result of a central Dyn2 homodimer with two Pac11 pep2 binding at the exterior of the central dimerization site to complete two antiparallel β-sheets. The Dyn2 and Pac11 pep2 crystal structure shows two central β-sheets (Fig. 2-2A); each composed of four antiparallel strands from one Dyn2 monomer (in order β1, β4, β5, β2), a β-strand from the corresponding Dyn2 monomer (β3') and a Pac11 pep2 β-strand (residues 75-85), with two helices from each monomer flanking the β-sheets. There is

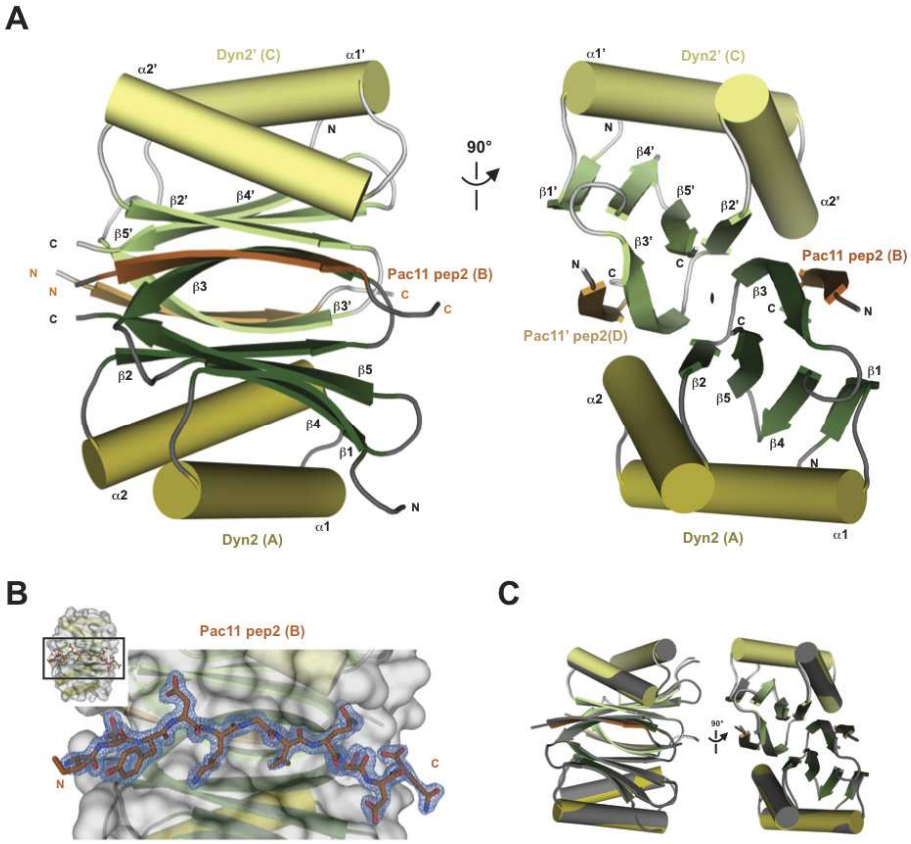

Figure 2-2. The structure of Dyn2 in complex with Pac11 pep2 shows a Dyn2 dimer bound to two Pac11 pep2s that form the end β-strands on two antiparallel β-sheets formed within the core of the Dyn2 dimer.

A. Cartoon rendering of the Dyn2-Pac11 pep2 quaternary structure shows Dyn2 monomer one (chain A) in dark green (β-strands) and dark yellow (α-helices), Pac11 pep2 β-strand one (chain B) in dark orange, the second Dyn2 monomer (chain C) in light green (β-strands) and light yellow (α-helices), and the second Pac11 pep2 β-strand (chain D) in light orange. A two-fold non-crystallographic symmetry operator about the z-axis (90° rotation figure at right) shows how the two Dyn2-Pac11 pep2 monomers relate to each other in the asymmetric unit. **B.** Stick rendering of Pac11 pep2 (dark orange) is shown bound in the Dyn2 (gray surface on top of cartoon) binding cleft between Dyn2 monomers. $2F_o$-F_c electron density map of the Pac11 pep2, contoured to 1.5σ, is shown in blue mesh. **C.** The symmetry mate of Dyn2 (chain E) and Pac11 pep2 (chain F) complex completes the dimer from the native chain E Dyn2 and F Pac11 pep2. The Cα atoms from the chain E/F dimer (gray) align to an RMSD of 0.182 Å (over 168/194 atoms) on the original chains A-D (colored).

a two-fold non-crystalographic symmetry operator lengthwise between the β-sheets, which relates the Dyn2 monomers to each other rotationally in formation of the dimer. The two Pac11 pep2 strands each complete an antiparallel β-sheet of Dyn2 and are parallel to each other so the amino terminus of each strand extends in the same direction. The crystal structure is a complex of 2 Dyn2 : 2 Pac11 pep2 from crystals that diffracted to 1.90 Å resolution in the $C222_1$ space group (Table 2-1). The structure was solved using the Dyn2 dimer stripped of the bound Nup159 peptide (4DS1) for a molecular replacement model (Romes, 2012). The Pac11 pep2 was modeled into clear electron density for all 11 residues (Fig. 2-2B). The structure was refined to R and R_{free} factors of 16.0% and 21.2%, respectively (Table 2-1). The crystallographic asymmetric unit contains three Dyn2 monomers and three Pac11 pep2s (data not shown). The third Dyn2 and Pac11 pep2 unit is a composite dimer with the next symmetry mate showing a slight torque about the y-axis. The dimer that is composed of a Dyn2-Pac11 pep2 unit from one symmetry mate and one Dyn2-Pac11 pep2 unit from another symmetry mate aligns with the original dimer (Fig. 2-2C) to an RMSD of 0.182 Å (C_a aligned over 168 out of 194 atoms).

The Dyn2 and Pac11 pep2 structure shows a conservation of hydrogen bonds and an extensive van der Waals network which signifies the importance of the QT motif in Dyn2 binding the peptide. The Pac11 pep2 binding site is mainly composed of an anti-parallel β-strand interaction between Dyn2 β3 and the Pac11 pep2 mediated by eight hydrogen bonds between the amino and carboxyl groups of the backbone (Fig. 2-3A). The stick diagram of this binding site shows there are additional hydrogen bond contributions from the side chains of Dyn2 β3 and the Pac11 pep2 as well as R39' and E38' from the corresponding Dyn2 dimer. The positively charged K12 from Dyn2 β1, and the large, hydrophobic Y78, and Y80

Table 1: Data Collection and Refinement Statistics

Wavelength (Å)	0.97920
Space group	$C222_1$
Cell dimensions (Å)	
a	101.5
b	112.7
c	56.4
Resolution (Å)	50.0-1.90 (1.97-1.90)
Reflections	
Measured	117,213
Unique	25,589
Completeness (%)	98.5 (88.8)
Mean redundancy	4.6 (3.6)
$\langle I/\sigma \rangle$	15.5 (2.5)
R_{sym} [a]	0.09 (0.41)

Refinement

Resolution (Å)	37.7-1.90 (1.97-1.90)
R [b] / R_{free} (%) [c]	16.0 (19.9) / 21.2 (27.0)
No. reflections, R/R_{free}	23575 (2089) / 2000 (178)
Total atoms	2617
Protein/water	2343/274
Stereochemical ideality (rmsd)	
Bonds/angles (Å/°)	0.007/1.04
Mean B-factors (Å^2)	
MC/SC/water	15.7/24.5/20.6
B-factor rmsd (Å^2)	
MC/SC	2.1/4.4
Ramachandran analysis	
Favored/allowed (%)	97.8/2.2

Parentheses list statistics for the high resolution shell

[a] $R_{sym} = \Sigma_h \Sigma_i |I_i(h) - \langle I(h) \rangle| / \Sigma_h \Sigma_i I_i(h)$ where $I_i(h)$ is the integrated intensity of the ith reflection with the Miller Index h and $\langle I(h) \rangle$ is the average over Friedel and symmetry equivalents.

[b] R value = $\Sigma (|F_{obs}| - k|F_{calc}|) / \Sigma |F_{obs}|$.

[c] R_{free} is calculated using a 7.8% subset of the data that are removed randomly from the original data and excluded from refinement.

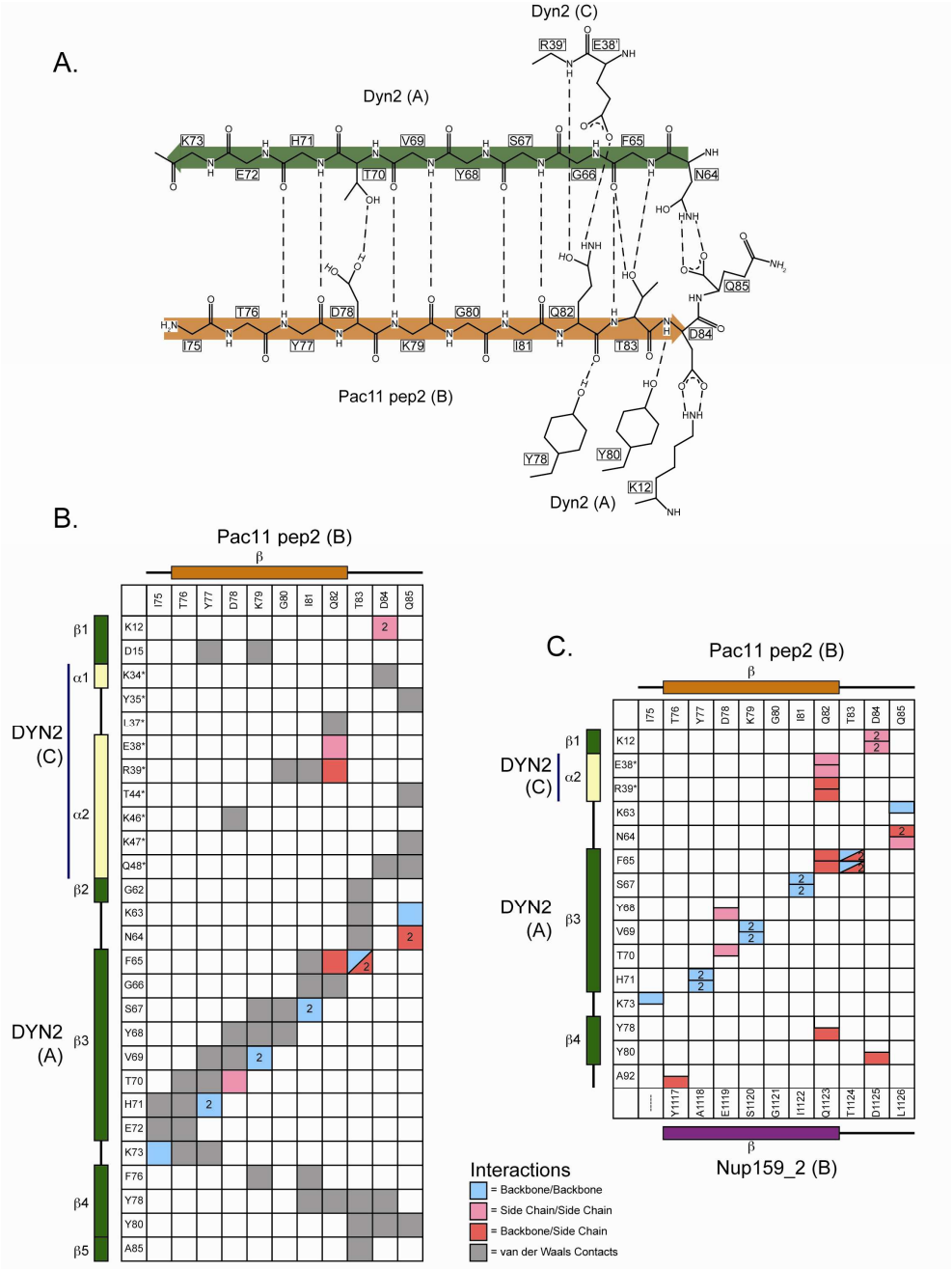

Figure 2-3. The crystal structure of Dyn2 in complex with Pac11 pep2 shows an extensive hydrogen bonding network that involves backbone/backbone β-strand interactions as well as involvement by the residue side chains.

A. A two-dimensional diagram of the hydrogen bonding network and salt bridges (dashed lines) that occur between Pac11 pep2 chain B (orange) and Dyn2 chains A and C (green). **B.** and **C.** Interaction grids between Pac11 pep2 chain B (top, horizontal) and Dyn2 chains A and C (vertical). Outside the grid is displayed the secondary structure (β-strands orange and

green, α-helices in yellow) and which chain contains the individual residues. Hydrogen bond interactions (distances less than or equal to 3.5 Å) are delineated as backbone/backbone (blue), side chain/side chain (pink), and backbone/side chain (red), and van der Waals contacts in gray (less than or equal to 4.5 Å). **C.** Hydrogen bonding network represented between Dyn2/Pac11 pep2 is compared to previously reported interaction between Dyn2 and Nup159 pep2 (bottom, horizontal axis), so the top half of a grid square represents the Pac11 pep2 hydrogen bond and the bottom half represents the corresponding Nup159 pep2 hydrogen bond (Romes, 2012).

(both Dyn2 β4) contribute four total hydrogen bonds. The largest number of Pac11 pep2 hydrogen bonds and van der Waals contacts are made with Q82 and T83 (Fig. 2-3B). The six hydrogen bonds and nine additional van der Waals interactions contribute to the stability and specificity of Dyn2 recognizing Pac11 pep2. Dyn2 also binds Nup159 with the same QT motif at residues 1123 and 1124 (Fig. 2-3C), and in the same anti parallel β-strand configuration (Romes, 2012). Many of the same contacts are made between Dyn2 and Nup159 as with Pac11 pep2 even though many of the other residue identities are not conserved between Nup159 pep2 and Pac11 pep2. Q82 of Pac11 pep2 makes three of the four hydrogen bonds and all of the T83 bonds that are made for Nup159 pep2 to secure specificity. All of the Pac11 pep2 and Nup159 pep2 residues make at least one hydrogen bond with Dyn2 (with the exception of Pac11 T76 and the conserved G80 in Pac11 and G1121 in Nup159).

WT Dyn2 is primarily a dimer in solution and binds Pac11 pep2 with 620 nM affinity. Isothermal microtitration calorimetry of Pac11 pep2 binding to WT Dyn2 shows an average binding affinity (K_D) of 620 nM ± 270 nM (Fig. 2-4A). The Pac11 pep2 bound WT Dyn2 exothermically at 26°C, and was fit with a single site binding model. The experiment was done in triplicate and averaged with the standard deviation to show good agreement (N = 1.05 ± 0.02 sites, ΔH = -5175 ± 139 cal/mol, ΔS = 11.3 ± 1.5 cal/mol/deg). Previous

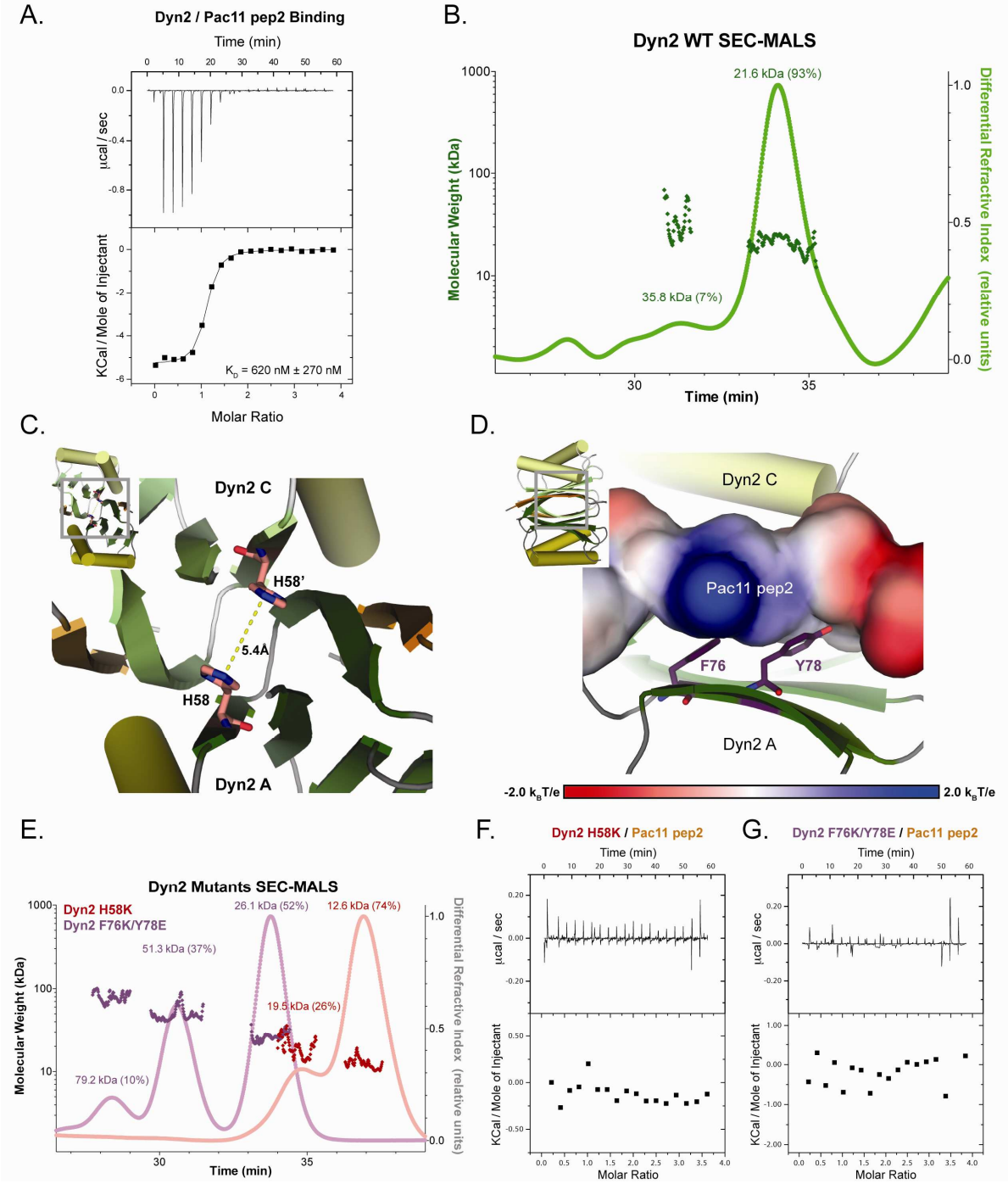

Figure 2-4. Dyn2's ability to dimerize and bind Pac11 pep2 is abrogated through key mutations.

A. Pac11 pep2 binds to Dyn2 with a 2:2 binding stoichiometry in an exothermic interaction and with a K_D of 620 nM as measured by isothermal microtitration calorimetry. The upper binding isotherm shows 19 x 2 µL injections of 1.0 mM Pac11 pep2 into 200 µL of 50 µM Dyn2. The bottom panel shows the data fit to a single binding site model from one of three independent experiments, with averaged K_D (+/- standard deviation of three experiments).

B. The SEC-MALS of WT Dyn2 was measured by a 50 μL injection of 6 mg/mL (green) at pH 6.8. The differential refractive index measurements were normalized to the tallest, dimer peak (21.6 kDa). The peaks are labeled with the measured molecular weight (dark green) and the fraction of total injected mass in each peak (in parentheses). This construct of WT Dyn2 has a calculated molecular weight of 10,852 Da. **C.** The crystal structure of Dyn2 is shown in ribbons and cylinders (colored as in Fig. 2-2) with H58 from each dimer shown in salmon-colored sticks. The zoom window shows that the H58 imidazole rings stack 5.4 Å apart. **D.** The crystal structure of Dyn2 (ribbons and cylinders) highlights the location of Dyn2, chain A F76 and Y78 (purple sticks) binding to the Pac11 pep2 (electrostatic shown on surface). The electrostatic surface of Pac11 pep2 is rendered from -2.0 k_BT/e (red) to +2.0 k_BT/e (blue). **E.** A 50 μL injection of 10 mg/mL Dyn2 H58K mutant (pink) or 6 mg/mL Dyn2 F76K/Y78E mutant (light purple) for SEC-MALS at pH 6.8. The differential refractive index measurements for each mutant were individually normalized to the tallest peak (H58K to the 12.6 kDa peak, F76K/Y78E to the 26.1 kDa peak). Each peak shows the measured molecular weight (H58K in red, F76K/Y78E in purple) and the fraction of total injected mass in each peak (in parentheses) **F.** and **G.** ITC of Dyn2 mutations interacting with Pac11 pep2. The upper panels show 19 x 2 μL injections of 1.0 mM Pac11 pep2 into 200 μL of 50 μM Dyn2 H58K (**F.**), or Dyn2 F76K/Y78E (**G.**). Neither experiment shows detectable binding of Pac11 pep2.

Dyn2/Lc8 binding experiments show that WT Dyn2 is capable of binding peptides with endothermic or exothermic modes as Dyn2 does with binding Nup159 pep2 endothermically at 17.9 μM and Nup159 pep4 exothermically at 13.1 μM (Romes, 2012). Lc8 also binds similar length peptides exothermically with K_Ds between 1 μM for Bmf and 7 μM for nNOS (Radnai, 2010). Therefore, Dyn2 binding Pac11 pep2 is more than an order of magnitude tighter than binding Nup159 peptides and on the tighter side of the Lc8 homologs. The first Pac11 binding site was synthesized to measure binding, but it was too hydrophobic to solubilize for ITC experiments. In the same buffer conditions as the binding experiments we show that WT Dyn2 forms mostly a dimer at pH 6.8 as measured by SEC-MALS (Fig. 2-4B), as was previously described in Romes, 2012. Here we show that 93% of the total injected mass was found to form a dimer at 21.6 kDa (calculated molecular weight of the WT Dyn2 monomer is 10.852 kDa, with the GPLGS cloning fragment). 7% of the total injected mass eluted in a wide, but small peak, which usually indicates an inability to separate two

species. The differential refractive index was used to calculate the molecular weight of this peak at 35.8 kDa, this suggests it is composed of trimer and tetramer of WT Dyn2.

An H58K mutation in the Dyn2 dimerization site and a F76K/Y78E double mutation at the peptide-binding site temper Dyn2's ability to dimerize and/or bind the Pac11 pep2. A single mutation in the dimerization site of Lc8 at H55 to a lysine (K) was previously reported to preference an Lc8 monomer at pH 3-8 where Lc8 is mostly at dimer at pH 4-8 (Nyarko, 2005). We hypothesized that the dimerization in the equivalent H58 lysine mutant of Dyn2 would cause a similar preference for a Dyn2 monomer at neutral pH. H55 in Lc8 acts as a switch that favors a folded monomer when the imidazole ring is in the protonated form, below the pKa of this particular histidine at pH 4.5 (Nyarko, 2005). In Dyn2 H58 the imidazole rings are a distance of 5.4 Å apart in the central core of the dimerization interface (Fig. 2-4C). When H55 in Lc8 (or H58 in Dyn2) is mutated to a residue with a pKa not sensitive to this particular pH region the decoupled protonation state stays as a monomer or dimer at any pH that allows Dyn2 to maintain the fold. When we mutated H58 to a lysine, the charge repulsion caused Dyn2 to preferentially form monomers at pH 6.8 (Fig. 2-4E, pink/red). The SEC-MALS for Dyn2 H58K shows that 74% of the Dyn2 is in the monomer form at 12.6 kDa (Dyn2 H58K calculated molecular weight is 10.843 kDa) and 26% in the dimer population at 19.5 kDa. Dyn2 H58K in the same buffer was also unable to bind Pac11 pep2 at the same concentrations as measured for the WT Dyn2 (Fig. 2-4F). Small endothermic peaks were observed in the Dyn2 H58K/Pac11 pep2 binding reaction that are attributed to the high concentration of Pac11 pep2 which was offset by the large exothermic contribution of Pac11 pep2 binding to the WT Dyn2 in Fig. 2-4A. To ensure that Pac11 pep2 was not able to bind to Dyn2 H58K we increased the concentrations of Dyn2 H58K and

Pac11 pep2 to the highest concentrations attainable that were still soluble. At 0.3 mM Dyn2 H58K and 3.0 mM Pac11 pep2 there was a significant exothermic contribution by the Pac11 pep2 (Fig. S2-1D) as determined by a control of 3.0 mM Pac11 pep2 injected into buffer (Fig. S2-1C). After subtracting the control experiment from the 3.0 mM Pac11 pep2/0.3 mM Dyn2 H58K binding experiment it was evident that no significant binding was taking place. Since the Pac11 pep2 shows such a large exothermic heat of dilution at high concentrations, we additionally desalted Pac11 pep2 with a Sephadex desalting column and measured 0.5 mM desalted Pac11 pep2 injected into 50 μM Dyn2 H58K and found there was no significant binding (Fig. S2-1A).

A double mutation of Dyn2 at the peptide-binding site was designed specifically for Pac11 pep2's electrostatic profile (Fig. 2-4D). Pac11 pep2 contains an electropositive charge (K79) and an electronegative charge (D84) that form van der Waals contacts with F76 and Y78 of Dyn2 (Fig. 2-3B) but the F76 and Y78 are not predicted to disturb the dimerization site of Dyn2. We designed Dyn2 mutations to have charge repulsions so that F76 is mutated to lysine to oppose K79 on Pac11, and Y78 is mutated to glutamate to oppose the D84 according to the crystal structure. The SEC-MALS for Dyn2 F76K/Y78E demonstrates that at pH 6.8 the dimer is still maintained with 52% of the total mass fraction at 26.1 kDa (Dyn2 F76K/Y78E calculated molecular weight is 10.799 kDa) (Fig. 2-4E, purple). There are also two other oligomer populations at 51.3 kDa (37% mass fraction) and 79.2 kDa (10% mass fraction) that are inexplicably more prominent in the double mutant than in the WT Dyn2 (Fig. 2-4B). Dyn2 F76K/Y78E was unable to bind Pac11 pep2 as measured by ITC at the same concentrations as WT (Fig. 2-4G). We also measured Dyn2 at 0.3 mM Dyn2 F76K/Y78E with 3.0 mM injected Pac11 pep2 (Fig. S2-1E) and saw a similar Pac11 pep2

dependence in the control that was corrected by subtracting the control heats of dilution from the Dyn2 F76K/Y78E/Pac11 pep2 reaction and resulted in no significant binding. Measuring 0.5 mM desalted Pac11 pep2 into 50 μM Dyn2 F76K/Y78E also resulted in no significant binding as was seen in all of Dyn2 mutant experiments (Fig. S2-1B). These results indicate that Dyn2 H58K shows consistent behavior to the Lc8 counterpart of forming mostly a dimer that in this case is unable to bind the Pac11 pep2. The Dyn2 F76K/Y78E is able to maintain the homodimer in solution at pH 6.8, but peptide binding is abrogated for Pac11 pep2.

Discussion

The dynein light chain, Dyn2 was first characterized as a dynein associating protein, but studies have not been able to determine Dyn2's purpose, other than as a general scaffolding protein that binds to the dynein intermediate chain, Pac11. The dynein intermediate chain has been shown to abrogate force production of the dynein complex when bound to NudE (McKenney, 2011), but whether Dyn2 or other dynein light chains are present and necessary for this process is unclear. This and previous studies have determined through sequence alignments and deletion studies that dynein intermediate chains contain more than one possible binding site for the dynein light chains near the N-terminus. The intermediate chain in higher eukaryotes has been shown to bind one of each of the three dynein light chains, however yeast species only contain the Dyn2 dynein light chain which binds in two putative locations that align with the Lc8 and TcTex binding sites on the IC in higher eukaryotes (Stutchell-Brereton, 2011). Here we show that the Dyn2/Lc8 binding sequence motif is highly conserved across many species of yeast and higher metazoans, but the second Dyn2 binding site in yeast diverges in higher metazoans to form the homologous

TcTex binding location. We confirm that Dyn2 binds Pac11 at the second Dyn2 binding site exothermically through isothermal microtitration calorimetry. We report that Dyn2 binds Pac11 pep2 with a K_D of 620 nM, which is bound more tightly than previous Dyn2 binding interactions, and among the tightest found for Dyn2/Lc8 binding to date. We also obtained a 1.90 Å crystal structure of a Dyn2 homodimer bound to two Pac11 pep2. The co-crystal complex of Dyn2 and Pac11 pep2 showed an extensive hydrogen-bonding network that supports the result that Dyn2 binds Pac11 pep2 exothermically. The hydrogen-bonding network compares to a previous structure of Dyn2 bound to the nuclear pore protein, Nup159 to illuminate the importance of the QT motif in binding to Dyn2. Glutamine 82 and threonine 83 in Pac11 pep2 each contribute three hydrogen bonds in the Pac11 network, and the corresponding Q1123 in Nup159 pep2 contributes four hydrogen bonds with three from T1124 to form the Dyn2-specific network. Both the ITC binding studies and co-crystalization of Dyn2 and Pac11 pep2 support our hypothesis that Dyn2 acts as a dimerization machine to assist Pac11 homodimerization through mediation of Dyn2. We confirmed through an H58K point mutation in the core of the Dyn2 structure that Dyn2 homodimerization is necessary to bind the Pac11 pep2, as has been shown for the higher eukaryote homolog, Lc8 (Wang, 2003). We showed through SEC-MALS that Dyn2 H58K forms primarily a monomer in solution that was unable to bind the Pac11 pep2 using a number of different concentrations and conditions in ITC. This histidine to lysine mutation was shown to mimic the behavior of an Lc8 phosphomimetic which preferences the Lc8 monomer in solution (Song, 2008). Phosphorylation of Lc8 therefore regulates the dimerization and binding to target proteins by dissociating the dimer, much like protonation of H55 (or H58 in Dyn2) dissociates the dimer. Additionally we designed a F76K/Y78E double point mutant in Dyn2 that shows the ability

to dimerize in solution through SEC-MALS, but the double mutation abrogates the ability of Dyn2 to bind to the Pac11 pep2. The F76K/Y78E Dyn2 mutant was designed specifically for ablating the interaction with Pac11 pep2, however we hypothesize that this specific mutation would also be useful for Dyn2 binding sites that contain a (+)xxQT(-) motif (where + indicates a positively charged residue K/R/H and – indicates a negatively charged D/E). This F76K/Y78E Dyn2 mutant also showed an unexplained higher population of larger order oligomers than the corresponding SEC-MALS of the Dyn2 WT at the same concentrations. We hypothesize that these higher order oligomers form in the F76K/Y78E mutant due to an increase in ionic interactions. The ionic strength of the buffer is low with only 50 mM NaCl, so we could test our hypothesis by increasing the NaCl concentration of the buffer to determine whether the pronounced higher oligomer peaks remain, indicating oligomer associations through ionic interactions. In the future we aim to utilize the H58K and F76K/Y78E mutants to determine whether Dyn2's interaction with Pac11 modulates the *in vitro* processivity and localization of the dynein complex through Dyn2's function as a dimerization machine for Pac11.

References

1. Adams, P. D., Afonine, P. V., Bunkóczi, G., Chen, V. B., Davis, I. W., Echols, N., Headd, J. J., Hung, L.-W., Kapral, G. J., Grosse-Kunstleve, R. W., McCoy, A. J., Moriarty, N. W., Oeffner, R., Read, R. J., Richardson, D. C., Richardson, J. S., Terwilliger, T. C., and Zwart, P. H. (2010) *Acta Cryst*. **D66,** 213-221

2. Brunger, A. T. (1992) *Nature* **355,** 472-475

3. Emsley, P., Lohkamp, B., Scott, W., and Cowtan, K. (2010) *Acta Cryst*. **D66,** 486-501

4. Kardon, J. R., Reck-Peterson, S. L., and Vale, R. D. (2009) *PNAS* **106**, 5669-5674

5. McKenney, R. J., Weil, S. J., Scherer, J., and Vallee, R. B. (2011) *J. Biol. Chem*. **286**, 39615-39622

6. Nyarko, A., Cochrun, L. Norwood, S., Pursifull, N., Voth, A., and Barbar, E. (2005) *Biochemistry* **44**, 14248-14255

7. Otwinowski, Z., and Minor, W. (1997) *Methods in Enzymology*, Volume **276**: Macromolecular Crystallography, part A, p.307-326, Academic Press, New York, NY

8. Radnai, L., Rapali, P., Hodi, Z., Suveges, D., Monar, T., Kiss, B., Becsi, B., Erdodi, F., Buday, L., Kardos, J., Kovacs, M., and Nyitray, L. (2010) *J. Biol. Chem*. **285,** 38649-38657

9. Rapali, P., Radnai, L., Suveges, D., Harmat, V., Tolgyesi, F., Walgren, W. Y., Katona, G., Nyitray, L., and Pal, G. (2011) *PLoS One* **6,** e18818

10. Romes, E. M., Tripathy, A., and Slep, K. C. (2012) *J. Biol. Chem*. **287**, 15862-15873

11. Song, C., Wen, W., Rayala, S. K., Chen, M., Ma, J., Zhang, M., and Kumar, R. (2008) *J. Biol. Chem*. **283**, 4004-4013

12. Stuchell-Brereton, M. D., Siglin, A., Li, J., Moore, J. K., Ahmed, S., Williams, J. C., and Cooper, J. A. (2011) *Mol. Biol. Cell* **15,** 2690-2701

13. Wang, W., Lo, K. W., Kan, H., Fan, J., and Zhang, M. (2003) *J. Biol. Chem*. **278,** 41491-41499

14. Williams, J. C., Xie, H., and Hendrickson, W. A. (2005) *J. Biol. Chem*. **280**, 21981-21986

15. Williams, J. C., Roulhac, P. L., Roy, A. G., Vallee, R. B., Fitzgerald, M. C., and Hendrickson, W. A. (2007) *Proc. Natl. Acad. Sci*. **104,** 10028-10033

16. Wyatt, P. J. (*1993*) *Anal. Chim. Acta **272,*** 1-40

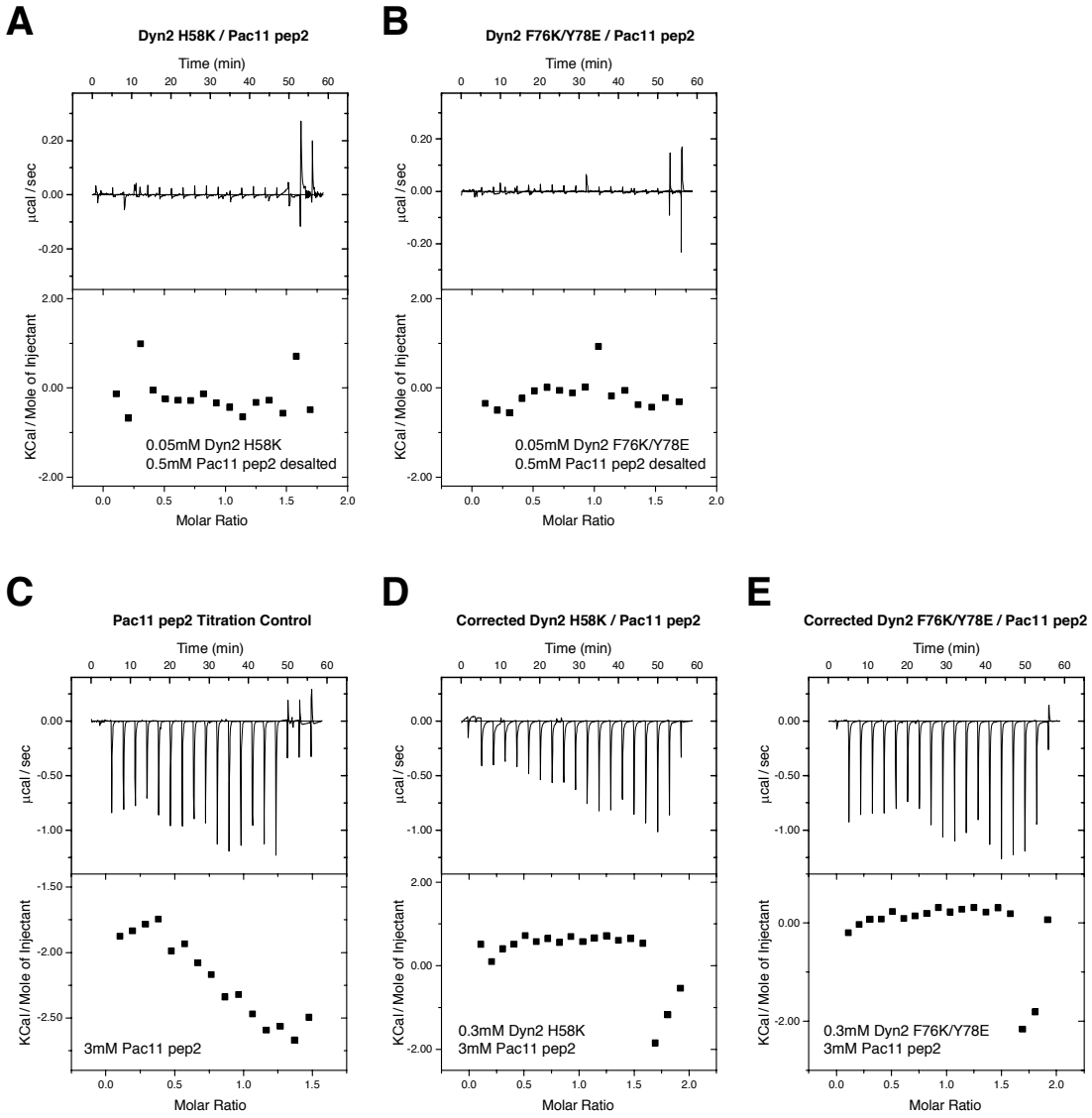

Supplemental Figure 2-1. Pac11 pep2 does not bind to Dyn2 H58K or Dyn2 F76K/Y78E as measured by ITC.

A. and **B.** 0.5 mM desalted Pac11 pep2 was injected into 200 µL of 50 µM Dyn2 H58K or Dyn2 F76K/Y78E in 19 x 2 µL injections and no measurable binding was observed as indicated by the relatively straight line of integrated heats of dilution in the bottom panels. **C.** The control of 19 x 2 µL injections of 3.0 mM Pac11 pep2 into 200 µL of buffer B showed significant heats of dilution (upper panel) and a trend upon integrating values (lower panel). **D.** and **E.** 19 x 2 µL injections of 3.0 mM Pac11 pep2 were introduced to 200 µL of 0.3 mM Dyn2 H58K or Dyn2 F76K/Y78E showing significant heats of dilution in the top panels. The values in the control lower panel (**C.**) were subtracted from **D.** and **E.** heats of dilution to correct for Pac11 pep2 into buffer B heat contribution (lower panels).

CHAPTER 3

THE STRUCTURE AND BINDING MODE OF THE DYNEIN LIGHT CHAIN, LC8, WITH AN ESSENTIAL CENTRIOLE DUPLICATION FACTOR, ANA2

Preface

This work is a manuscript in progress with unfinished experiments. Karen Plevock cloned Lc8 into the pGEX-6P-2 vector. Lauren Slevin assisted me in the isothermal microtitration calorimetry experiments and preparing crystals for diffraction. Lauren also performed fluorescence microscopy experiments on Lc8 and Ana2 localization in S2 cells, but that work is not reflected here. I designed and performed the remaining biophysical experiments and protein preparation. My advisor, Kevin Slep, and I designed the binding and crystallization experiments, and Kevin Slep, Lauren Slevin and I wrote and edited the manuscript.

Romes, EM, Slevin, LK, Plevock, K, and Slep, K. (manuscript in progress).

Summary

Centriole duplication is an important process in the life cycle of a cell, which is highly regulated so that a cell is able to properly segregate chromosomal DNA and prevent genomic instability and nuclear fallout. Centrioles nucleate a procentriole orthogonal to the existing centriole (Nigg, 2011) and proceed through a duplication cycle, which includes initiation/licensing, elongation, termination, and new centriole maturation (Azimzadeh, 2012). The initiation step in the cycle utilizes the highly regulated Sas6 to form the initial

structure of the procentriolar cartwheel (Brito, 2012). Sas6 binds to another essential centriole duplication protein, Ana2, which is responsible for nucleating a single procentriole off of a mother centriole, and without which a cell is likely to have fewer than two centrioles during mitosis (Arquint, 2012). Ana2 binds to a dynein light chain, Lc8 to regulate spindle positioning and to assist Ana2 in dimerization (Wang, 2011). Here we demonstrate that Lc8 binds Ana2 exothermically at two locations with one canonical QT binding motif (pep1) and an affinity of 0.54 μM, and the second site is a QC motif (pep2) with a binding affinity of 12.7 μM. We present the 1.83 Å crystal structure of Lc8 bound to Ana2 pep1, which demonstrates that Lc8 binds Ana2 pep1 in a similar manner as previously described crystal structures. We will continue to refine this crystal structure and the structure of Lc8 bound to Ana2 pep2 to answer whether the previously uncharacterized non-canonical QC binding motif displays a different hydrogen-bonding interaction network than what has been previously described. We also aim to determine whether Lc8 functions as a dimerization machine responsible for dimerizing Ana2 at the site of centriole duplication.

Experimental Procedures

Cloning and Expression of full length Lc8

Full length Lc8 was cloned from *Drosophila melanogaster* into the pGEX-6P-2 expression vector (GE Healthcare) using the polymerase chain reaction. pGEX-6P-2-Lc8 was transformed into *E. coli* BL21 DE3 (pLysS) and grown under ampicillin selection in 6 L of LB media at 37°C. At an optical density of 0.8 (600 nm), GST-Dyn2 expression was induced using 0.1 mM isopropyl-1-thio-β-D-galactopyranoside for 16 hours at 18°C. Cells were harvested by centrifugation at 2100 x g for 10 min. at 4°C and the pellets resuspended in

buffer A: 150 mL of 25 mM Tris, pH 8.0, 300 mM NaCl, and 0.1% β-mercaptoethanol, and stored at -20°C.

Protein Purification

Lc8 was purified as described in Romes, 2012. Briefly, Lc8 was expressed in BL21 DE3 (pLysS) cells at 18° C for 16 hours. Cells were lysed by sonication and the supernatant was first purified on a Glutathione-S-sepharose column and the GST tag was cleaved with PreScission protease (GE Healthcare). The cleaved protein was additionally purified by SP Sepharose Fast Flow column (GE Healthcare) and the peak fractions were exchanged into the final MES buffer: 25 mM MES at pH 6.0, 50 mM NaCl, and 0.1% β-mercaptoethanol. Lc8 was concentrated to about 0.5 mM and snap frozen in liquid nitrogen and stored at -80°C until further use. The final Lc8 contains an N-terminal GPLGS cloning artifact.

Synthesis of Ana2 Peptides

Ana2 peptides were synthesized at the UNC Microprotein Sequencing and Peptide Synthesis Facility and lyophilized peptides were reconstituted in final MES buffer. The sequences for Ana2 peptides are pep1 (NYTICAGTQTDP, residues 159-168) and pep2 (NYSSTTGTQCDI, residues 237-246), which includes an N-terminal exogenous Asn and Tyr for peptide concentration determination.

Crystallization

Lc8 and Ana2 pep1 complex: final concentrations of 0.5 mM Lc8 and 0.6 mM Ana2 pep1 in final MES buffer were incubated for 30 minutes on ice. Crystallization followed the hanging drop protocol using 2 μL of the Lc8-Ana2 pep1 mixture and 2 μL of the 1 mL well solution: 0.3 M magnesium acetate tetrahydrate, 0.1 M cacodylic acid sodium salt, pH 6.5 and 26% (w/v) polyethylene glycol 8000. Crystals grew at 20°C into rods within three days and

remained at full size for up to three weeks. Crystals were transferred into fomblin oil (Sigma) for cryoprotection and flash frozen in liquid nitrogen.

Lc8 and Ana2 pep2 complex: final concentrations of 0.75 mM Lc8 and 0.9 mM Ana2 pep2 in final MES buffer were incubated for 30 minutes on ice. Crystallization followed the hanging drop protocol using 2 μL of the Lc8-Ana2 pep2 mixture and 2 μL of the 1 mL well solution: 20% (w/v) polyethylene glycol 3350 and 0.35 M potassium phosphate monobasic. Crystals grew at 20°C into thin plates within seven days. Crystals were transferred into fomblin oil (Sigma) for cryoprotection and flash frozen in liquid nitrogen.

Data Collection, Structure Determination, and Refinement

Diffraction data were collected on Lc8-Ana2 pep1 and pep2 crystals at the Advanced Photon Source SER-CAT beamline 22-ID with 1° oscillations over 180° from a single crystal. Data were indexed, integrated and scaled using HKL2000 (Otwinowski, 1997). The Lc8-Ana2 pep1 structure was determined using the AutoMR molecular replacement program (PHENIX crystallographic suite (Adams, 2010)) and a modified 2PG1 (Williams, 2007) coordinate file in which a monomeric, apo Lc8 search model was used. The model was built using AutoBuild (PHENIX) (Adams, 2010) and refined iteratively through manual builds in Coot (Emsley, 2010) followed by refinement runs using phenix.refine (PHENIX) (Adams, 2010). Refinement statistics were monitored using a Free R, calculated using 5.7% of the data, randomly excluded from refinement (Brunger, 1992).

Isothermal Microtitration Calorimetry

ITC experiments were carried out at 26°C in final MES buffer on a Microcal AutoITC200 (GE Healthcare). Lyophilized peptides were solubilized in final MES buffer. 19 x 2 μL injections of 1.0 mM Ana2 pep1 were automatically injected into 200 μL of 50 μM Lc8 and

2.0 mM pep2 was automatically injected into 200 μL of 100 μM Lc8. The resulting binding isotherms (Fig. 3-1) were analyzed using the Origin 7.0 software package (OriginLab) and were fit to a one-site binding model. Ana2 peptide control experiments were performed to determine heat of dilution contribution where 19 x 2 μL injections of 1.0 mM Ana2 pep1 or 2.0 mM Ana2 pep2 was injected into 200 μL of final MES buffer. The resulting binding isotherm for the Ana2 pep1 control was not significant to subtract from the raw experimental values, so the final 5 injection values (where binding was saturated out) were averaged and this value was subtracted from each injection as an internal control. Ana2 pep2 external control registered a significant endothermic heat contribution so these control values were individually subtracted from the raw experimental values for Lc8 binding Ana2 pep2 (see Fig. S3-1 for control binding isotherms). Experiments were conducted in triplicate, the internal or external controls were subtracted, and the resulting heats of dilution were averaged to determine respective mean K_D values with standard deviations as shown.

Results

Lc8 binds the traditional QT motif, Ana2 pep1 with 0.54 μM affinity and the non-traditional QC motif, Ana2 pep2 with 12.7 μM affinity. The interactions between Lc8 and Ana2 pep1/pep2 were determined by ITC to investigate strength and mode of binding. Previous studies have shown that Dyn2 dimers (the *S. cerevisiae* Lc8 homolog) are capable of binding Nup159 target peptides with two different binding modes (Romes, 2012). Although most Lc8 binding interactions determined to date are exothermic in nature, Lc8 is also capable of binding target peptides with affinities ranging from 0.06 μM (Swallow) to 100 μM (Pak1) (Benison, 2009; Williams, 2007). We determined that Lc8 binds to both

Ana2 pep1 and Ana2 pep2 with an exothermic binding mode (Fig. 3-1 A,B), which indicates they both form extensive hydrogen bonding networks with Lc8. Ana2 pep1 bound to Lc8 with 0.54 μM affinity (Fig. 3-1A), which is comparable to 0.62 μM affinity that Pac11 pep2 binds to Dyn2 (Romes, unpublished). The Ana2 pep1 heats of dilution did not contribute significantly to the overall binding of Lc8 as determined by an external control (Fig. S3-1A), so an internal subtraction of the saturated peaks at the end of the binding curve was sufficient

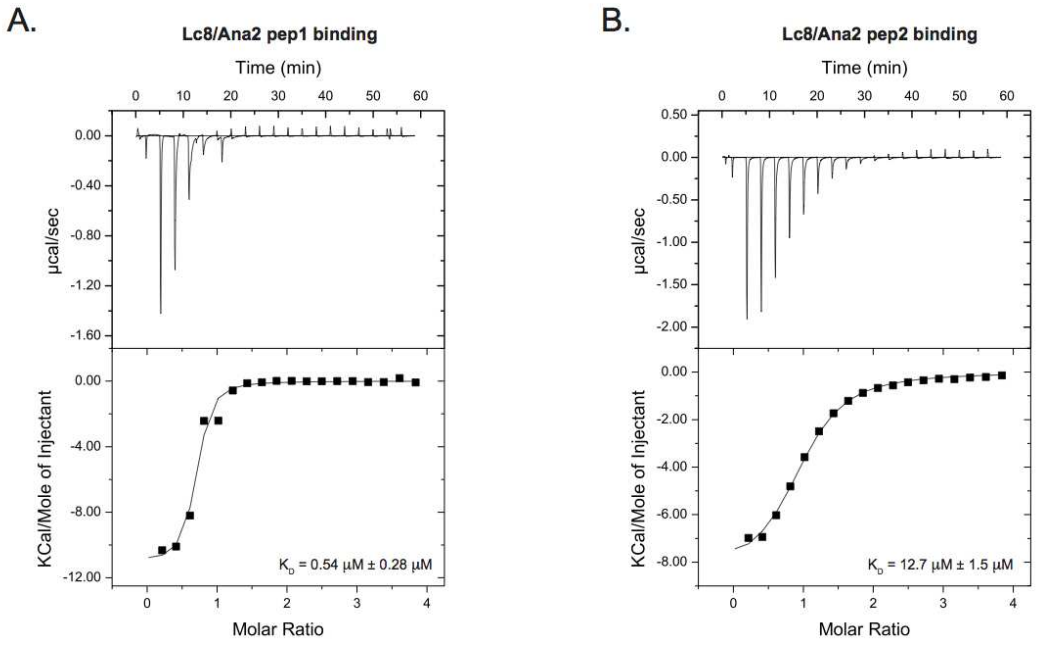

Figure 3-1. Lc8 interacts with two Ana2 peptides with an exothermic binding mode but exhibits different affinities.

The upper panel displays the injection thermograms of Lc8 bound over the period of time (min). The lower panel displays the integrated heats of dilution and the values were fit to a one-site binding model using Origin 7.0 software (OriginLab). **A.** 19 x 2 μL injections of 1.0 mM Ana2 pep1 were automatically injected into 200 μL of 50 μM Lc8 to measure the thermal heats of dilution. The exothermic profile of the binding curve was internally corrected and fit with Ana2 pep1 binding Lc8 with 0.54 μM affinity. **B.** 19 x 2 μL injections of 2.0 mM Ana2 pep2 were automatically injected into 200 uL of 100 μM Lc8 to measure binding heats. The resulting isotherm was externally corrected and fit with Ana2 pep2 binding Lc8 with 12.7 μM affinity.
Lc8-Ana2 pep1: K_D = 0.54 ± 0.28 μM, ΔH = -1.08E4 cal/mol, ΔS = -7.1 cal/mol/deg, N = 0.61 sites; Lc8-Ana2 pep2: K_D = 12.7 ± 1.5 μM, ΔH = -8700 cal/mol, ΔS = -6.8 cal/mol/deg, N = 0.94 sites.

for eliminating the contribution of Ana2 pep1 heat in buffer. Lc8 bound to Ana2 pep2 less strongly with a K_D of 12.7 μM (Fig. 3-1B). The concentrations necessary to accurately measure Ana2 pep2 binding to Lc8 were higher than for pep1, and injecting Ana2 pep2 into buffer (Fig. S3-1B) contributed to the measurable heat of the system, so values from the external control of Ana2 pep2 injections into buffer were individually subtracted from each binding injection for Ana2 pep2 into Lc8.

Lc8 forms crystallized complexes with Ana2 peptides, but only Ana2 pep1 was able to resolve a structure without further optimization. We were able to optimize crystallization and x-ray diffraction conditions for the complex of Lc8-Ana2 pep1 to process the raw diffraction and solve the structure to 1.83 Å in the $P2_12_12_1$ space group. The diffraction data were indexed, integrated and scaled with HKL2000 (Otwinowski, 1997) to obtain a 1.83 Å data set with 96% completion and 12.3 $\langle I/\sigma \rangle$ (signal over noise). We modified pdb 2PG1 (Williams, 2007) to contain only an Lc8 monomer for a molecular replacement solution for the Lc8-Ana2 pep1 structure. There are four Lc8-Ana2 pep1 molecules in the asymmetric unit. Each asymmetric unit contains two Lc8 homodimers with each homodimer binding two Ana2 pep1 within the medial peptide-binding cleft. The Ana2 pep1 electron density was strongly indicated as binding to all four Lc8 monomers and was built in *de novo* and has currently been refined to 18.2 R working and 22.6 R_{free} values.

The crystal morphology of Lc8-Ana2 pep2 was a series of thin, epitaxial plates, which were very different from pep1 morphology. The epitaxial plates indicated that the twinned crystals were diffracting as split and smeared spots in the x-ray diffraction pattern.

Table 1: Data Collection and Refinement Statistics	
Wavelength (Å)	1.00000
Space group	$P2_12_12_1$
Cell dimensions (Å)	
a	51.5
b	77.9
c	108.9
Resolution (Å)	50.0-1.83 (1.90-1.83)
Reflections	
Measured	108,631
Unique	37,745
Completeness (%)	95.7 (96.8)
Mean redundancy	2.9 (2.5)
I/σ	12.3 (2.0)
R_{sym} [a]	0.08 (0.45)
Refinement	
Resolution (Å)	46.5-1.83 (1.87-1.83)
R[b] / R_{free} (%)[c]	18.2 (25.4) / 22.6 (27.4)
No. reflections, R/R_{free}	35,748 (2081) /1,997 (119)
Total atoms	3270
Protein/water	2914/177
Stereochemical ideality (rmsd)	
Bonds/angles (Å/°)	0.007/1.05
Ramachandran analysis	
Favored/allowed (%)	96.2/1.1

Parentheses list statistics for the high resolution shell

[a] $R_{sym} = \Sigma_h\Sigma_i|I_i(h) - < I(h) >|/\Sigma_h\Sigma_i I_i(h)$ where $I_i(h)$ is the integrated intensity of the ith reflection with the Miller Index h and $<I(h)>$ is the average over Friedel and symmetry equivalents.

[b] R value = $\Sigma (|F_{obs}| - k|F_{calc}|)/ \Sigma|F_{obs}|$.

[c] R_{free} is calculated using a 5.7% subset of the data that are removed randomly from the original data and excluded from refinement.

As a result, we were unable to resolve the peaks for proper indexing and further crystal optimization will be needed to resolve these issues.

The Lc8-Ana2 pep1 crystal structure reveals that Lc8 binds to Ana2 pep1 in the same binding pocket and orientation as previous Lc8 structures. The crystal structure of the Lc8 homodimer bound to the dynein intermediate chain (Williams, 2007) was previously shown

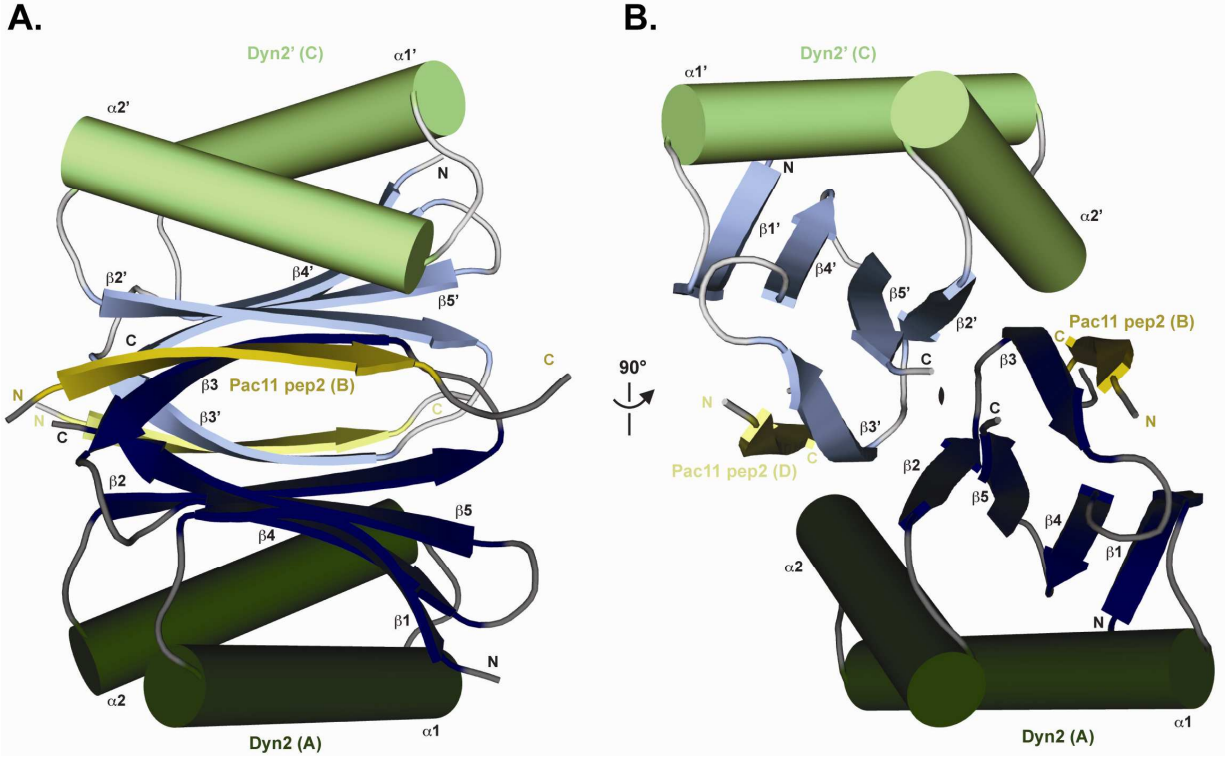

Figure 3-2. The crystal structure of the Lc8-Ana2 pep1 is a 2:2 complex formed by an Lc8 homodimer binding two Ana2 pep1.

A. and **B.** The Lc8 monomer is composed of two α-helices from each monomer on the top and bottom of two antiparallel β-sheets. Chain A monomer of Lc8 is represented in dark colors with α-helices in dark green cylinders and β-strands in dark blue cartoon. Chain B is the second Lc8 monomer in light colors with helices in light green cylinders and β-strands in light blue cartoon. The Ana2 pep1 are in dark yellow (Chain C) and light yellow (Chain D) cartoon. **B.** The Lc8-Ana2 pep1 complex is turned 90 degrees about the y-axis to demonstrate the two-fold non-crystallographic symmetry operator through the center of the dimer about the z-axis.

to be two α-helices from each monomer flanking two β-sheets that are parallel, but composed of antiparallel β-strands (Fig. 3-2A). Each β-sheet is composed of five β-strands in order of β1-β4-β5-β2-β3' where the ultimate β-strand is contributed by the corresponding dimer pair. There is a non-crystallographic symmetry operator that relates the Lc8-Ana2 monomers to each other through a two-fold rotation (Fig. 3-2B). The Lc8 binding site for peptides with a canonical or non-canonical QT motif is a β-strand-β-strand interaction where

the peptide completes the β-sheet following the β3' strand. We found that the 1.83 Å crystal structure of the Lc8-Ana2 complex forms the same secondary structures and Lc8 binds the Ana2 pep1 in the same binding pocket.

Discussion

Previous work shows that Ana2 is essential for localizing Sas6 to a procentriole during centriole duplication (Stevens, 2010). Ana2/STIL/Sas-5 have proven to be necessary for promoting the growth of only one procentriole on a mother, a process which ensures that the proper number of centrioles are formed to prevent genomic instability due to improper chromosome segregation (Nigg, 2011). In addition, centriole position is crucial to determining spindle orientation which is especially important in polarized, dividing cells (Wang, 2011). Ana2 was shown to interact with a dynein light chain, Lc8, and both are necessary for properly positioned mitotic spindles (Wang, 2011). Wang, et al. determined that the N-terminus and central coiled-coil of Ana2 are important for interacting with Lc8, and the N-terminal 274 residues are sufficient for Ana2's function in centriole duplication and positioning mitotic spindles (Wang, 2011). Our work aims to better define the role for the Lc8-Ana2 interaction in centriole duplication and positioning spindles, and specific regions required for this interaction to occur.

We determined that Lc8 binds two locations on Ana2 in a similar manner as previous examples of Lc8 bind to target peptides. We utilized ITC to show that Lc8 binds two different QT motifs, one canonical and one non-canonical. Both of the binding motifs are within the N-terminal region that Wang, et al. determined to be sufficient for Ana2's function in centrioles. The more N-terminal binding motif is canonical because it contains both Q and

T at residues 165 and 166, while the second Ana2 peptide contains the non-canonical QC motif at residues 243 and 244. The canonical Ana2 pep1 bound Lc8 with a K_D of 0.54 μM, and the non-canonical Ana2 pep2 bound Lc8 with a K_D of 12.7 μM. They both exhibited common exothermic binding modes, which are indicative of a strong hydrogen-bonding network between Lc8 and Ana2. The structural complex of Lc8 and Ana2 pep1 confirmed this extensive hydrogen-bonding network.

The x-ray crystal structure of Lc8 and Ana2 pep1 demonstrates that Lc8 is able to bind Ana2 at the first putative binding site in a manner consistent with other Lc8 structures. We aim to continue refining this Lc8-Ana2 pep1 complex in order to obtain a structure sufficient for publication and to properly determine the individual binding interactions that occur through the hydrogen-bonding network. We have determined through structural analysis of this Lc8-Ana2 pep1 complex that the Lc8 binding pocket is not as wide as the Dyn2 binding pocket from Romes, 2013 (data not shown). Peptides that are able to bind in the Dyn2 binding pocket may not be able to do so in the Lc8 binding pocket due to steric hindrance. We hypothesize that the binding pocket for Lc8 binding to Ana2 pep2 may be slightly shifted to accommodate the non-canonical cysteine instead of a sterically smaller, canonical threonine in Ana2 pep1.

We will continue to optimize conditions for Lc8 and Ana2 pep2 crystallization and x-ray diffraction. We hypothesize that much of the hydrogen-bonding network will be the same between the Ana2 pep1 and Ana2 pep2 structures with Lc8, but that small differences will account for the difference in binding affinity. We are also interested in refining the regions of Ana2 that play a role in centriole duplication and whether Lc8's role as a dimerization machine for Ana2 is essential for their individual roles in mitotic spindle orientation.

References

1. Adams, P. D., Afonine, P. V., Bunkóczi, G., Chen, V. B., Davis, I. W., Echols, N., Headd, J. J., Hung, L.-W., Kapral, G. J., Grosse-Kunstleve, R. W., McCoy, A. J., Moriarty, N. W., Oeffner, R., Read, R. J., Richardson, D. C., Richardson, J. S., Terwilliger, T. C., and Zwart, P. H. (2010) *Acta Cryst*. **D66,** 213-221

2. Arquint, C., Sonnen, K. F., Stierhof, Y.-D., and Nigg, E. A. (2012) *J. Cell Sci*. **125**, 1342-1352

3. Azimzadeh, J., and Bornens, M. (2012) *J. Cell Sci*. **120**, 2139-2142

4. Benison, G., Chiodo, M., Karplus, P. A., and Barbar, E. (2009) *Biochemistry* **48**, 11381-11389

5. Brito, D. A., Gouveia, S. M., and Bettencourt-Dias, M. (2012) *Curr. Opin. Cell Biol*. **24**, 4-13

6. Brunger, A. T. (1992) *Nature* **355,** 472-475

7. Emsley, P., Lohkamp, B., Scott, W., and Cowtan, K. (2010) *Acta Cryst*. **D66,** 486-501

8. Nigg, E. A., and Stearns, T. (2011) *Nat. Cell Biol*. **13**, 1154-1160

9. Otwinowski, Z., and Minor, W. (1997) *Methods in Enzymology*, Volume **276**: Macromolecular Crystallography, part A, p.307-326, Academic Press, New York, NY

10. Romes, E. M., Tripathy, A., and Slep, K. C. (2012) *J. Biol. Chem*. **287**, 15862-15873

11. Stevens, N. R., Dobbelaere, J., Brunk, K., Franz, A., and Raff, J. W. (2010) *J. Cell Biol*. **188**, 313-323

12. Wang, C., Li, S., Januschke, J., Rossi, F., Izumi, Y., Garcia-Alvarez, G., Gwee, S. S. L., Soon, S. B., Sidhu, H. K., Yu, F., Matsuzaki, F., Gonzalez, C., and Wang, H. (2011) *Dev. Cell* **21**, 520-533

13. Williams, J. C., Roulhac, P. L., Roy, A. G., Vallee, R. B., Fitzgerald, M. C., and Hendrickson, W. A. (2007) *Proc. Natl. Acad. Sci*. **104,** 10028-10033

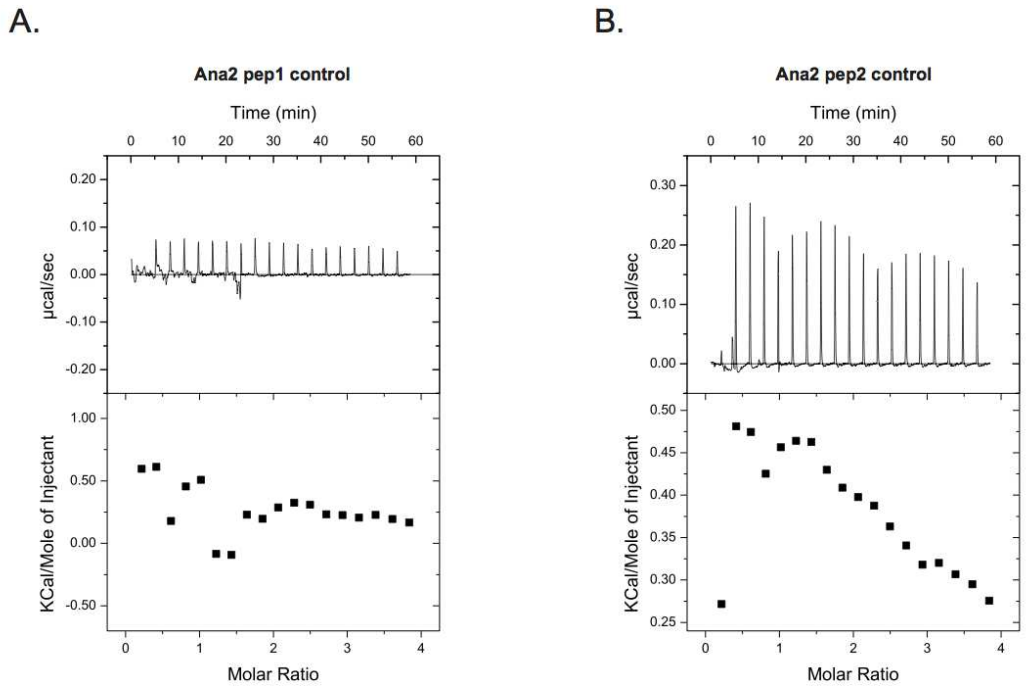

Supplemental Figure 3-1. Ana2 peptide ITC controls were necessary to determine the peptide contribution to the overall heat of dilution in each injection.

A. 19 x 2 µL injections of 1.0 mM Ana2 pep1 were automatically injected into final MES buffer to measure the heats of dilution for the control (upper panel). The lower panel shows that the integrated heats of dilution do not show significant values for subtracting from the experimental values of Ana2 pep1 into Lc8. **B.** Heats of dilution for 19 x 2 µL injections of 2.0 mM Ana2 pep2 (upper panel) show significant heat contributions that change over the course of the control experiment. The integrated injection peaks (lower panel) were then individually subtracted from each value in the experiment of 2.0 mM Ana2 pep2 into 0.1 mM Lc8.

CHAPTER 4

THE STRUCTURE OF A YEAST DYN2-NUP159 COMPLEX AND THE MOLECULAR BASIS FOR THE DYNEIN LIGHT CHAIN – NUCLEAR PORE INTERACTION

Preface

This work was previously published in Journal of Biological Chemistry. Ashutosh Tripathy helped me design and assisted me in the size exclusion chromatography-multi-angle light scattering experiments as well as the isothermal microtitration calorimetry. I performed the remaining experiments. My advisor, Kevin Slep, designed the project and we wrote and edited the manuscript.

Romes, EM, Tripathy, A, Slep, K. (2012) *J. Biol. Chem.* 287 (19): 15862-73.

Summary

The Nuclear Pore Complex gates nucleocytoplasmic transport through a massive, eight-fold symmetric channel capped by a nucleoplasmic basket and structurally unique, cytoplasmic fibrils whose tentacles bind and regulate asymmetric traffic. The conserved Nup82 complex, composed of Nsp1, Nup82 and Nup159, forms the unique cytoplasmic fibrils that regulate mRNA nuclear export. While the nuclear pore complex plays a fundamental, conserved role in nuclear trafficking, structural information about the cytoplasmic fibrils is limited. Here, we investigate the structural and biochemical interactions between *S. cerevisiae* Nup159 and the nucleoporin: Dyn2. We find that Dyn2 is

predominantly a homodimer and binds arrayed sites on Nup159, promoting Nup159's parallel homodimerization. We present the first structure of Dyn2, determined at 1.85 Å resolution, complexed with a Nup159 target peptide. Dyn2 resembles homologous metazoan dynein light chains, forming homodimeric composite substrate binding sites that engage two independent 10 residue target motifs, imparting a β-strand structure to each peptide via anti-parallel extension of Dyn2's core β-sandwich. Dyn2 recognizes a highly conserved QT motif, while allowing sequence plasticity in the peptide's flanking residues. Isothermal titration calorimetric analysis of Dyn2's comparative binding to two Nup159 target sites shows similar affinities (18 and 13 μM), but divergent thermal binding modes. Dyn2 homodimers are arrayed in the crystal lattice, likely mimicking Dyn2's arrayed architecture on Nup159's multivalent binding sites. Crystallographic inter-dimer interactions potentially reflect a cooperative basis for Dyn2-Nup159 complex formation. Our data highlights the determinants that mediate oligomerization of the Nup82 complex and promote a directed, elongated cytoplasmic fibril architecture.

Experimental Procedures

Cloning and Expression of Full Length Dyn2 from S. cerevisiae - Full length Dyn2 was cloned from *S. cerevisiae* S288c into the pGEX-6P-2 expression vector (GE Healthcare) using the polymerase chain reaction and BamHI and EcoRI engineered flanking restriction sites. The Dyn2 insert was sequence verified against Genbank accession NC_001136. pGEX-6P-2-Dyn2 was transformed into *E. coli* BL21 DE3 (pLysS) and grown under ampicillin selection in 6 L of LB media at 37°C. At an optical density of 0.8 (600 nm), GST-Dyn2 expression was induced using 0.1 mM isopropyl-1-thio-β-D-galactopyranoside for 16 hours

at 18°C. Cells were harvested by centrifugation at 2100 x g for 10 min. at 4°C and the pellets resuspended in buffer A: 150 mL of 25 mM HEPES, pH 6.8, 300 mM NaCl, and 0.1% β-mercaptoethanol, and stored at -20°C.

Protein Purification - Resuspended cell pellets were thawed and lysed by sonication at 4°C. 0.1 mM phenylmethylsulfonyl fluoride was added to the lysate and cell debris was pelleted by centrifugation at 23,000 x g for 45 min. Supernatant was loaded onto a 5 ml Glutathione Sepharose Fast Flow affinity column (GE Healthcare). GST-tagged Dyn2 was eluted from the glutathione column with 100 ml of 3 mM glutathione pH 8.0 in buffer A. The GST-Dyn2 eluate was exchanged into buffer B (25 mM HEPES, pH 6.8 and 0.1% β-mercaptoethanol) using an Amicon Ultra 10 kDa spin concentrator (Millipore) and incubated for 16 hours with PreScission protease (GE Healthcare). The cleaved protein was loaded onto an SP Sepharose Fast Flow column (GE Healthcare) and eluted over a linear 0-1 M NaCl gradient in buffer B. Dyn2 peak fractions were pooled and exchanged into 50 mM NaCl, 25 mM HEPES, pH 6.8, and 0.1% β-mercaptoethanol using an Amicon Ultra 3 kDa spin concentrator (Millipore) and concentrated to 5 mg/mL, snap frozen in liquid nitrogen and stored at -80°C. All purification procedures were executed at 4°C. The final, purified Dyn2 protein contained an N-terminal GPLGS cloning artifact.

Synthesis of Nup159 Peptides - Nup159 pep1 (YSADFDVQTSL, residues 1103-1113), pep2 (NYAESGIQTDL, residues 1116-1126), pep3 (YVKHNSTQTVK, residues 1141-1151), pep4 (YAVDNGLQTEP, residues 1153-1163), and pep5 (YTCNFSVQTFE, residues 1165-1175) (Fig. 4-1C) were synthesized at the UNC Microprotein Sequencing and Peptide Synthesis Facility. Pep1, pep3, pep4 and pep5 were designed with an amino terminal

tyrosine in order to quantify the peptide concentration once solubilized. Lyophilized peptides were solubilized in 50 mM NaCl, 25 mM HEPES, pH 6.8 and 0.1% β-mercaptoethanol.

Crystallization - 1.0 mM Dyn2 was incubated with 1.5 mM Nup159 pep2 in 50 mM NaCl, 25mM HEPES, pH 6.8, and 0.1% β-mercaptoethanol for 30 minutes on ice. Crystallization followed the hanging drop protocol using 1 μL of the Dyn2-Nup159 pep2 mixture and 1 μL of the 1 mL well solution: 0.3 M ammonium acetate, pH 5.5, 5% methyl pentanediol, and 35% polyethylene glycol 4000. Crystals grew at 20°C to 200 x 200 x 600 μm over the course of a week. Crystals were transferred to fomblin oil (Sigma) for cryoprotection and flash frozen in liquid nitrogen.

Data Collection, Structure Determination, and Refinement - Dyn2-Nup159 pep2 crystals were maintained at 100 K under a cryo-cooled nitrogen stream and diffraction data collected using a Rigaku Micromax 007HF x-ray generator (copper anode, 1.54 Å wavelength), Osmic mirrors and a Rigaku Saturn 944+ CCD in the UNC Macromolecular X-Ray Crystallography Core Facility. 0.5° oscillations were collected over 160° from a single crystal. Data were indexed, integrated and scaled using HKL2000 (Otwinowski, 1997) (Table 4-1). The structure was determined using the AutoMR molecular replacement program (PHENIX crystallographic suite (Adams, 2010)) and a modified 2PG1 (Williams, 2007) coordinate file in which a monomeric, apo *Drosophila* LC8 search model was used. The model was built using AutoBuild (PHENIX) (Adams, 2010) and refined iteratively through manual builds in Coot (Emsley, 2010) followed by refinement runs using phenix.refine (PHENIX) (Adams, 2010). Refinement statistics were monitored using a Free R, calculated using 10% of the data, randomly excluded from refinement (Brunger, 1992). The final model includes two Dyn2 molecules (chains A and C: residues 7-92), two Nup159 pep2 molecules

(chain B: residues 1117-1126; chain D: residues 1116-1126 with N1116 modeled as alanine) and 217 water molecules.

Size Exclusion Chromatography and Multi Angle Light Scattering - 100 μL of 200 μM Dyn2 was injected onto a Wyatt WTC030S5 silicone size exclusion column (for elution of 5,000 – 1,250,000 Da proteins) in 50 mM NaCl, 25 mM HEPES, pH 6.8, 0.1% β-mercaptoethanol, and 0.2 g/L sodium azide, and passed in tandem through a Wyatt DAWN HELEOS II light scattering instrument and a Wyatt Optilab rEX refractometer. The light scattering and refractive index data were used to calculate the weight-averaged molar mass (M_W) and the mass fraction in each peak using the Wyatt Astra V software program (Wyatt Technology Corp.) (Wyatt, 1993).

Isothermal Microtitration Calorimetry - ITC experiments were carried out at 15°C in buffer B: 50 mM NaCl, 25 mM HEPES, pH 6.8, and 0.1% β-mercaptoethanol on a Microcal AutoITC200 (GE Healthcare). Peptides were exchanged into buffer B using G-25 Sephadex Quick Spin Columns (Roche). 17 x 2 μL injections of 1 mM pep2 or pep4 were automatically injected into 200 μL of 100 μM Dyn2. The resulting binding isotherms (Fig. 4-6 A,B) were analyzed using the Origin 7.0 software package (OriginLab) and were fit to a one-site binding model. Experiments were conducted in triplicate and averaged to determine respective mean K_D values with standard deviations as shown.

Protein Data Bank Accession Number - Coordinates for the Dyn2-Nup159 complex have been deposited in the Research Collaboratory for Structural Bioinformatics PDB under accession code 4DS1.

Results

S. cerevisiae Dyn2 is a member of the conserved dynein light chain family - The dynein light chain, a component of the cytoplasmic dynein motor complex, is highly conserved from yeast to human (Fig. 4-1A). The dynein light chain is 90% identical across higher eukaryotes ranging from *C. elegans* to human, with significant identity extending to lower eukaryotes, as exemplified by the 50% identity between *S. cerevisiae* Dyn2 and *D. melanogaster* LC8. Across organisms, evidence points to the dynein light chain's role as a factor that promotes substrate dimerization. While the dynein light chain is a component of the dynein microtubule motor complex, it is not exclusive to this complex. Recent work has shown that approximately 25% of the *S. cerevisiae* dynein light chain member, Dyn2, is associated with the nuclear pore complex. Dyn2 associates with the Nup82 cytoplasmic fibril complex, binding to pentavalent motifs arrayed in Nup159's Dynein light chain Interaction Domain (DID) (Fig. 4-1 B-D) (Stelter, 2007). The Dyn2 binding motifs share a canonical QT motif with variable flanking components. Similar tandem binding sites have recently been mapped in the Dynein Intermediate Chain, Pac11, and shown to mediate Dyn2 interaction (Fig. 4-1 C,D) (Stuchell-Brereton, 2011). To understand the molecular basis of the Dyn2-Nup159 interaction, we cloned Dyn2 from *S. cerevisiae* (S288c) genomic DNA into the *E. coli* expression vector pGEX-6P-2, expressed and purified Dyn2 to homogeneity, removing the N-terminal GST tag. Nup159 peptides corresponding to the second and fourth Dyn2 DID binding sites (pep2 and pep4) were synthesized, purified by HPLC chromatography and verified by mass spectrometry analysis. Pep4 incorporated an N-terminal tyrosine to facilitate concentration determination while pep2 concentration was determined using its endogenous tyrosine.

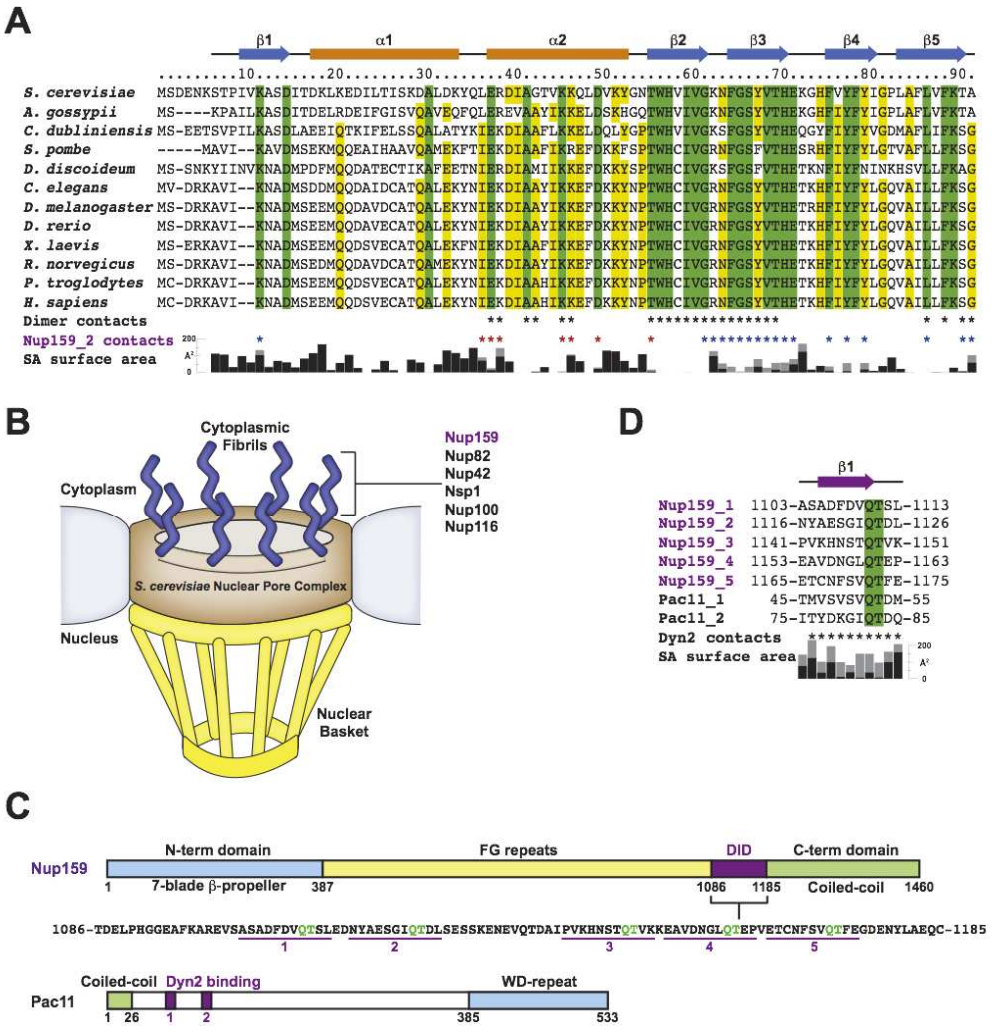

Figure 4-1. ***S. cerevisiae*** **Dyn2 is a conserved dynein light chain involved in diverse macromolecular complexes including the nuclear pore complex and the cytoplasmic dynein motor complex.**

A. Sequence alignment of 12 dynein light chain family members ranging from *S. cerevisiae* to human. Residues aligned with 100% and 80% identity are colored green and yellow respectively. Amino acid numbers and secondary structure elements, based on the *S. cerevisiae* Dyn2 structure are shown above the alignment. Residues involved in Dyn2 dimerization and Dyn2-Nup159 pep2 binding are indicated below the alignment by asterisks based on EMBL-EBI PDBe PISA (Protein Interfaces, Surface and Assemblies); black: Dyn2:Dyn2 chain A:C interactions; red: Dyn2:Nup159 pep2 chain A:D or chain C:B interactions; blue: Dyn2:Nup159 pep2 chain A:B or chain C:D interactions. Solvent accessible (SA) surface area for respective Dyn2 chain C residues is indicated below the alignment, calculated in the presence (black) and absence of the Nup159 pep2 chain D (gray) using the Accessible Surface Area Analysis tool in CCP4 (Collaborative, 1994). **B.** Cartoon diagram of the Nuclear Pore Complex illustrating the cytoplasmic localization of Nup159 and the Nup82 complex to cytoplasmic fibrils. **C.** Domain architecture of known Dyn2 binding proteins: Nup159 and Pac11. Nup159 is composed of an N-terminal β-propeller

domain involved in Dbp5 binding, central FG-rich repeats common to nucleoporins, a Dynein light chain interacting domain (DID) composed of five QT consensus motifs (residues 1103-1177) with Dyn2 binding activity, and a C-terminal region involved in Nup159 anchoring to the Nuclear Pore Complex (Stelter, 2007; Del Priore, 1997; Weirich, 2004). Pac11, the yeast dynein intermediate chain, shares architectural similarities with Nup159, composed of an N-terminal coiled-coil domain, tandem Dyn2 QT binding motifs, and a C-terminal WD-40 repeat domain, predicted to be a β-propeller. **D.** Sequence alignment of the Dyn2 binding motifs from Nup159 and Pac11 highlighting the invariant QT motif. Nup159 pep2 secondary structure is indicated above the alignment. Nup159 pep2 residues involved in Dyn2 binding are indicated by asterisks below the alignment, as is SA surface area, calculated in the presence (black) and absence of Dyn2 chains (gray).

The Dyn2 homodimer forms two composite substrate binding sites using a central β-sandwich and flanking α2-helices – To elucidate the structural determinants underlying the Dyn2-Nup159 interaction, we screened mixtures of Dyn2 and Nup159 pep2 and pep4 for co-crystallization. We obtained crystals of the Dyn2-Nup159 pep2 (residues 1116-1126) complex using a 1:1.5 molar ratio of Dyn2 and Nup159 pep2 respectively. The crystals diffracted to 1.85 Å resolution and belonged to the space group $P2_12_12_1$. We solved the structure by the molecular replacement method using a peptide-free monomeric chain derived from the *Drosophila* dynein light chain (2PG1) that showed 50% sequence identity with Dyn2 (Williams, 2007). Two Dyn2 chains occupy the asymmetric unit, homodimerized around a non-crystallographic two-fold axis. Clear electron density was evident for two Nup159 pep2 chains, each bound to the Dyn2 homodimer. The R and R_{free} values for the Dyn2-Nup159 pep2 structure are 15.1% and 18.0% respectively. Crystallographic data and refinement statistics are presented in Table 4-1. Dyn2 homodimerizes across a composite central β-sandwich (Fig. 4-2A). Each β-sheet is composed of five β-strands arranged in an anti-parallel organization: β1-β4-β5-β2-β3' in which the final β3' strand is provided by the homodimeric mate. The prime interface between Dyn2 molecules is mediated by the anti-parallel β2-β3' strand interaction. Here, the β2-β3' and β2'-β3 strand interactions

Table 1: Data Collection and Refinement Statistics

Wavelength (Å)	1.54178
Space group	$P2_12_12_1$
Cell dimensions (Å)	
a	33.9
b	48.0
c	110.7
Resolution (Å)	50.0-1.85 (1.92-1.85)
Reflections	
Measured	80,909
Unique	15,121
Completeness (%)	93.9 (62.7)
Mean redundancy	5.4 (2.5)
I/σ	24.8 (5.9)
R_{sym} [a]	0.05 (0.15)

Refinement

Resolution (Å)	29.3-1.85 (1.92-1.85)
R[b] / R_{free} (%)[c]	15.1 (17.8) /18.8 (24.4)
No. reflections, R/R_{free}	13,573/1508
Total atoms	1761
Protein/water	1541/221
Stereochemical ideality (rmsd)	
Bonds/angles (Å/°)	0.006/1.02
Mean B-factors (Å^2)	
MC/SC/water	13.9/20.0/28.5
B-factor rmsd (Å^2)	
MC/SC	1.4/2.5
Ramachandran analysis	
Favored/allowed (%)	98.4/1.6

Parenthesis list statistics for the high resolution shell

[a] $R_{sym} = \Sigma_h\Sigma_i|I_i(h) - < I(h) >|/\Sigma_h\Sigma_i I_i(h)$ where $I_i(h)$ is the integrated intensity of the ith reflection with the Miller Index h and $<I(h)>$ is the average over Freidel and symmetry equivalents.

[b] R value = Σ ($|F_{obs}| - k|F_{calc}|$)/ $\Sigma|F_{obs}|$.

[c] R_{free} is calculated using a 10% subset of the data that are removed randomly from the original data and excluded from refinement.

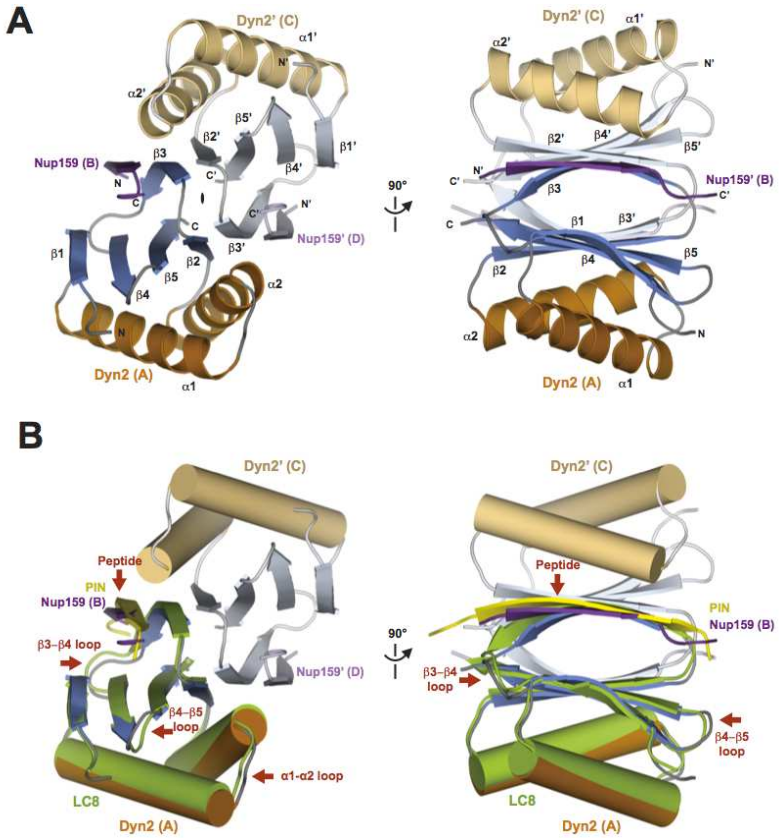

Figure 4-2. Structure of the Dyn2-Nup159 pep2 complex shows a quaternary complex composed of a Dyn2 dimer, bound to two Nup159 pep2 peptides through parallel, composite β-sheets.

A. Cartoon diagram of the Dyn2-Nup159 complex. Dyn2 chain A is shown in orange (α-helices) and dark blue (β-strands), Dyn2 chain C is shown in beige (α-helices) and light blue (β-strands). The two-fold non-crystallographic symmetry operator that relates the Dyn2 and Nup159 chains in the asymmetric unit is indicated about the z-axis. Image at right shows the complex after a 90° rotation about the y-axis. **B.** The complex as shown in the two orientations in A, with Dyn2 chain A superimposed on the human dynein light chain, LC8 (light green) bound to a PIN peptide (yellow) (pdb 1CMI) after a least squares fit with an RMSD of 0.6 Å over 87 aligned residues (Liang, 1999). Helices are shown in cylindrical format. Structural differences between Dyn2 and human LC8 are indicated by red arrows, and are dominated by loop regions as well as the bound peptides.

encompass the non-crystallographic two-fold operator that relates each Dyn2 molecule. Flanking the central β-sandwich, each Dyn2 molecule contributes an α1 and α2 helix that bridge β1 and β2. The α1-α2 helix-turn-helix motifs symmetrically pack against the two β-sheets that form the central β-sandwich. The Dyn2 homodimer symmetrically binds two

Nup159 peptides; the basis for the interaction is an extension of each β-sheet through an anti-parallel strand that is stabilized through buttressing interactions with the neighboring α2-helix.

Dyn2 architecture is homologous to other dynein light chain structures determined to date, with the highest structural homology to the human dynein light chain 8 (LC8) complexed with a peptide from the Protein Inhibitor of Neuronal Nitric Oxide Synthase (PIN) (pdb 1CMI), 0.6 Å Cα RMSD over 87 residues (47% identity, Fig. 4-2B), and ranged among dynein light chain structures to 2.3 Å Cα RMSD over 81 residues when compared to the dynein light chain structure 1YO3 from *Plasmodium falciparum* (37% identity) (Liang, 1999; Vedadi, 2007). The main elements that show structural diversity between Dyn2 and the *Drosophila* LC8 structure (1CMI) are restricted to loop regions, specifically the α1-α2 loop, the β3-β4 loop and the β4-β5 loop. The core secondary structure elements of the domain show little plasticity. Diversity of allowable residues in the target peptide N-terminal to the canonical QT motif, in turn show structural diversity in the target β-strand backbone bound to the dynein light chain, as shown in the overlay of the Dyn2-Nup159 peptide structure with the human LC8-PIN peptide structure (Fig. 4-2B, Fig. S4-1).

The Dyn2 homodimerization interface involves an extensive hydrophobic and electrostatic interface that buries approximately 940 $Å^2$ of solvent accessible surface area on each Dyn2 molecule. Core β-strand-β-strand hydrogen bonding networks extend the anti-parallel sheets across homodimeric mates (β2-β3' and β2'-β3), augmented through additional backbone-side chain electrostatic interactions as well as van der Waals contacts between side chains (Fig. 4-3A). Helix α2' packs against the β3 strand and buttresses the dimerization

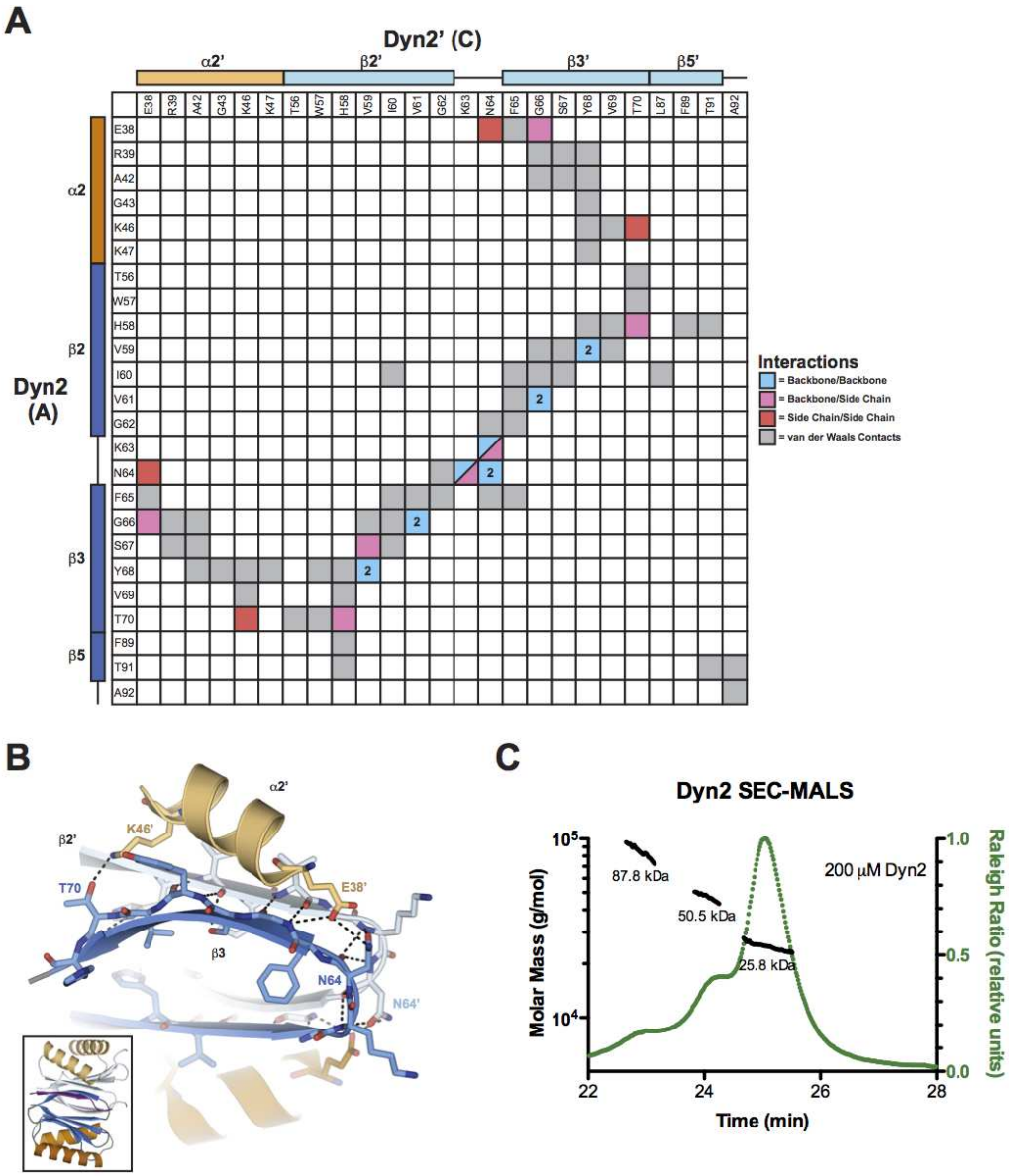

Figure 4-3. Dyn2 homodimerizes via an extensive network of van der Waals contacts and hydrogen bonds.

A. Interaction matrix, showing the pseudo-symmetric bonding and contact networks formed between Dyn2 protomers A and C in the complex. Secondary structure elements corresponding to the residues of each protomer are indicated along the axes of the matrix. Backbone/backbone, backbone/side chain, side chain/side chain, and van der Waals interactions are indicated in blue, pink, red, and grey respectively and correlate with distances less than or equal to 3.5 Å (hydrogen bonds) and 4.5 Å (van der Waals contacts). Numbers in cells indicate the total number of hydrogen bonds (greater than one) between two residues. **B.** Diagram of key residues and structural elements involved in the Dyn2-Dyn2 interface. The Dyn2 homodimer is shown as colored in Fig. 4-1. Specific Dyn2 residues mediating homodimerization are shown in stick format. Hydrogen bonds are indicated as dashed lines. The interface involves extensive antiparallel β-strand-β-strand interactions as

well as contributions from the α2 helices that flank the central β-sandwich. Inset shows the relative orientation of the complex. **C.** SEC-MALS analysis of Dyn2, injected at an initial concentration of 200 μM (green) in 100 μL. The Raleigh Ratio elution profile was normalized. Dyn2 predominantly forms a dimer in solution at pH 6.8, with additional, higher-order tetrameric and octameric species detected as well. The Dyn2 construct analyzed has a calculated monomeric molecular weight of 10,852 Da.

interface through the use of charged side chains, primarily E38' and K46', that afford van der Waals contacts as well as hydrogen bonding to β3 residues N64 and T70 respectively (Fig. 4-3 A,B). Overall, the homodimerization interface involves a pseudo-symmetric set of reciprocal interactions involving conserved residues (Figs. 4-1A, 4-3A).

Dyn2 exists as a multimer in solution – While the crystal structure of the Dyn2-Nup159 pep2 complex showed Dyn2 in a homodimeric state, we wanted to determine whether this dimeric form existed in solution in the absence of bound peptide. To determine Dyn2's oligomeric state, we utilized size exclusion chromatography coupled with multi-angle light scattering (SEC-MALS). We analyzed the elution and mass profiles of purified Dyn2 injected at an initial concentration of 200 μM. The Dyn2 elution profile contained three main peaks with masses respectively calculated at 25.8 kDa, 50.5 kDa and 87.8 kDa. On average, 87% of the eluted mass fraction was in the 25.8 kDa peak (Fig. 4-3C). The theoretical calculated molecular mass of our Dyn2 construct is 10,852 Da. Thus, under the conditions analyzed, peptide-free Dyn2 was found primarily as a homodimer with the remaining population in higher-order oligomeric states.

The Dyn2 homodimer binds parallel Nup159 peptides using a conserved composite binding site – Nup159 contains a pentameric array of Dyn2 binding sites (Stelter, 2007). In the structure we present here, the Dyn2 homodimer is complexed with two Nup159 peptides

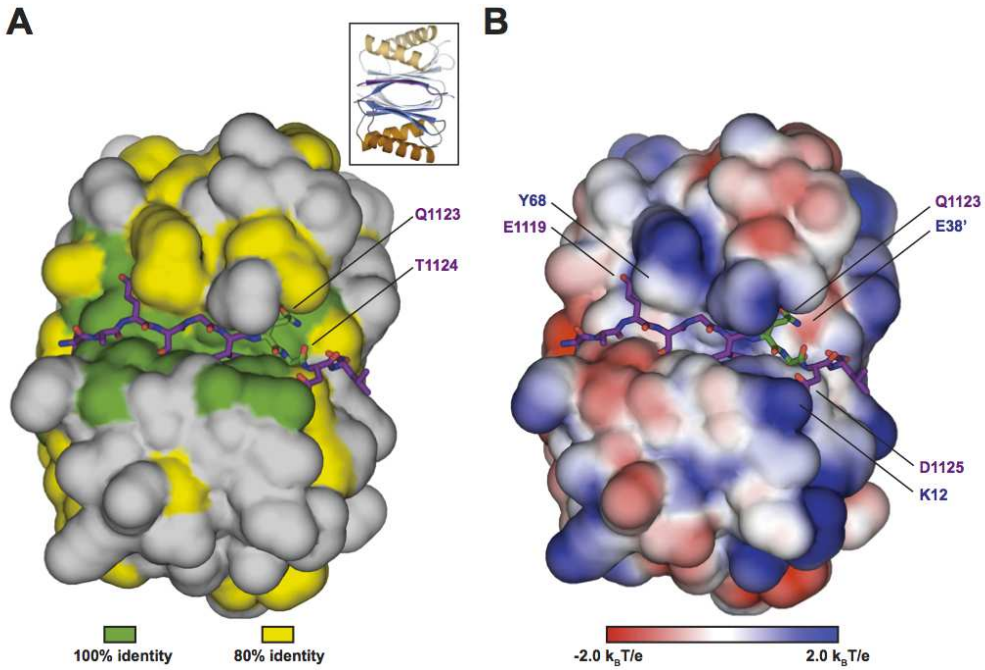

Figure 4-4. Dyn2 binds substrates through a highly conserved, positively charged composite groove formed by Dyn2 dimerization.

A. Conservation, as highlighted in Fig. 4-1A (green: 100% identity, yellow: 80% identity, as determined across twelve diverse species), mapped on the Dyn2 dimer shown in surface representation. Nup159 pep2 is shown in stick format in purple, inserted in the highly conserved interdimer groove. The highly conserved QT substrate motif (green sticks) is located C-terminal to the Nup159 pep2 β-strand. Conservation however, is equally distributed across the Dyn2 substrate-binding region. Inset shows the relative orientation of the complex in cartoon format colored as in Fig. 4-2A. **B.** Electrostatic surface calculated using APBS to generate solvent accessible surface potentials that are shown in k_BT/e, colored according to the key shown (Baker, 2001). Nup159 pep2 is shown in purple stick format with specific Dyn2 residues involved in hydrogen bond contacts labeled. The conserved QT motif is shown in green stick format. Dyn2:Nup159 pep2 interactions include Y68:E1119, E38':Q1123 and K12:D1125. The complex is oriented as in A.

corresponding to the second Dyn2 binding site in the Nup159 DID. The Nup159 peptide binds in a conserved pocket formed at the Dyn2 homodimer interface, consisting of both hydrophobic and charged residues (Fig. 4-4B). Nup159 pep2 (chain B) buries 911 $Å^2$ of solvent accessible surface area while each of the Dyn2 molecules bury 512 and 129 $Å^2$, for a collective 641 $Å^2$ of solvent accessible surface area buried at a single Nup159 pep2 binding

site. 16 of the 25 Dyn2 residues involved in Nup159 peptide binding are 100% invariant across the twelve species shown in Fig 4-1A, and 22 of the 25 are at least 80% invariant across these species (Fig. 4-4A). In Nup159, the glutamine (Q1123) and threonine (T1124) that constitute signature dynein light chain binding determinants, bind to the periphery of the peptide binding cleft in an area of high dynein light chain conservation. Analysis of the Dyn2 electrostatic surface shows that the peptide binding cleft is composed of mixed charges near the peptide N-terminal region while positive charges dominate the electrostatic potential at the peptide's C-terminal region. Key salt bridges in the complex include interactions between the invariant Dyn2 K12 and Nup159 D1125 as well as Dyn2 E38' and Nup159 Q1123. The Nup159 peptides form a β-strand interaction, extending the central β-sheets formed by Dyn2 homodimerization. The Nup159 β-strand runs anti-parallel to the Dyn2 β3 strand and extends across seven residues, terminating at the glutamine, Q1123, that composes the QT motif (Fig. 4-4, 4-5). The Nup159 Q1123 side chain forms a network of hydrogen bonds with the start of the neighboring Dyn2 α2' helix; capping the end through interactions with the R39' backbone amine as well as one of the E38' side chain □arboxyl oxygens. In addition, the Q1123 side chain forms a hydrogen bond with the F65 backbone amine on β3. Q1123's backbone is stabilized through a hydrogen bond to Dyn2's Y78 hydroxyl group (Fig. 4-5 A-C). T1124 from the Nup159 QT motif forms extensive contacts with Dyn2 F65, engaging the F65 backbone carbonyl and amine through hydrogen bonds from its own backbone amine and side chain hydroxyl group. The T1124 side chain γC also forms van der Waals contacts with the F65 benzene ring. Preceding the QT motif, the N-terminal six Nup159 residues primarily use an anti-parallel β-strand-β-strand hydrogen bond network as well as van der Waals contacts to bind the conserved Dyn2 groove, indicative of the highly variable

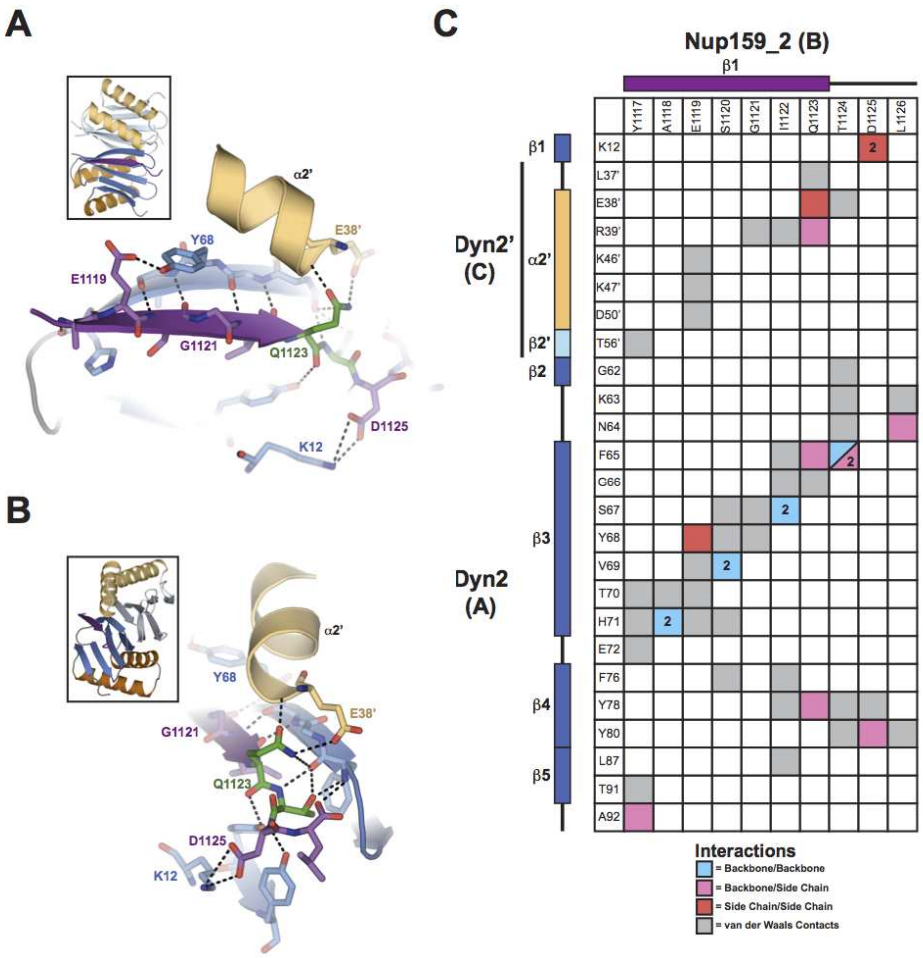

Figure 4-5. The Dyn2:Nup159 pep2 interaction is mediated by an extensive interaction network that recognizes ten contiguous Nup159 residues, dually conferring specificity and substrate plasticity.

A. and **B.** Close up of residues involved in the Dyn2:Nup159 pep2 interaction. Secondary structure elements are shown as in Fig. 4-2A, with specific residues that mediate the Dyn2:Nup159 pep2 interaction shown in stick format and their corresponding hydrogen bonding network shown with dashed lines. **C.** Interaction matrix, showing the contact networks formed between Dyn2 protomers A and C with Nup159. Secondary structure elements and protomer designation are indicated along matrix axes. Backbone/backbone, backbone/side chain, side chain/side chain, and van der Waals interactions are indicated in blue, pink, red and gray respectively and correlate with distances less than or equal to 3.5 Å (hydrogen bonds) and 4.5 Å (van der Waals contacts).

composition accepted in dynein light chain targets. Overall, the Nup159 pep2:Dyn2 interface is mediated by extensive hydrogen bonding and van der Waals contacts involving ten residues in the Nup159 peptide. All Nup159 residues modeled contact one Dyn2 protomer

and six of these ten residues make additional contacts with the Dyn2' homodimeric mate, indicating that high-affinity Dyn2-substrate recognition is mediated via Dyn2 dimerization. The Nup159 pep2:Dyn2 interface buries 1565 $Å^2$ of solvent accessible surface area at each binding site. The two Nup159 peptides bound to the Dyn2 homodimer run parallel to each other, related by a two-fold symmetry axis, with their mid points separated by approximately 20 Å.

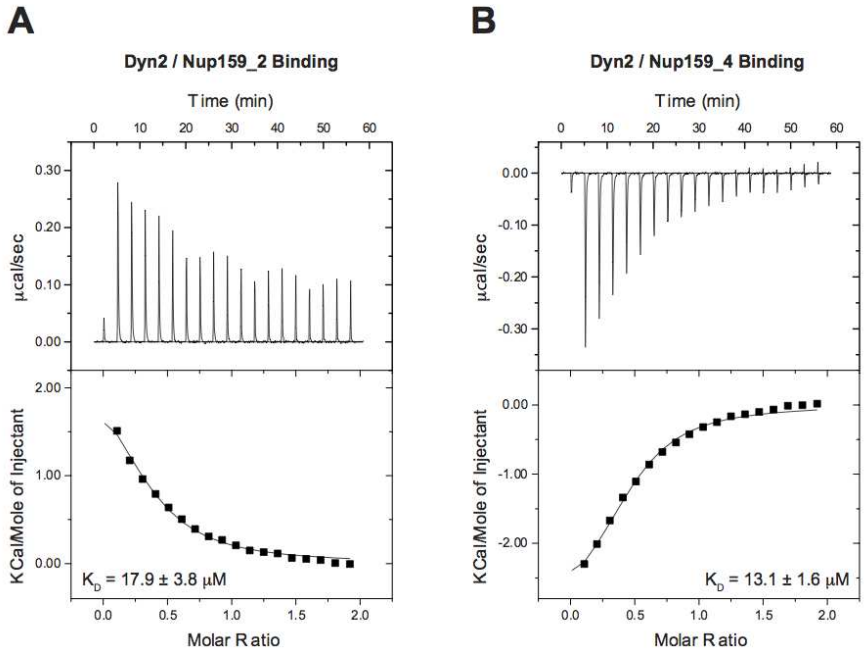

Figure 4-6. The Dyn2 interaction with Nup159 pep2 and pep4 occur in a 1:1 stoichiometry, and exhibit similar affinities but differ in their thermal binding modes.

A. 17 x 2 µL of 1 mM Nup159 pep2 was injected into 200 µL of 100 µM Dyn2. The thermogram (upper panel) displays µcal/sec over the injection period (min). **B.** 17 x 2 µL of 1 mM Nup159 pep4 was injected into 200 µL of 100 µM Dyn2. Dyn2 binding to Nup159 pep2 (A) displayed an endothermic binding isotherm, while Dyn2 binding to Nup159 pep4 (B) showed exothermic binding. Thermograms (upper panels) were integrated and the resulting isotherm was fit to a one-site binding model (lower panels) through iterative fitting. K_D values presented (inset, lower panel) are the average of three independent experiments: Dyn2-Nup159 pep2: K_D = 17.9 ± 3.8 µM, ΔH = 2500 cal/mol, ΔS = 31 cal/mol/deg, N = 0.33 sites; Dyn2-Nup159 pep4: K_D = 13.1 ± 1.6 µM, ΔH = -4000 cal/mol, ΔS = 8.6 cal/mol/deg, N = 0.39 sites.

Nup159 DID sites two and four respectively bind Dyn2 with 17.9 and 13.1 μM affinity, using differential thermal binding modes – To determine the affinities between Dyn2 and the five Nup159 Dyn2 binding sites in the DID, we synthesized the respective peptides and performed isothermal titration calorimetry, titrating peptides into the calorimeter cell containing Dyn2. Each Nup159 peptide binding experiment was performed in triplicate and the fitted values were averaged. Each individual binding experiment was best fit to a one-site model (using the Dyn2 monomer concentration) (Wyatt, 1993). Pep2 showed an endothermic isotherm (Fig. 4-6A) while pep4 showed an exothermic isotherm (Fig. 4-6B). The experimentally determined affinities between Dyn2 and Nup159 pep2 and pep4 are shown in Fig. 4-6 and have K_Ds equal to 17.9 and 13.1 μM respectively. Pep3 did not show sufficient signal to noise and was not soluble at the concentrations needed to determine binding accurately. Pep1 and Pep5 are highly hydrophobic and once solubilized, failed to show binding to Dyn2 as determined using isothermal titration calorimetry (data not shown). This may be due to the weaker binding affinities for these peptides as was qualitatively shown in the aforementioned PepScan assay (Stelter, 2007), or due to a folded/aggregated state that precluded Dyn2 from binding.

Translational arrangement of the Dyn2 homodimer facilitates contiguous binding to arrayed QT motifs – The arrangement of delineated QT motifs in Nup159 are nearly contiguous, separated by one or two amino acids except for a tentative QT region linking sites two and three that showed no Dyn2 binding activity in the previously mentioned PepScan assay (Stelter, 2007). In the same investigation, electron microscopy of the Dyn2:Nup159 DID complex showed five densities arranged like beads on a string, leading

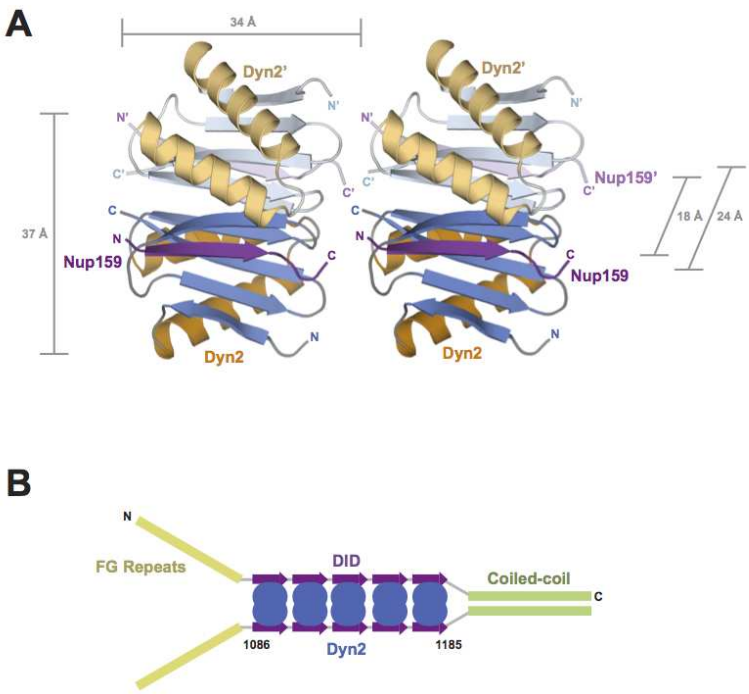

Figure 4-7. Crystallographic contacts array Dyn2 dimers linearly in an arrangement that affords polarized binding to arrayed Dyn2 binding motifs.

Dyn2-Nup159 crystallographic symmetry mates shown in cartoon representation, colored as in Fig. 4-2A. Dyn2 interdimer interactions coupled with parallel, arrayed binding motifs on Nup159 likely promote linear, cooperative binding activity between Dyn2 dimers and Nup159.

the authors to propose a model in which five Dyn2 dimers bound parallel Nup159 DID arrays (Stelter, 2007). Stelter et al. modeled the bound Dyn2 dimers in a translational array. In the $P2_12_12_1$ lattice presented here, we note a translational arrangement of Dyn2 dimers in the crystal lattice, that supports the Stelter et al. Dyn2:Nup159 complex model. As shown in Fig. 4-7, Dyn2:Nup159 pep2 complexes are translationally arranged in the crystal, with a 34 Å translational component approximately collinear to the Nup159 peptide, effectively placing the C-terminus of one Nup159 peptide proximal to the N-terminus of the neighboring Nup159 peptide. Five Dyn2 dimers in this crystal lattice span 170 Å, on par with the 20 nm

filaments observed by Stelter et al. in electron micrographs of the Dyn2:Nup159 DID complex.

Discussion

The dynein light chain, while a component of the cytoplasmic dynein motor complex, is promiscuous and has been identified as a component in numerous, diverse complexes. A universal role postulated for the dynein light chain is to serve as a dimerization machine. In *S. cerevisiae*, 25% of the Dyn2 cytoplasmic pool is found associated with the nuclear pore complex (Stelter, 2007). Nup159, a component of the Nup82 complex of the cytoplasmic fibrils, was identified as a Dyn2 binding partner that promotes stable association of the Nup82 complex with the NPC (Stelter, 2007). Nup159's pentameric array of Dyn2 binding sites link the N-terminal FG repeat region with the C-terminal NPC anchor region (Yoshida, 2011).

Our analysis of Dyn2 homodimer binding to individual Nup159 peptides showed similar affinities for pep2 and pep4, at 17.9 μM and 13.1 μM respectively, while binding for pep1, pep3, and pep5 could not be experimentally determined based on properties of the individual peptides as synthesized. Binding curves fit best to a one-site binding model and are comparable to LC8 binding to peptides of similar size: DYNLL1 binds a seven amino acid peptide from Bmf with a K_D of 1.1 μM and similarly sized nNOS peptide with a K_D of 7.0 μM (Radnai, 2010). The affinities determined between Dyn2 and the Nup159 peptides do not take into account potential cooperativity between arrayed Dyn2 homodimers based on interactions we observed in translational symmetry mates in the Dyn2:Nup159 crystal. The affinities and differential thermal binding modes determined for Nup159 pep2 and pep4

reflects plasticity in the Dyn2 binding pocket. The Dyn2 binding site does not have many steric occlusions, and can thereby accommodate sequence diversity as observed with the LC8 family (Fan, 2001; Radnai, 2010; Rapali, 2011). The Dyn2:Nup159 crystal structure shows that extensive backbone/backbone interactions mediate the anti-parallel β-sheet extension. This backbone-based interaction affords tight binding while simultaneously enabling diversity in the side chains that flank the core, conserved QT binding motif. The QT motif is present in most Dyn2/LC8 binding peptides characterized to date and constitutes the C-terminal flank of the target peptide's β-strand. The QT motif contributes a network of hydrogen bonds and van der Waals contacts with the dynein light chain's conserved grove, directly contacting residues from each subunit of the homodimer. The amino acid diversity flanking the QT motif likely underlies the differential affinities and thermal binding modes observed across dynein light chain targets. Pep4 exhibited exothermic binding, indicative of a strong enthalpic, electrostatically-driven interaction, while pep2 exhibited endothermic binding, indicative of a hydrophobic, entropically-driven interaction. Pep2 and pep4 each have electrostatic and hydrophobic residues. A key hydrophobic determinant that may underlie the endothermic binding observed with Nup159 pep2, is the tyrosine residue at position 1117, 6 residues upstream of the QT motif (i.e. Q-6; see Fig. 4-1D). The corresponding residue in Nup159 pep4 is an alanine. The Nup159 pep2 Q-6 tyrosine makes numerous van der Waals contacts with the Dyn2 homodimer (Fig. 4-5C). Peptide-specific exothermic and endothermic binding has been observed with Dyn2 homologs from other species and highlights the sequence diversity within target sites that dynein light chains are capable of accommodating (Benison, 2008; Radnai, 2010; Rapali, 2011; Hodi, 2006; Wagner, 2006; Nyarko, 2011).

Our work represents the first biophysical and structural characterization of the yeast dynein light chain, Dyn2. At physiological conditions, Dyn2 exists predominantly in the homodimeric state. As a homodimer, Dyn2 is positioned to interact with target sites and induce and stabilize parallel dimerization in these target proteins. Dimerization machines can crosslink targets, homo or heterodimerize targets, serve to architecturally extend a target, as well as promote a target's avidity for binding partners. The Dyn2:Nup159 structure creates a foundation for understanding Dyn2's role in the NPC as a dimerization machine that can scaffold Nup159 and extend the protein at least 170 Å (5 x 34 Å). Our structural and biophysical investigations of the Dyn2:Nup159 interaction have additional implications for Dyn2's mode of interaction and function with the dynein intermediate chain, Pac11, its potential role in promoting Pac11 dimerization and aiding in the recruitment of the dynein activation complex, dynactin (Stuchell-Brereton, 2011).

References

1. Adams, P. D., Afonine, P. V., Bunkóczi, G., Chen, V. B., Davis, I. W., Echols, N., Headd, J. J., Hung, L.-W., Kapral, G. J., Grosse-Kunstleve, R. W., McCoy, A. J., Moriarty, N. W., Oeffner, R., Read, R. J., Richardson, D. C., Richardson, J. S., Terwilliger, T. C., and Zwart, P. H. (2010) *Acta Cryst*. **D66,** 213-221

2. Baker, N. A., Sept, D., Joseph, S., Holst, M. J., and McCammon, J. A. (2001) *Proc. Natl. Acad. Sci. USA* **98,** 10037-10041

3. Benison, G., Karplus, P. A., and Barbar, E. (2008) *J. Mol. Biol*. **384,** 954-966

4. Brunger, A. T. (1992) *Nature* **355,** 472-475

5. Collaborative Computational Project, Number 4 (1994) *Acta Cryst. D* **50,** 760-763

6. Del Priore, V., Heath, C. V., Snay, C. A., MacMillan, A., Gorsch, L. C., Dagher, S., and Cole, C. N. (1997) *J. Cell Sci*. **110**, 2987-2999

7. Emsley, P., Lohkamp, B., Scott, W., and Cowtan, K. (2010) *Acta Cryst*. **D66,** 486-501

8. Fan, J., Zhang, Q., Tochio, H., Li, M., and Zhang, M. (2001) *J. Mol. Biol*. **306,** 97-108

9. Hodi, Z., Nemeth, A. L., Radnai, L., Hetenyi, C., Schlett, K., Bodor, A., Perczel, A., and Nyitray, L. (2006) *Biochemistry* **45,** 12582-12595

10. Liang, J., Jaffrey, S. R., Guo, W., Snyder, S. H., and Clardy, J. (1999) *Nat. Struct. Biol*. **6,** 735-740

11. Nyarko, A., Hall, J., Hall, A., Hare, M., Kremerskothen, J., and Barbar, E. (2011) *Biophys. Chem*. **159,** 41-47

12. Otwinowski, Z., and Minor, W. (1997) *Methods in Enzymology*, Volume **276**: Macromolecular Crystallography, part A, p.307-326, Academic Press, New York, NY

13. Radnai, L., Rapali, P., Hodi, Z., Suveges, D., Monar, T., Kiss, B., Becsi, B., Erdodi, F., Buday, L., Kardos, J., Kovacs, M., and Nyitray, L. (2010) *J. Biol. Chem*. **285,** 38649-38657

14. Rapali, P., Radnai, L., Suveges, D., Harmat, V., Tolgyesi, F., Walgren, W. Y., Katona, G., Nyitray, L., and Pal, G. (2011) *PLoS One* **6,** e18818

15. Stelter, P., Kunze, R., Flemming, D., Hoepfner, D., Diepholz, M., Philippsen, P., Boettcher, B., and Hurt, E. C. (2007) *Nat. Cell Biol*. **9,** 788-796

16. Stuchell-Brereton, M. D., Siglin, A., Li, J., Moore, J. K., Ahmed, S., Williams, J. C., and Cooper, J. A. (2011) *Mol. Biol. Cell* **15,** 2690-2701

17. Vedadi, M., Lew, J., Artz, J., Amani, M., Zhao, Y., Dong, A., Wasney, G. A., Gao, M., Hills, T., Brokx, S., Qiu, W., Sharma, S., Diassiti, A., Alam, Z., Melone, M., Mulichak, A., Wernimont, A., Bray, J., Loppnau, P., Plotnikova, O., Newberry, K., Sundararajan, E., Houston, S., Walker, J., Tempel, W., Bochkarev, A., Kozieradzki, I., Edwards, A., Arrowsmith, C., Roos, D., Kain, K., and Hui, R. (2007) *Mol. Biochem. Parasitol.* **151,** 100-110

18. Wagner, W., Fodor, E., Ginsburg, A., and Hammer, J. A. 3rd (2006) *Biochemistry* **45,** 11564-11577

19. Weirich, C. S., Erzberger, J. P., Berger, J. M., and Weis, K. (2004) *Mol. Cell* **16,** 749-760

20. Williams, J. C., Roulhac, P. L., Roy, A. G., Vallee, R. B., Fitzgerald, M. C., and Hendrickson, W. A. (2007) *Proc. Natl. Acad. Sci.* **104,** 10028-10033

21. Wyatt, P. J. (*1993*) *Anal. Chim. Acta* ***272*****,** 1-40

22. Yoshida, K., Seo, H., Debler, E. W., Blobel, G., and Hoelz, A. (2011) *PNAS* **108,** 16571-16576

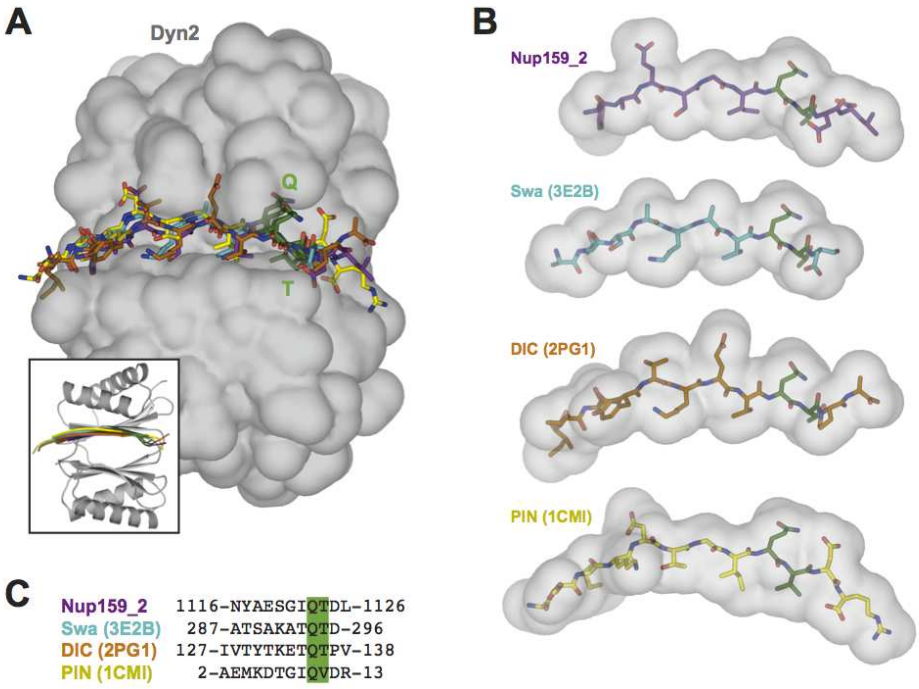

Supplemental Figure 4-1. The dynein light chain is highly plastic with regard to target peptide binding.

A. Superpositioning of four dynein light chain target peptides solved to date. Peptides are modeled in the presence of Dyn2 after a least squares fit of each structure's respective dynein light chain (not shown). Dyn2 is shown in gray surface representation. Peptides are shown in stick format. Nup159 peptide two is shown in purple. The Swallow (Swa) peptide is shown in blue (pdb 3E2B), the dynein intermediate chain (DIC) is shown in orange (pdb 2PG1) and the PIN peptide (1CMI) is shown in yellow (Williams, 2007; Benison, 2008; Liang, 1999). Inset shows the orientation of Dyn2 and the peptides in cartoon format. **B.** The peptides shown in A are presented in stick format and surface representation to highlight unique and differential features. The N-terminal region of the peptides show the greatest diversity. The conserved QT motif is towards the C-terminal region and is colored in green stick format. C. Sequence alignment of the peptides shown in B. The QT motif is highlighted in green, showing divergence in the PIN peptide: QV.

CHAPTER 5

DISCUSSION AND FUTURE WORK

Discussion

The importance of studying the dynein light chain, Dyn2/Lc8

The dynein light chain, Dyn2/Lc8 has, until recently been discussed in light of its function at the dynein complex for which it was named. More recent publications illuminate Dyn2/Lc8's ability to interact with a number of cellular targets that function in very specialized and highly regulated roles (McCauley, 2007; Lightcap, 2008; Espindola, 2000; Benison, 2007). Here we explore Dyn2/Lc8's interaction at the dynein complex, as well as two of Dyn2/Lc8's additional roles in dimerizing Nup159 at the nuclear pore complex, and dimerizing Ana2 in the early stages of centriole duplication.

The phenotype of Lc8/Dyn2 is not lethal in any of the model organisms surveyed to date, however, the severity of the deletion phenotypes for Lc8/Dyn2's binding partners can be cataclysmic and result in an inviable cell. When Lc8 is mutated to a null protein there can be slight defects in spindle orientation, which can result in a small percentage of cells dividing incorrectly or delayed in anaphase (Wang, 2011; Stuchell-Brereton, 2011). In the case of Dyn2's interaction at the nuclear pore protein, Nup159, the phenotype for *dyn2Δ* is a viable cell that may have slightly decreased fitness compared to WT (Breslow, 2008), but does not compare to the inviable cell in the null mutation of Nup159 (Stelter, 2007). A similar cellular defect is found when Lc8's binding partner, Ana2, is overexpressed in

Drosophila cells there is widespread over-proliferation of centrioles that results in genomic instability and can have the consequence of nuclear fallout (Stevens, 2010). It is the fact that Dyn2/Lc8 binds to these important cellular targets that makes Dyn2/Lc8 of great interest in optimizing target protein function, or as a point of regulation in the cell. Many of our outstanding questions involve how Dyn2/Lc8 modulates a protein's behavior through its function as a scaffolding protein.

In this body of work we show that Dyn2 forms a stable homodimer in solution, just as its higher eukaryote counterpart, Lc8, which acts as a scaffolding protein to encourage or stabilize dimerization of target proteins as a "dimerization machine". Dyn2/Lc8 is capable of binding to multiple cellular target proteins through a conserved QT sequence motif at the dynein intermediate chain, the centriole duplication factor, Ana2, and at the nuclear pore complex with Nup159. Here we show the first published structure of the *S. cerevisiae*, Dyn2, for which there is only 50% sequence identity between Dyn2 and the *Drosophila*, Lc8 (Romes, 2012). We show that there is structural commonality between Dyn2 and Lc8 that illustrates their ability to both bind the conserved QT motif in spite of their sequence identity difference. Dyn2's promiscuity in binding partners is highlighted by its flexibility to bind peptides with varying sequence outside of the QT motif and with different thermodynamic binding modes.

Dyn2/Lc8 is expressed ubiquitously throughout the cell, and has taken up a promiscuous role in binding many different protein targets with more than one type of thermodynamic binding mode. Dyn2/Lc8's deletion mutant or null mutation phenotype indicates that it is not an essential protein in the cellular contexts where it is found, but we

hypothesize that it acts as a point of regulation when it is phosphorylated and increases its binding partner's efficiency for binding other target proteins through homodimerization.

Dyn2 interacts at the dynein complex to homodimerize the intermediate chain, Pac11

The dynein holoenzyme is involved in many different, very important cellular contexts that determine cell viability in higher eukaryotes, and the efficiency of spindle movement during *S. cerevisiae*'s cell division. The dynein intermediate chain, Pac11 has been shown to bind to the dimerization domain of the dynein heavy chain to act as a scaffolding protein that binds many dynein-associating factors. The dynein light chain is an associating factor that binds directly to Pac11 to act as a scaffold for Pac11 to dimerize. There are two putative Dyn2 binding sites on Pac11 that contain conserved QT binding motifs, and we confirm that the second site binds to a Dyn2 homodimer with an extensive hydrogen bonding network and a strong affinity. We obtained a 1.90 Å crystal structure of the 2:2 Dyn2-Pac11 pep2 complex, which highlights Dyn2's ability to mediate dimerization of Pac11. The Q82 and T83 of Pac11 pep2 provide five hydrogen bonds for the extensive hydrogen bonding network and feature their prominence as the Dyn2 binding recognition motif. We found that Dyn2 binds to the Pac11 pep2 with a 620 nM affinity, which is the strongest Dyn2 interaction characterized to date. Through our exploration of the Dyn2-Pac11 pep2 complex we characterized distinct mutational sites that separately abrogate Dyn2 dimerization and Dyn2 binding to the Pac11 pep2. A single point mutation of H58K in the core of the dimerization interface acted like a switch to ablate Dyn2's ability to form a stable dimer in solution, as was shown for the corresponding H55 in Lc8 (Nyarko, 2005). Although the distance between the H58 imidazole rings is 5.4 Å, it appears that protonation at low pH or disturbance of this particular residue through mutation is enough to affect the delicate balance of dimerization.

Romes, 2012 details the extensive hydrogen bonding network and van der Waals forces involved in dimerization of Dyn2 that contribute to dimerization affinity. The dimerization affinity was measured for Lc8 to be 12 μM and showed that the Lc8 monomer β3 strand gained order upon dimerization and upon binding to a target protein/peptide (Nyarko, 2005).

Consistent with previous Lc8 findings, disturbance of homodimerization consequently abrogated Dyn2's ability to bind to the Pac11 pep2, which shows that homodimerization of Dyn2 is necessary for binding to the Pac11 pep2. Our work and others' work demonstrates the necessity of Dyn2/Lc8 dimerization for forming the peptide-binding cleft to build the extensive hydrogen-bonding network (Romes, 2012; Wang, 2003; Benison, 2009). We saw in the case of Dyn2 binding Nup159 pep2 that key residues (E38 and R39) in the second Dyn2 monomer contributed hydrogen bonds along with a number of van der Waals interactions throughout the second α-helix which all encourage stabilized binding.

We designed a double mutation in the peptide-binding pocket at F76K/Y78E to set up a charge repulsion with the intention of ablating peptide binding but maintaining the Dyn2 dimerization interface. We confirmed that the F76K/Y78E mutations allowed Dyn2 to dimerize in solution, but abolished the ability to bind to the Pac11 pep2. We hypothesize that this Dyn2 double mutant may be utilized to eliminate Dyn2 binding interactions in target proteins with a (+)xxQT(-) motif (where + indicates a K/R/H residue and – indicates a D/E residue).

In our binding assays we were unable to show that Dyn2 binds to previously determined binding motifs in Nup159 pep1, pep3, and pep5 as well as Pac11 pep1 due to the peptides' insoluble nature and inherent hydrophobicity. We hypothesize that Dyn2 would bind at these locations in the context of the full length Nup159 or Pac11. The first Pac11 pep1 binding site

aligns with the TcTex binding site for higher eukaryotes and begs the question why higher eukaryotes evolved the ability to bind to a different dynein light chain at this site. Although we were unable to answer whether there are intrinsic differences in Dyn2 binding to the two Pac11 binding sites, we surmise that since there are sequence differences between these two sites, Dyn2 is able to overcome these possible thermodynamic or steric differences through its flexible binding pocket as it binds promiscuously to other target proteins throughout the cell.

Lc8 homodimerizes the essential centriole duplication protein, Ana2

The process of centriole duplication is a highly regulated and conserved mechanism for duplicating the machinery, which controls many functions of proper DNA segregation during cellular division (Nigg, 2011). Centrioles duplicate exactly once every cell cycle to yield a pair composed of one mother centriole and a maturing orthogonal centriole (Kitagawa, 2011). In the initiation phase of duplication a few necessary proteins, including Sas6 and its binding partner, Ana2, form a single procentriole (Carvalho-Santos, 2010). Overexpression of Ana2 results in multiple procentrioles and can lead to genomic instability (Arquint, 2012). Ana2 and its binding partner, Lc8 are both important for the spindle orientation in asymmetric cell division (Wang, 2011). Previously Lc8 was not known to have a significant phenotype (Zhang, 2009), so this is the first example of Lc8's independent and Ana2-dependent function in asymmetric cell division. The Lc8 binding sites on Ana2 was hypothesized to be located within a central domain, which contains a coiled-coil (Wang, 2011), but not much was known about how this interaction might abrogate their function in orienting the spindle.

We have solved the 1.83 Å crystal structure of the Lc8 homodimer in complex with two bound Ana2 pep1s. This structure demonstrates that Lc8 binds Ana2 pep1 in the same peptide-binding pocket where the conserved QT motif aligns and makes similar binding contacts as other Lc8-peptide binding interactions. We are continuing to refine the Lc8-Ana2 pep1 crystal structure so that we may dissect the binding interactions that make this a tight binding interaction for Lc8. We have also obtained crystals for the Lc8-Ana2 pep2 in different crystallization conditions and with a completely dissimilar morphology. We were not able to obtain adequate diffraction of these crystals so we will continue to optimize and refine the conditions so that we may determine the differences between Lc8 binding a canonical QT motif versus a non-canonical QC motif from the second Ana2 binding site.

Here we show that Lc8 binds to Ana2 exothermically through two binding sites, one of which contains a canonical QT binding motif (site 1), and the other a non-canonical QC motif (site 2). We demonstrate through ITC that Lc8 binds the canonical binding motif with the higher affinity of 0.54 μM, and the non-canonical binding motif with 12.7 μM affinity. Both of these affinities are within the typical range of Lc8 binding affinities, however it is unusual that Lc8 is able to bind to two different sites on the same protein with affinities on either end of Lc8's usual binding range. The second Lc8 binding site is just C-terminal to Ana2's central coiled-coil domain, and both binding sites are located within a region of Ana2 that was shown to be important for Ana2 localization to the centrioles (Wang, 2011).

Dyn2 interacts with five consecutive Nup159 binding sites within the nuclear pore complex cytoplasmic fibril

The nuclear pore is a structure that gates all asymmetric traffic into and out of the nucleus (Fahrenkrog, 1998). The pore is especially significant in controlling the export of mRNA out

of the nucleus and into the cytoplasm for translation (Cole, 2006). On the cytoplasmic side of the nuclear pore there are structures called the cytoplasmic fibrils, which act as the last checkpoint in gating, and may assist in pulling through the pore larger transiting complexes (Zhao, 2002). Previous work has shown that Dyn2 interacts with one of the essential cytoplasmic fibril proteins, Nup159 in a domain near the C-terminus that helps to anchor Nup159 into the nuclear pore (Stelter, 2007; Stuchell-Brereton, 2011). Here we are interested in the biophysical role that Dyn2 plays in functionally dimerizing Nup159 through binding and structural assays.

We demonstrate the first published structure of Dyn2 in complex with a Nup159 pep that shows the importance of the Dyn2 QT binding motif. We parse out the network of hydrogen bonding interactions between Dyn2 and Nup159 pep2, as well as the importance of salt bridges for recognition and additional stability in this binding reaction. We see that although the Dyn2 binding site is not a charged environment, there are charged residues on either end of the binding pocket that form electrostatic interactions with oppositely charged residues on the Nup159 peptide. The five sequential Dyn2 binding motifs on Nup159 contain very different sequence, but highlight Dyn2's malleable binding requirements that support binding driven by binding affinity and not induced fit or sterics.

We show that Dyn2 can bind two Nup159 peptides in solution with similar affinities but different binding modes through ITC. Dyn2 binds to Nup159 pep2 with 17.9 μM affinity and an endothermic profile which suggests a rearrangement of structural waters and the composite consolidation of hydrophobic residues within the binding interaction. Nup159 pep4 binds to Dyn2 with a similar 13.1 μM affinity, but in an exothermic binding profile

which is common for many binding interactions. This is the first example of Dyn2 or Lc8 binding along the same protein with two different binding modes.

We hypothesize with the support of these data that Dyn2 binds the consecutive Nup159 binding sites with cooperativity to increase the avidity of the Dyn2-Nup159 interaction. This zippering affect of cooperativity allows Dyn2 to have a lower binding affinity than has been seen for most Dyn2/Lc8 binding interactions, but still mediate a productive Nup159 dimer. We also envision that Nup159 dimerizing through Dyn2 allows it to have less dedicated peptide sequence than would be required for a full coiled-coil dimerization so that Nup159 can utilize that sequence to further extend into the cytoplasm.

Dyn2 binds target proteins with a large number of hydrogen bonds that are highly conserved within the Nup159 and Pac11 networks.

Our studies on Dyn2 and Lc8 have uncovered the mode with which the Dyn2/Lc8 homodimer uses to recognize and bind a variety of target proteins. Here we showed that the Dyn2 peptide-binding pocket sequence is well conserved among an alignment of 12 species (Fig. 4-4A). We find that the Dyn2 binding pocket does not contain charged residues except two peripheral lysines that only make salt bridge contacts with specific binding sequences (Fig. 4-4B). We therefore conclude that Dyn2 does not bind proteins through charge-charge interaction, but instead utilizes an extensive network of hydrogen bonds and van der Waals contacts (Fig. 4-5C; Fig. 2-3B). We also found that a number of different types of hydrogen bond contacts are conserved between the Nup159 pep2 and Pac11 pep2 binding interfaces with Dyn2 (Fig. 2-3C). We hypothesize that the extensive hydrogen-bonding network and van der Waals forces contribute to the μM binding affinities that are observed between Dyn2 and the target peptides we have measured here.

Future Work

We would like to further investigate the purpose of Dyn2/Lc8 as a dimerization machine in these various cellular contexts. Since we see Dyn2/Lc8 as a ubiquitous protein that is able to promiscuously bind various target proteins through malleable binding requirements, we anticipate that further examples of Dyn2/Lc8 dimerizing important protein targets will surface. We recognize that although Dyn2/Lc8 are dynein light chains in name it is probable that this was not their original functional location. Some species of plants and algae contain only the Lc8 light chain, but do not contain the dynein motor for intracellular transport. We are curious how Dyn2/Lc8 evolved the ability to bind to new targets throughout the cell, and why many of these targets exhibit strong null phenotypes, which suggests the target proteins' importance in their various cellular contexts.

Much of our future work revolves around determining the importance of Lc8/Dyn2's dimerization of target proteins. We are currently collaborating with Arne Gennerich to determine whether Dyn2's ability to dimerize the dynein intermediate chain, Pac11 modulates processivity or velocity of dynein along microtubule tracks. The point mutations we developed from biophysical and structural studies will hopefully allow the Gennerich lab to parse out the importance of the Dyn2-Pac11 dimerization interaction for dynein.

Since Lc8 and Dyn2 are so ubiquitously expressed and utilized throughout the cell in a number of different contexts, we would like to investigate how Lc8/Dyn2 is regulated. We believe that Lc8/Dyn2-mediated dimerization is the perfect point of regulation. Song et al. have shown that Lc8 is phosphorylated on Ser88 (Dyn2 contains a Thr91 that aligns with Ser88) to cause dissociation of the dimer, which in turn ablates Lc8's ability to bind target proteins (Song, 2008; Benison, 2009). We aim to determine whether Dyn2 and Lc8 are

phosphorylated at the dynein complex, at the nuclear pore, and at centriole duplication. We will utilize the phosphomimetic mutation used in Benison et al. to assay the importance of Dyn2/Lc8 phosphorylation in dimerization (Benison, 2009).

Additionally, we aim to determine whether Lc8 interacts with Ana2 at the site of centriole duplication to modify centriole number in dividing *Drosophila* S2 cells by ablating the Lc8 binding sites on Ana2. Studies to date have not shown what role Lc8-mediated dimerization plays, and whether the Ana2 coiled-coil is sufficient for dimerization. We propose a simple SEC-MALS Ana2 experiment to determine the oligomer state of Ana2 in the absence of Lc8. This experiment would illuminate whether full length Ana2 is capable of dimerizing without Lc8 mediation. We also aim to look at the dimerization state of an Ana2 construct that contains the two Lc8 binding sites and the putative coiled-coil, to determine whether this is the minimal domain for dimerization. Additionally we are still refining structural data of the Lc8-Ana2 pep1 co-crystallization structure, and we aim to solve the structure of the Lc8-Ana2 pep2 complex. We hypothesize that the Lc8-Ana2 pep2 complex may explain how Lc8 is capable of binding such different sequences, even when the canonical QT motif is not maintained.

With the biophysical information we have gathered on Lc8/Dyn2's mechanism for binding target peptides in the dynein complex, at centriole duplication, and in the nuclear pore, we have developed Dyn2 mutational tools that may help us determine whether dimerization is necessary or just helps to optimize function for Pac11, Ana2, and Nup159. If dimerization of these and other target proteins increases their avidity for other protein-protein interactions, then Dyn2/Lc8-mediated dimerization affords optimized binding, much in the same way that it is easier to catch a ball with two hands than with a single hand.

References

1. Arquint, C., Sonnen, K. F., Stierhof, Y.-D., and Nigg, E. A. (2012) *J. Cell Sci.* **125**, 1342-1352

2. Benison, G., Karplus, P. A., and Barbar, E. (2007) *J. Mol. Biol.* **371,** 457-468

3. Benison, G., Chiodo, M., Karplus, P. A., and Barbar, E. (2009) *Biochemistry* **48**, 11381-11389

4. Breslow,D. K., Cameron, D. M., Collins, S. R., Schuldiner, M., Stewart-Ornstein, J., Newman, H. W., Braun, S., Madhani, H. D., Krogan, N. J., and Weissman, J. S. (2008) *Nat. Methods* **5**, 711-718

5. Carvalho-Santos, Z., Machado, P., Branco, P., Tavares-Cadete, F., Rodrigues-Martins, A., Pereira-Leal, J. B., and Bettencourt-Dias, M. (2010) *J. Cell Sci.* **123**, 1414-1426

6. Cole, C. N., and Scarcelli, J. J. (2006) *Curr. Opin. Cell Biol.* **18**, 299-306

7. Espindola, F.S., Suter, D. M., Partata, L. B. E., Cao, T., Wolenski, J. S., Cheney, R. E., King, S. M., and Mooseker, M. S. (2000) *Cell Motil. Cytoskeleton* **47**, 269-281

8. Fahrenkrog, B., Hurt, E. C., Aebi, U., and Pante, N. (1998) *J. Cell Biol.* **143,** 577-588

9. Kitagawa, D., Vakonakis, I., Olieric, N., Hillbert, M., Keller, D., Olieric, V., Bortfeld, M., Erat, M. C., Fluckiger, I., Gonczy, P., and Steinmetz, M. O. (2011) *Cell* **144**, 364-375

10. Lightcap, C. M., Sun, S., Lear, J. D., Rodeck, U., Polenova, T., and Williams, J. C. (2008) *J. Biol. Chem.* **283,** 27314-27324

11. McCauley, S. D., Gilchrist, M., and Befus, A. D. (2007) *Life Sci.* **80,** 959-964

12. Nigg, E. A., and Stearns, T. (2011) *Nat. Cell Biol.* **13**, 1154-1160

13. Nyarko, A., Cochrun, L. Norwood, S., Pursifull, N., Voth, A., and Barbar, E. (2005) *Biochemistry* **44**, 14248-14255

14. Romes, E. M., Tripathy, A., and Slep, K. C. (2012) *J. Biol. Chem.* **287**, 15862-15873

15. Stevens, N. R., Dobbelaere, J., Brunk, K., Franz, A., and Raff, J. W. (2010) *J. Cell Biol.* **188**, 313-323

16. Stuchell-Brereton, M. D., Siglin, A., Li, J., Moore, J. K., Ahmed, S., Williams, J. C., and Cooper, J. A. (2011) *Mol. Biol. Cell* **15,** 2690-2701

17. Wang, C., Li, S., Januschke, J., Rossi, F., Izumi, Y., Garcia-Alvarez, G., Gwee, S. S. L., Soon, S. B., Sidhu, H. K., Yu, F., Matsuzaki, F., Gonzalez, C., and Wang, H. (2011) *Dev. Cell* **21**, 520-533

18. Wang, W., Lo, K. W., Kan, H., Fan, J., and Zhang, M. (2003) *J. Biol. Chem.* **278,** 41491-41499

19. Zhang, J., Li, S., Musa, S., Zhou, H., and Xiang, X. (2009) *J. Biol. Chem.* **284**, 34760-34768

20. Zhao, J., Jin, S. B., Bjorkroth, B., Wieslander, L., and Daneholt, B. (2002) *EMBO* **21**, 1177-1187